August 2015

# Sediment Records from Coastal Ponds: Temporal Archives of Storm Inundation and Environmental Change

Christine M. Brandon
*University of Massachusetts - Amherst*

# SEDIMENT RECORDS FROM COASTAL PONDS: TEMPORAL ARCHIVES OF STORM INUNDATION AND ENVIRONMENTAL CHANGE

A Dissertation Presented

by

CHRISTINE MARIE BRANDON

Submitted to the Graduate School of the
University of Massachusetts Amherst in partial fulfillment
of the requirements for the degree of

DOCTOR OF PHILOSOPHY

May 2015

Geosciences

SEDIMENT RECORDS FROM COASTAL PONDS: TEMPORAL ARCHIVES OF STORM INUNDATION AND ENVIRONMENTAL CHANGE

A Dissertation Presented

by

CHRISTINE MARIE BRANDON

Approved as to style and content by:

_____
Jonathan D. Woodruff, Chair

_____
William D. McCoy, Member

_____
Don J. DeGroot, Member

_____
Julie Brigham-Grette, Department Head
Geosciences Department

**DEDICATION**

For Patrick
whose unwavering love, support, and patience are the foundation of this work

**ACKNOWLEDGEMENTS**

The old saying that “it takes a village to raise a child” can also be applied to creating a dissertation. Here, I’d like to acknowledge the contributions of my “village.”

First, and foremost, I’d like to thank my advisor, Jon Woodruff for being a role model of academic excellence and integrity. Through his advice, tutelage, and copious patience I’ve become a far better researcher, teacher, and scientific writer over the years. I am forever grateful that he accepted me as a “walk-in” student.

Next, I’d like to thank my committee members Don DeGroot and Bill McCoy. This research and dissertation have greatly benefitted from their input and their advice has helped shape the direction of this project.

I’d like to recognize the coauthors on the scientific articles that form the basis of this work: Jeff Donnelly, Richard Sullivan, Philip Orton, and the late Phil Lane. They have contributed immensely to the research by performing field work, sharing field and lab resources, and developing numerical models. They have also reviewed countless drafts of these articles and have added a richness and depth to the work that would not have otherwise been there.

This research would not have been possible without those who helped me in the field: Hannah Baranes, Jeff Donnelly, Brecia Douglas, Andrea Hawkes, Phil Lane, Dana MacDonald, Chris Maio, Skye Moret, Richard Sullivan, Michael Toomey, Peter van Hengstom, Davin Wallace, Jon Woodruff, and Sam Zipper. Every one of them enhanced the field experience in some way for me, whether it was through teaching me how to operate various pieces of equipment, ingenious solutions to unexpected problems, good humor, hard work, or tasty cooking. I’d also like to thank Andy Sheldon, a retired geology professor, who, out of his love of science, provided me with data from Spring Creek Pond and a canoe trip to the marsh.

I would still be sieving sediment if not for the help of my undergraduate lab assistants Shakib Ahmed, Olivia Beaulieu, Hayley Kinney, Melanie Koerth, and Lisa Kumpf. Their willingness to tackle tedious work and do it accurately has spoiled me in the best way, in that I don't know what it's like to have a "bad" assistant.

I'd also like to thank those people who were not coauthors but still contributed significantly to the research. Kerry Emanuel provided "synthetic hurricanes" for St. Marks Florida and John Warner taught me how to use ROMS; both provided a deeper understanding of numerical modeling. Thanks also to Jim Elsner for helping me understand bootstrapping techniques.

I would be remiss if I did not thank Stephanie Madsen for helping me properly prepare carbon-14 samples for submittal and knowing where everything is in the Woods Hole lab; Anna Martini for analyzing my sediment samples for mercury; and Carla Dellatte at the Staten Island Museum for her assistance with the historical research and for reminding me to eat something during the day. Thanks also to Mike Rhodes and Pete Dawson for their assistance with the Itrax (and allowing me to run samples at odd hours) and John Sweeney for being able to build anything.

I'd also like to thank the grad students and post docs of the sedimentology lab throughout the years: Hannah Baranes, Ehmed El'Zidani, Kinuyo Kanamaru, Tom Naughton, Zach Stromer, Davin Wallace, and Brian Yellen. Not only have they helped in tangible ways, like running samples for me on the gamma counter, but through discussions with them, my knowledge of sedimentology has been greatly enhanced.

Chris Condit also deserves recognition, perhaps as the founder of this village. I'm still not entirely certain of the details, but I believe he is partly, if not wholly, responsible for my admittance to the Geosciences Department.

Financial support for this dissertation came from various sources. I'd like to thank the UMass Geosciences department for giving me a teaching assistantship for two years as well as two Gloria Radke Memorial Scholarships; the UMass Astronomy department for giving me three semesters as a teaching assistant; and the Springfield Water and Sewer Commission, Hudson River Graduate Fellowship (02-13), and the Woods Hole Guest Student Program for summer support. This work was also funded under various National Science Foundation grants (including instrument and facility support via grant IF-0949313 and RAPID grant #1313859), Hudson River Foundation Expedited Grant #004/12E, and the Dalio Explore Fund. The oyster modeling performed by Phil Orton was supported by a NOAA-RISA funded project (Consortium for Climate Risk in the Urban Northeast) and a grant of computer time from the City University of New York High Performance Computing Center under NSF Grants CNS-0855217, CNS-0958379 and ACI-1126113.

Finally, I'd like to thank my friends and family who have supported me and patiently listen to me talk about sand and hurricanes for the past six years. I would especially like to thank my "scientist husband", Patrick for intuitively knowing when I needed to be left to my work and when I needed a video game break.

**ABSTRACT**

SEDIMENT RECORDS FROM COASTAL PONDS: TEMPORAL ARCHIVES OF STORM INUNDATION AND ENVIRONMENTAL CHANGE

MAY 2015

CHRISTINE MARIE BRANDON, B.S., UNIVERSITY OF MASSACHUSETTS AMHERST

M.A. BOSTON UNIVERSITY

Ph.D. UNIVERSITY OF MASSACHUSETTS AMHERST

Directed by: Jonathan D. Woodruff

Hurricanes are powerful storms that can cause billions of dollars in damage and kill many people when they strike populated coastal areas. Understanding how frequently coastal cities can expect storms of a certain magnitude would help inform more effective mitigation and adaptation strategies. Unfortunately, current estimates of hurricane frequency rely on numerical models based on weather observations that, on the east coast of the United States, only extend ~150 years into the past. While this is sufficient for estimating the characteristics (i.e. wind speed and storm surge height) of annual or decadal storms, the properties of larger, rarer, and more destructive storms have much uncertainty associated with them. Therefore, longer records of storm activity are needed to more accurately estimate the characteristics of these storms.

Such records can be found in coastal ponds. Nearshore sediments entrained in storm surges can form overwash deposits in these ponds. These deposits are easily distinguishable from lacustrine sediments due to their different grain size, organic content, and mineralogy. The grain size distribution and thickness of each deposit are related to the height and duration of the storm surge which created it and in turn this storm surge is related to the magnitude of the

storm, itself. Additionally, lacustrine sediments can record regional changes in sediment supply and deposition rate.

Here, I present a 2500 year long reconstruction of hurricane intensity and activity from St. Marks, Florida and a 3000 year long reconstruction from Staten Island, New York. The St. Marks record reveals millennial-scale changes in hurricane intensity that may be related to the past position of the Loop Current (an oceanic surface current). The Staten Island reconstruction contains deposits of every recorded storm which produced a >2 m surge in New York City, including an 1821 hurricane which was more powerful than Hurricane Sandy. Finally, the Staten Island record shows a sudden decrease in hurricane deposits before 1600 CE, coincident with European colonization of the area. This is due to the removal of the oyster beds from the harbor which protected the coast from storm induced erosion.

**TABLE OF CONTENTS**

Page

**LIST OF TABLES**

Table Page

**LIST OF FIGURES**

Figure Page

# CHAPTER 1

# INTRODUCTION

The overarching question of this dissertation is "what information can the geological record of overwash deposits reveal about the storm surge and tropical cyclone history of a particular site?" or, stated more colloquially, "what can sand tell us about hurricanes?" Answering this seemingly simple question involves understanding the complex interplay between sediment transport and deposition, coastal dynamics, sea-level rise, storm surge, waves, hurricane properties (including wind speed, forward velocity, track, landfall location, and impact angle), and a site's geologic history. The following chapters offer some advances in this area which is a hotbed of active research in the paleotempestology community.

It is also a societally relevant question as tide gauge records of hurricane storm surge on the United States' east coast only extend ~150 years into the past. This short time span is insufficient to estimate the return periods of rarer (and usually larger and more destructive) storms, yet current calculations of the return periods of storms like Hurricane Sandy, which made landfall in New Jersey in 2012 Common Era (CE), are based on extrapolation from this data. Therefore, developing centennial to millennial-scale records of hurricane activity will help increase the accuracy of these estimates. Additionally, studying the frequency of hurricane strikes in the past, under different climate regimes, can offer insight into how hurricane frequency might change in the future.

Chapter 2 of this dissertation consists of a paper that was published in Geochemistry, Geophysics, Geosystems in 2013. It presents a 2500 year long record of hurricane activity from St. Marks, located on Florida's Gulf Coast. A new numerical model was developed that produced estimates of hurricane wind speed based on the maximum grain size measured in each storm

surge deposit. This allowed a reconstruction of the Saffir-Simpson categories of hurricanes that affected the area through time and revealed a period of increased frequency of major (category 3 or larger) hurricane strikes from 1700 to 600 years before present (BP, where present is defined as 1950 CE). It is hypothesized that this is the result of the Loop Current, a warm surface ocean current, extending closer to our site than it does today. This would prevent the weakening of large hurricanes that occurs when they advect cold, subsurface water to the surface and instead allow them to remain at nearly full strength when they make landfall.

Chapter 3 focuses on the historical record (~400 years) of hurricane strikes in Staten Island, New York and was published in Scientific Reports in 2014. All overwash deposits found in Seguine Pond, a coastal, backbarrier pond, correspond to > 2 m high storm tides measured in the Battery tide gauge record or reported in historical documents. Hurricane Sandy's deposit provides a modern constraint on overwash deposition in the pond and is compared to older deposits, including one from an 1821 CE hurricane. The maximum grain size of the 1821 Hurricane's deposit was larger than that of Hurricane Sandy's deposit, suggesting that the 1821 storm produced a larger storm tide. The thickness of the deposits was also qualitatively related to the inundation period of the surges and suggests that Hurricane Sandy's much thicker deposit is due to its much longer inundation period. These findings are supported by Sea, Lake, and Overland Surges from Hurricanes (SLOSH) modelling results.

Chapter 4 is currently undergoing peer review and will be published in a special issue of Earth Surface Processes and Landforms. It presents a ~3000 yearlong record of environmental change from three sites on Staten Island (including the site visited in chapter 3) and hurricane strikes from Seguine Pond. Three distinct regimes are delineated by changes in percentage of sand, background magnetic susceptibility, spikes in magnetic susceptibility (a proxy of overwash deposition), and sediment color. The three regimes correspond to a time of barrier stabilization

(~3000 yrs. BP), a time of no overwash deposition (~3000 to 350 yrs. BP), and a time of overwash deposition and increased terrestrial sediment input to the ponds (~350 yrs. BP to present). We propose that oyster beds, which once covered Raritan Bay and New York Harbor, acted as coastal protection by preventing storm waves from eroding the coast until ~350 yrs. BP when overharvesting by European colonists removed them. Increases in terrestrial deposition at the same time are probably the result of land clearance by the colonists. Numerical modeling results suggest that oyster beds could reduce wave heights by ~30% and therefore attenuate their erosive ability; however, very little effect is seen on the storm surge itself.

Finally, this dissertation concludes with a summary of the three research papers.

# CHAPTER 2

## TROPICAL CYCLONE WIND SPEED CONSTRAINTS FROM RESULTANT STORM SURGE DEPOSITION: A 2500 YEAR RECONSTRUCTION OF HURRICANE ACTIVITY FROM ST. MARKS, FL

### 2.1 Abstract

Recent work suggests that the patterns of intense (≥ category 3 on the Saffir-Simpson scale) hurricane strikes over the last few millennia might differ from that of overall hurricane activity during this period. Prior studies typically rely on assigning a threshold storm intensity required to produce a sedimentological overwash signal at a particular coastal site based on historical analogs. Here we improve on this approach by presenting a new inverse-model technique that constrains the most likely wind speeds required to transport the maximum grain size within resultant storm deposits. As a case study the technique is applied to event layers observed in sediments collected from a coastal sinkhole in northwestern Florida. We find that 1) simulated wind speeds for modern deposits are consistent with the intensities for historical hurricanes affecting the site, 2) all deposits throughout the ~2500 year record are capable of being produced by hurricanes, and 3) a period of increased intense hurricane frequency is observed between ~1700 and ~600 yrs BP and decreased intense storm frequency is observed from ~2500 to ~1700 and ~600 yrs BP to the present. This is consistent with prior reconstructions from nearby sites. Changes in the frequency of intense hurricane strikes may be related to the degree of penetration of the Loop Current in the Gulf of Mexico.

## 2.2 Introduction

The number of studies pertaining to tropical cyclone (called "hurricane" in the North Atlantic Ocean) proxies preserved within the geologic record have increased rapidly over the last two decades. This relatively new field of paleotempestology is fueled by a growing appreciation for the application of these records in hurricane risk assessments (e.g. Murnane et al., 2000; Nott, 2004; Elsner et al., 2008), and in identifying past long-term shifts in hurricane climatology (e.g. Mann et al., 2009). Many studies have been conducted to extend the hurricane strike record at various locations in the western North Atlantic by identifying deposits in the sediment record left by hurricane storm surges and wave run-up (Liu and Fearn, 1993, 2000; Donnelly et al., 2001a, 2001b; Donnelly and Woodruff, 2007; Scileppi and Donnelly, 2007; Woodruff et al., 2008b; Boldt et al., 2010; Wallace and Anderson, 2010; Lane et al., 2011). Other proxies of paleo-hurricane activity include extreme-precipitation events associated with hurricanes using $\delta^{18}O$ records from speleothems (Malmquist, 1997; Frappier et al., 2007) and tree rings (Miller et al., 2006); increased river run-off and its effect on the growth and luminescence of coral (Lough, 2007; Nyberg et al., 2007); and coarse deposits interpreted as intense terrestrial flooding events (Noren et al., 2002; Besonen et al., 2008). Together, these proxy records provide an increasing body of knowledge of paleo-hurricane history in the Gulf of Mexico and the Northwestern Atlantic Ocean.

In prior work, past geologic reconstructions of tropical cyclone activity have mainly documented changes in the reoccurrence rates of hurricanes above some assumed threshold based on modern calibration. In addition to documenting event occurrences, grain size distributions within hurricane deposits also provide information on the intensity of flooding by past hurricane strikes (Woodruff et al., 2008b). However, the overall flooding magnitude at a location is influenced by factors in addition to the storm intensity. For example, a category 1

storm that directly hits a site could produce a similar storm surge as a category 5 storm making landfall much farther away. Accurate methods for back-calculating hurricane wind speed from resultant deposits must therefore account for these uncertainties.

In this study we present a new ~2500 year reconstruction of hurricane occurrences based on event-deposits preserved within a coastal sinkhole in western Florida. We use a series of nested modeling techniques to develop relationships between storm intensity and the maximum grain size that the resulting flows can carry to the site (i.e. transport competence). The obtained wind speed/transport competence relationship is then used to constrain the likely wind speed required to transport the maximum grain size observed within each individual deposit and to provide a reconstruction of hurricane intensity at the site.

**2.3 Regional setting and site description**

Spring Creek Pond (SCP), the coastal sinkhole considered in this study, is located ~2.8 km inland from Apalachee Bay and is part of the Big Bend region of Florida's northwest coast (Figure 2.1a). The pond is nearly circular and has a diameter of ~120 m. While much of the pond has an average depth of ~1 m, the sinkhole itself is ~15 m deep and has a diameter of ~60 m (darker portion of water in Figure 2.1b). The elevation of this freshwater pond is approximately 2.75 m above mean sea level. Between the pond and the coast the relatively undeveloped terrain is lightly forested and gradually slopes seaward.

Hurricanes commonly affect Apalachee Bay, with the eye of a hurricane currently passing within 93 km (50 nautical miles) of the site on average once every 13 years (NOAA/National Weather Service, available from http://www.nhc.noaa.gov/climo/#returns). The bay is 400 $km^2$ in area, with an average submerged depth of 3 m (USEPA, 1999; Lane et al., 2011), a topographic and bathymetric across-shore gradient of 1:5000 (Hine et al., 1988), and an

astronomical tidal range of 0.7 m (Lane et al., 2011; NOAA, 2012). Hurricane-induced flooding within the Bay is particularly destructive because its concave coastline focuses storm surge, the shallow bathymetric depth allows a larger surge to form, and the shallow topographic slope allows these surges to inundate great distances inland (Jelesnianski et al., 1992; Lane et al., 2011).

The underlying bedrock of the coast and coastal shelf of Apalachee Bay (and a large portion of Florida) is Eocene/Oligocene age limestone, emplaced when the area was submerged beneath a shallow sea (Hine et al., 1988; Wright et al., 2005). Today's karst landscape is the result of dissolution of the limestone bedrock over millions of years. Sinkhole formation is an ongoing process and readily occurs in the saltwater/freshwater coastal mixing zone (Randazzo and Jones, 1997). During the Miocene, another time when this area was submerged, quartz sands from the erosion of the Appalachian Mountains were overlain on the limestone bedrock (Hine et al., 1988). Today, this sand is available for mobilization by hurricane storm surge and deposition in sinkhole ponds. Many of these ponds are deep and steep-sided thereby preventing remobilization of sediment after deposition.

Mullet Pond, a sinkhole which was previously used in a paleotempest study (Lane et al., 2011), lies ~20 km to the south of SCP (Fig. 2.1). The authors reconstructed a ~4500 year, decadally-resolved, storm history of the area. This record was further analyzed for differences between "low-threshold" storm layers (i.e. the threshold above which most %coarse anomalies were identified as storm-related) and "high-threshold" storm layers (storms which left deposits exceeding the highest %coarse anomaly left by a historic storm, in this case, Hurricane Elena in 1985 CE). Little variability was observed in low-threshold deposits at 95% confidence, but high-threshold deposits show periods of increased storm activity ~3800 cal. yrs. before present (BP) (~300 year period), ~3550 yrs. BP (~100 year period), ~3300 yrs. BP (~100 year period), 2800-

2300 yrs BP, 1200 yrs. BP (50-100 year period), 900 years BP (~50 year period), 700 years BP (~100 year period) and decreased activity around 1800, 1650, 350, and 150 years BP. This finding is somewhat different from earlier findings by Liu and Fearn (2000) for Western Lake located ~150 km to the west. Results from Western Lake show a drop in hurricane activity beginning ~1000 years ago (Liu and Fearn, 2000), but this could be related to coastal barrier dynamics changing the sensitivity of the site to overwash (Otvos, 2001). Additional records from the Apalachee region are nonetheless required to evaluate whether the patterns in overwash described by Lane et al. (2011) can be reproduced at nearby sites.

Changes in relative sea-level can greatly impact the occurrence of hurricane overwash at a site and therefore warrant consideration. Several studies have reconstructed sea-level curves for the Gulf of Mexico (Stapor et al., 1991; Tanner, 1992; Morton et al., 2000; Törnqvist et al., 2004; Wright et al., 2005; Donnelly and Giosan, 2008; Milliken et al., 2008); however, there is some disagreement among these results. Some authors propose that sea-level has continuously risen throughout the Holocene, with the rate of sea-level rise decreasing over time (Otvos, 2001; Törnqvist et al., 2004; Wright et al., 2005; Donnelly and Giosan 2008; Milliken et al., 2008). Others have proposed more complicated sea-level curves which include sea-level "highstands" or periods of time when sea-level was higher than it is today (Stapor et al., 1991; Tanner, 1992; Morton et al., 2000; Blum et al., 2002). Proponents of mid-Holocene highstands use geomorphic observations and radiocarbon data from beach ridges to support the idea that these features were formed by wave deposition, and due to their heights, must have been formed at a time of higher-than-present sea-level. Donnelly and Giosan (2008) offer an alternative explanation; that these ridges were formed during times of increased storm activity in the Gulf of Mexico, which increased the overall wave climate, leading to construction and preservation of these ridges. Further, Lane et al. (2011) found no indication of open marine sequences within the sediments

and foraminifera assemblages at Mullet Pond, which refutes a mid-Holocene high-stand in sea-level. We rely on the sea-level rise data of Wright et al. (2005) and Törnqvist et al. (2006) which indicates a continuously, nearly linear rising sea-level rate of ~0.4 mm/yr for the region over the last ~3,000 years.

### 2.4 Methods

#### 2.4.1 Field work

Spring Creek Pond was visited during a field campaign in November 2011. The site was initially surveyed with a hand-held depth sounder and sub-bottom sonar profiles operating at 10 kHz (although the presence of gas resulted in limited sub-bottom sonar penetration within sediments). To preserve the sediment-water interface an initial 306 cm surface drive was obtained using a modified Vohnout/Colinvaux piston corer (i.e. SCP D1), following methods similar to Donnelly and Woodruff (2007). Core SCP D1 was followed with a deeper piston vibracore (i.e. SCP D2) extending from 138 cm to 443 cm below the sediment-water interface. Both cores were obtained from approximately the center of the sinkhole (30° 5.892'N, 84° 19.681'W ± 3 m for SCP D1 and 30° 5.891', 84° 19.681'W ± 3 m for SCP D2, fig. 2.1b). These cores were then shipped to the University of Massachusetts Amherst where they were split, described, and stored at 4 °C refrigeration.

#### 2.4.2 Analysis of sediment cores

X-radiograph images of SCP D1 and SCP D2 split-cores were taken with an Itrax Core Scanner (Cox Analytical) at UMass Amherst (Croudace et al., 2006). The images have a resolution of 200 µm per pixel. The black and white inverted x-radiographs reveal density variations in the

core with siliciclastic sand layers appearing much lighter than the surrounding silty, highly-organic sediments (Figure 2.2a).

Sediment cores were analyzed at 1 cm intervals for percent coarse (%coarse) material, corresponding to the silt-sand transition (e.g. > 63 µm). These sub-samples were sieved wet in order to prevent the aggregation of finer particles by drying, with the percent water (%water) obtained from a separate sub-sample. The %water was calculated by measuring the mass of the initial sample, drying it in an oven at 100°C for 24 hours, and then weighing it again to obtain the dry mass. To determine the %coarse, another sub-sample was weighed wet with the separate %water measurements used to calculate the corresponding dry mass for the sample. Samples were then wet sieved at 63 µm with organics removed with 6% $H_2O_2$ at ~60 °C prior to analysis. Sediments retained in the 63 µm sieve were then dried in an oven at 100°C for 24 hours, and weighed to obtain the mass of coarse material and the corresponding %coarse relative to its calculated dry mass.

The grain size distribution of the > 63 µm portion of samples was obtained using a digital image processing, particle size and shape analyzer (Retsch Technology Camsizer), with distributions adjusted to account for %fines in each sample (i.e. < 63 µm ) lost through initial sieving. Grain size results are presented for $D_{90,}$ which is defined as the size for which 90% of all other grain sizes in a distribution are smaller than.

### 2.4.3 Radiometric dating

Cesium-137 ($^{137}Cs$) and lead-210 ($^{210}Pb$) were used to constrain modern deposition rates and the ages of historic storm deposits. The onset of $^{137}Cs$ in the sediment record is concurrent with the start of atmospheric nuclear weapons testing in 1954 CE, with the peak in $^{137}Cs$ activity dating to 1963 CE (Pennington et al., 1973) just before the signing of the Nuclear Test Ban

Treaty. $^{210}$Pb ages were obtained using techniques similar to those described in Woodruff et al. (2013a). First, excess (unsupported) $^{210}$Pb activity ($^{210}Pb_{ex}$) was obtained by subtracting the supported $^{210}$Pb, as measured by the activity of $^{214}$Pb (Chen et al., 2004) from the total $^{210}$Pb activity. Next, a best-fit linear regression of the logarithm of $^{210}$Pb excess versus the depth in the sediment was calculated (Faure, 1986; Koide et al., 1973; Robbins and Edgington, 1975), with the slope equal to the radioactive decay constant of $^{210}$Pb (0.03114 $yr^{-1}$) divided by the average sedimentation rate. Discrete ages for individual $^{210}$Pb measurements were obtained with the age-to-activity relationship described by Appleby and Oldfield (1978) when assuming a constant initial concentration of $^{210}Pb_{ex}$. Sediment samples were analyzed for $^{137}$Cs and $^{210}$Pb using a Canberra GL2020R Low Energy Germanium Detector at the University of Massachusetts Amherst. Each ~1.5-2.0 gram dried sample was placed in a 6 cm diameter plastic jar and counted for 48-96 hours. $^{137}$Cs activities were computed spectroscopically using the 661.7 keV photopeak, $^{210}$Pb activities were calculated using the 46.5 keV photopeak, and $^{214}$Pb activities were obtained with the combined 74.8 keV, 77.11 keV, 87.3 keV, 295.2 keV, and 351.9 keV photopeaks.

Carbon-14 ($^{14}$C) was used to date sediments older than the $^{210}$Pb and $^{137}$Cs derived age. Plant material at selected depths in the core was dated using Accelerator Mass Spectrometry (AMS) at the National Ocean Sciences Accelerator Mass Spectrometry Facility (NOSAMS) in Woods Hole, MA (Table 2.1). All radiocarbon ages were converted to years Before Present (BP) using IntCal09 (Reimer et al., 2004), where “present” is defined as 1950 CE by convention. Anomalously old radiocarbon samples resulting in age reversals were excluded from the age chronology (see Table 2.1).

### 2.4.4 Numerical modeling of storm inundation

Numerical simulations were performed to constrain the range of hurricanes with the competence to transport the observed grain sizes into Spring Creek Pond under modern hurricane climatology. We then assume that this relationship provides a reasonable representation for the combination of storm characteristics (including wind speed, storm size, landfall location, intensity, forward translation speed, angle of approach, etc.), for hurricanes impacting the site prior to the instrumental record. To overcome restrictions associated with the limited number of historical overwash events affecting the site, we employed the model described by Emanuel et al. (2006), and hereafter referred to as the MIT model. The MIT model is a coupled ocean-atmosphere, beta and advection hurricane model that generates a database of tropical cyclones that pass a set distance from a site under modern climatic conditions. In the MIT model, a synthetic storm is created by first generating a storm track (the location of the storm's eye with a temporal resolution of six hours) using a combination of historical storm track data and a synthetic wind field that conforms to monthly climatological means. Then, the storm's intensity is allowed to change based on a deterministic, coupled atmosphere-ocean model driven by shear derived from the synthetic wind field, monthly means of upper-ocean thermal structure, and potential intensity (the theoretical maximum intensity that a storm can achieve given certain environmental factors; see Emanuel et al. (2004)).

The Sea, Lake and Overland Surges from Hurricanes (SLOSH) model (Jelesnianski et al., 1992) was used with the Apalachicola (APC) grid to evaluate storm surge at the coast near Spring Creak Pond for each storm simulation from the MIT model. The National Weather Service SLOSH model simulates coastal inundation by solving differential equations (using finite-difference methods) which govern fluid motion. The hurricane, which is the driving force of the fluid motion, is modeled as a time-varying surface wind field and pressure gradient body force

(Jelesnianski et al., 1992). Of the 10,000 storms generated by the MIT model, 152 produced storm surges at the coastal grid cell closest to Spring Creek Pond that met or exceeded the 2.75 m elevation required to inundate the Spring Creek site. SLOSH simulations of time-varying water-level at this cell were extracted for each of these 152 storms.

Simulations of onshore inundation were performed using the Regional Ocean Modeling System (ROMS) (Warner et al., 2008) with a 2-D uniformly sloping grid and driven at its open boundary with water-level time-series obtained from the 152 SLOSH simulations. ROMS is a numerical model that calculates the movement of water and sediment in various ocean and riverine environments (Warner et al., 2008). It was used to model inundation at the Spring Creek site because it has a much finer horizontal resolution than the SLOSH model (10's of meters as opposed to 10's of kilometers for the SLOSH model) and is capable of resolving vertically varying flow fields, as well as resultant bottom shear stresses. While ROMS has the capability of creating a three- dimensional topography and bathymetry only a two-dimensional model was used here because of uncertainties associated with changing shoreline shape due to sea level rise over the course of the Holocene (Stapor et al., 1991; Morton et al., 2000; Törnqvist et al., 2004; Wright et al., 2005). The coastline at the site is therefore not known over the later Holocene in the detail needed to warrant the use of a three-dimensional model.

The landscape between the field site and the coast was modeled with a constant slope of $9.24 \times 10^{-4}$ (as measured using USGS digital elevation models), and a constant quadratic drag coefficient of 0.0025. This drag coefficient was chosen from the results of a ROMS model calibration using surge simulations produced by Hurricane Dennis in 2005 (see Dukhovskoy and Morey (2011)), and adjusted such that water levels reached, but did not exceed, Spring Creek Pond during the event (an observation consistent with first-hand accounts by local residents during the event). The ROMS model was given a horizontal resolution of 88 m and a vertical

topographic resolution of 7.7 cm which were chosen as a balance between modeling speed and accuracy of results. The vertical resolution of the surge is variable such that there is higher resolution close to the bed and lower resolution closer to the water's surface (Warner et al., 2008). Calculations were performed with a time-step of 30 seconds with results saved at 20 minute increments.

Among its many outputs, ROMS calculates the bottom shear stress along the path of inundation at every time step. The maximum bottom shear stress at the grid cell corresponding to the field site was extracted and used in the Shields equation to calculate the competence for transport at the site:

$$\tau = \theta_c(\rho_s - \rho_w)gD_{90} \quad (2.1)$$

where $\tau$ is the bottom shear stress, $\theta_c$ is the non-dimensional critical shields parameter, $\rho_s$ is the density of the sediment (2650 kg/m$^3$ for quartz sand), $\rho_w$ is the density of water (1000 kg/m$^3$), g is the acceleration due to gravity, and $D_{90}$ is taken as the maximum grain size that can be mobilized by the flow (Soulsby, 1997). Here we use a value of 0.047 for $\theta_c$ (Meyer-Peter and Müller, 1948; Julien and Wargadalam, 1995; Tjerry and Fredsøe, 2005). When combined, derived competence for transport for each of the 152 synthetic storms provides a relationship between the $D_{90}$ grain size measured in deposits at SCP and the most likely hurricane intensity responsible for each deposit, with data dispersion constraining the uncertainty in this relationship.

The distance between the coast and the site has likely decreased over the last few millennia as a result of sea-level rise. This leads to an increase in the sensitivity of the site to storm overwash and the maximum grain size advected to the site towards present. To account

for these changes the relationship between $D_{90}$ grain size and wind speed is derived at the grid cell correlating to the elevation of the site above sea-level at the time of deposition for each deposit within the Spring Creek Pond reconstruction. The data from Wright et al. (2005) and Törnqvist et al. (2006) were used to calculate a sea-level rise curve for this area, yielding an approximately linear rise of 0.4 mm/year (Figure 2.3). Since the vertical topographic resolution is 7.7 cm, the virtual site was moved to the next up-slope grid cell every 7.7 cm/0.04 cm/yr = 192.5 years, which is equivalent to a sea-level fall from the present to the past.

## 2.5. Results

### 2.5.1 Sediment Chronology

The age model for SCP D1 and SCP D2 is presented in Figure 2.4. The combined SCP record extends to a depth of 443 cm which corresponds to a maximum age of ~2580 years BP. The $^{14}C$ data indicate that prior to ~600 yrs BP, the sedimentation rate varied between 0.08 and 0.13 cm/yr. This rate increased to 0.31 cm/yr between ~600 and ~400 yrs BP and again to a rate of 0.38 cm/yr between ~400 to -4 yr BP (1954 CE). The latter rate was calculated using the average age of the oldest 2-σ range (leftmost gray box in Figure 2.4) for the topmost $^{14}C$ date. If the average age had been used like in the previous calculations, then the deposition rates would be 0.18 cm/yr between ~600 to ~400 yrs BP and 0.63 cm/yr between ~400 and -4 yrs BP, which are inconsistent with the deposition rates derived from the deeper radiocarbon dates as well as the historical deposition rates of 0.21-0.25 cm/yr based on $^{210}Pb$ derived chronologies and the 1954 CE onset of $^{137}Cs$ (Figure 2.4b). A 1963 CE peak in $^{137}Cs$ was not observed within SCP, potentially due to the disruption of surficial sediments during extraction and transport.

### 2.5.2 Sedimentology

Combined x-radiograph images and grain size data from SCP D1 and SCP D2 are presented in Figure 2.2, with Figure 2.5 showing data for the historic part of the sediment record. With few exceptions, significant peaks in %coarse correspond to peaks in $D_{90}$ (Figure 2.2b and 2.2c) and light-colored (dense) deposits in the x-radiograph (Figure 2.2a), a finding consistent with past observations of hurricane-induced deposition within coastal marshes (e.g. Boldt et al., 2010). In total, thirty-four dense layers in the x-radiograph are delineated as event deposits based on corresponding peaks in %coarse and $D_{90}$ grain size. Five of these deposits follow the 1851 CE onset of the best-track instrumental data-set based on the core's derived $^{137}Cs$, $^{14}C$, and $^{210}Pb$ age model (Figure 2.4). Lane et al. (2011) also observed five deposits between 1845 and 1950 CE at Mullet Pond and correlated these to known hurricane landfalls in 1852, 1894, 1926, 1929, and 1941 CE. Unfortunately, it is not known if these five deposits correspond to the five historical deposits seen in the Spring Creek record due to the temporal uncertainty of the emplacement of our deposits. An additional deposit was observed in the Lane et al. (2011) reconstruction following 1954 CE which potentially correlates to Hurricane Elena in 1985. This deposit is absent from the surficial sediments of the SCP core most likely due to disruption during transport of the core to UMass Amherst, as evidenced by a lack of the 1963 peak in $^{137}Cs$ in surficial SCP sediments.

$D_{90}$ grain sizes and %coarse for storm layers delineated at SCP range from 0.13 to 1.62 mm and 22% to 99%, respectively. Background (non-storm layer) material has $D_{90}$ grain sizes ranging from < 0.063 mm (the grain size at which the samples were sieved for %coarse) to 0.207 mm and %coarse ranging from 0 to 37.0%. While most of the inundation layers have grain sizes ranging from very fine- to medium-grained sand, a particularly prominent layer, centered at

223.5 cm depth, has very coarse grains ($D_{90}$=1.62 mm). A piece of a shell and some coral pieces were seen within this layer at 222.5 and 223.5 cm depth, supporting a marine origin.

### 2.5.3 Constraining storm wind speed

On the basis of bottom shear stresses derived from ROMS simulations for the 152 simulated storms with surge elevations > 2.5 m at the coast, 80 are capable of transporting sand-sized (≥ 0.063 mm) particles to Spring Creek Pond. Figure 2.6 plots the maximum wind speed at landfall for these 80 storms against the maximum grain size mobilized by each simulated event. When plotted together, the maximum wind speed ($V_{max}$) and surge grain size competence of transport (D) show an exponential relationship:

$$D = 10^{mV_{max}+b} \quad (2.2)$$

where m and b are the slope (0.01) and y-intercept (-1.8) of the linear regression of a log-log plot of the data, respectively.

Error bars presented in Figure 2.6 point to the range of storm intensities capable of transporting sediments of a given grain size, with scatter in the data pointing to the other storm characteristics in addition to peak wind speed at landfall also influencing the magnitude of local flooding (e.g. landfall location in relation to the site, storm size, forward translation speed, and angle of approach). Despite these other factors, a majority of the variance in grain size for deposits at the site (72%) can be explained by the landfall wind speed alone.

To assess the accuracy of the inverse-model we compare derived wind speeds for the five inundation deposits that occur during historic time to the measured landfall wind speeds of historic storms from the best-track dataset. Modern storms considered to potentially affect the

site are defined as those in the NOAA best-track dataset (Landsea et al., 2004), that passed within 150 km of the site at hurricane strength (wind speeds ≥ 119 km/h or 74 mph). The timing and derived wind speeds for the inundation deposits falls within the range of measured landfall wind speeds for these historic hurricanes. Therefore, the model generally reproduces the intensities of historical hurricanes affecting the site, providing support for applying the technique to pre-historic deposits at Spring Creek Pond.

In the Northern Hemisphere the front right quadrant of a hurricane is often the most damaging because counter-clockwise rotational winds and storm motion are in the same direction and combine to generate the greatest wind speeds. According to the NOAA best track dataset (Landsea et al., 2004), 14 hurricanes passed within 150 km of the field site since 1851 CE, five of which passed to the west (left) of SCP such that the most damaging front right quadrant of the storm impacted the site. Our sedimentary analysis also delineates five separate coarse deposits during this interval, a result similar to that from Mullet Pond by Lane et al. (2011). However, as discussed previously, none of the deposits at SCP date to younger than 1954 CE, which excludes 1 of the 5 hurricanes passing to the west of the site during the historical record. At least one of these event layers in SCP therefore reflects a hurricane passing to the east of SCP, such that the less severe front left quadrant impacted the site. Nonetheless, many of the more distal hurricanes that passed to the east of the site probably did not produce preserved deposits at SCP. This is likely one of the reasons our record does not capture all of the 14 historical hurricanes considered in Figure 2.7.

Further, the time period between many of these 14 hurricanes is often shorter than the temporal resolution of our sampling. A modern sedimentation rate of 0.25 cm/yr for SCP results in a temporal resolution of 4 years/cm. Of the 14 hurricanes to pass within 150 km of the SCP site 11 form four groups of storms too close together to be resolved individually within the SCP

core (1873, 1877 and 1880; two storms in 1886; 1894, 1898, and 1899; 1939 and 1941), with storms in 1852 and 1966 passing to the east of SCP. Therefore, the five historical deposits observed at SCP generally correspond to the number of deposits we expected after accounting for limits associated with temporal resolution and the intensity and landfall location of hurricanes impacting the site over the historical record.

### 2.5.4 Storm frequency and intensity

The complete time-series of inversely modeled wind speed for each coarse grained deposit within the SCP reconstruction are presented in Figure 2.7. Model results indicate that all deposits observed at the Spring Creek Pond site are capable of being produced by storms with hurricane strength winds. One storm was detected between ~2500 and ~1700 yrs BP (0.1 storms/century), fourteen storms between ~1700 to ~600 yrs BP (1.3 storms/century), and 19 storms between ~600 yrs BP to the present (3.2 storms/century). Nearly all of the major hurricanes (category 3 or greater) seen in this record occur during the period of activity from ~1700 to ~600 yrs BP (10 major hurricanes or 0.91 major hurricanes/century) and only one occurs post-600 yrs BP (0.17 major hurricanes/century).

The uniqueness of an anomalously coarse layer at 220 cm or ~600 yrs BP (Fig. 2.2) may indicate that it was formed by a process other than storm overwash. One possible origin of this unusually coarse deposit could be from a tsunami; however, this is unlikely due to the seismic stability of this area and its protection by Cuba and the Bahamas Platform from remotely generated tsunamis (Randazzo and Jones, 1997). Another possible origin could be from heavy rainstorms transporting the surrounding sand into the pond. This scenario also seems unlikely since there is no evidence of surface flow to the pond and the surrounding low-relief landscape is well-drained through the surficial Miocene sands underlain by fairly permeable limestone

topography (Puri and Vernon, 1964; Lane et al., 2011). Further, shells within the ~600 yr BP layer point to a marine origin, while well rounded sand grains in the deposit are indicative of beach material that has undergone some level of initial weathering by coastal processes. Additionally, inverse modeling results indicate that a hurricane of category 4 or 5 intensity is capable of producing the deposit. This result serves to highlight the significance of the exponential relationship between hurricane wind speed and competence of transport (i.e. Fig. 2.6), with major hurricanes transporting grains of significantly greater sizes than less intense events. Wind speed estimates for the ~600 yr BP event are 272 ± 40 km/h (169 ± 25 mph). This is far greater than the intensity for historical hurricanes affecting the site, however, Hurricane Camille (1969 CE) made landfall further to the east along the Gulf Coast of Mississippi with 306 km/h (190 mph) winds (NOAA, 2012), indicating that wind speed estimate for the 600 yr BP event does fall within the range of known landfall wind speeds in the region.

## 2.6 Discussion

### 2.6.1 Clustering of storms toward the present

A notable increase in the frequency of lower intensity hurricane events is observed following ~600 yrs BP, but the frequency of major hurricanes decreases during this same period. However, this increase in frequency is potentially an artifact due to i) a change in sensitivity of the site to overwash due to rising sea-level and ii) greater undercounting of actual events prior to 600 yrs BP due to lower sedimentation rates. First, with rising sea level, the number of storms affecting the site should increase in recent centuries because the shoreline is moving closer to the site, decreasing the distance storm-induced floods must travel over land, as well as lowering the site's altitude above sea level. The sea level has risen ~1 m over the time span covered by this record (calculated using the sea level curve from Donnelly and Giosan (2008)), resulting in a

lowering of the site from ~3.75 m to 2.75 m above sea level. This has consequently caused the shoreline to move ~1 km closer to the site (calculated from USGS digital bathymetry maps) allowing storm surges to advect larger sediment grains to the site. Secondly, in addition to rising sea level leading to an actual increase in the number of storms affecting Spring Creek Pond, an increasing deposition rate can also lead to an apparent increase in their frequency due to biasing associated with under-counting events in sediments with significantly slower deposition rates (Woodruff et al., 2008a). Figure 2.4 shows the $^{14}C$, $^{210}Pb$, and $^{137}Cs$ chronologies which reveal an increase in the deposition rate towards the modern age from an average of 1.0 mm/yr between ~2500 yrs BP and 600 yrs BP (calculated with the $^{14}C$ ages) to an average of 2.9 mm/yr between 600 yrs BP and the present (averaging the deposition rates from the ages of the youngest two $^{14}C$ samples, the 1954 CE onset of $^{137}Cs$, and the $^{210}Pb$ chronology). This allows more storms to appear individually because there is less time represented in each centimeter of sediment with many deposits older than 600 yrs BP possibly being amalgamations of two or more storms.

An increase in sedimentation rate towards the present is common to lacustrine and lagoonal sediments along the Gulf of Mexico and the North Atlantic coasts due to increased connectivity of these systems to the sea as sea-level rises, resulting in an increase in the amount of marine sourced material introduced to these back-barrier environments (Donnelly and Bertness, 2001; Donnelly et al., 2004; Gehrels et al., 2005; Woodruff et al., 2008a). Spring Creek Pond, however, is ~3 km inland and is not part of a coastal marsh system. Therefore, we do not believe that sea-level rise has contributed to the increased sedimentation rate at this site. Additional explanations include increased production from eutrophication and the compaction of older sediments. The underlying cause of the increased rate of sedimentation remains unclear. However, due to their concurrent timing, the increase in frequency of low intensity

hurricane events following 600 yrs BP is at least in part governed by the three-fold increase in sedimentation rate in the most recent centuries. It is possible that the frequency of low intensity hurricane landfalls at the site has also increased over this time period; however, biasing associated with changes in sedimentation make it difficult to assess the significance of any potential changes in the frequency of lower intensity events during this most recent interval.

### 2.6.2 Changes in Major Hurricane Frequency

Changes in the landfall frequency of all hurricane categories are difficult to assess at SCP due to significant changes in rates of sedimentation. Trends in intensity for higher magnitude events, however, show additional patterns less affected by undercounting biases associated with changes in sedimentation rate. This is because, i) these events occur less frequently and can be better resolved in a record of lower temporal resolution, and ii) more intense storms transport larger sediment grain sizes such that the maximum grain size within any deposit that is an amalgamation of several storms of different intensities will register as the most intense of these flood events.

In the SCP reconstruction the frequency of major hurricane strikes decreases from 0.91 storms/century between ~1700 to ~600 yrs BP to 0.17 storms/century between ~600 yrs BP and the present. This transition does not appear to be an artifact associated with an increase in sedimentation rate towards modern since the associated increase in temporal resolution should increase the number of deposits delineated in the record rather than decrease it. The drop in intense hurricane occurrences at 600 yrs BP is also inconsistent with increased sensitivity of the site to hurricane flooding from rising sea-level. We therefore conclude that the decrease in the number of major hurricanes at ~600 yrs BP represents a real drop in the frequency of these more intense events at SCP.

### 2.6.3 Paleoclimate Comparisons

The size of the SCP sinkhole is relatively small which limits the applicability for a transect of cores when compared to the larger back-barrier lagoons and marsh environments commonly used in other paleotempestological reconstructions. Alternatively, single core reconstructions from a series of nearby sinkholes provide a viable substitute to multi-core analyses from a larger individual back-barrier marsh or lagoonal site. This study benefits from the nearby sinkhole reconstruction of hurricane overwash by Lane et al. (2011) at Mullet Pond, with comparisons to the SCP record helping to circumvent limitations associated with a reconstruction derived from a single core location at a single site. No significant trends were observed within the Mullet Pond reconstruction with respect to the frequency of all hurricanes; however, similar to the SCP reconstruction the Mullet Pond record exhibits a notable increase in the number of major hurricanes between 1500 and 600 yrs BP (with peak activity ~700 yrs BP), followed by a decrease in major hurricane activity between 600 and yrs. BP and present (Figure 2.8a and b). Trends in the SCP reconstruction therefore help to verify the initial findings of Lane et al. (2011) and provide further support for significant variability in the frequency of major hurricanes impacting Apalachee Bay over the last few millennia.

Previous sedimentary reconstructions have related changes in hurricane activity to variations in North Atlantic sea surface temperatures (SSTs), the El Niño/Southern Oscillation (ENSO), and the North Atlantic Oscillation (NAO), (e.g. Mann et al., 2009; Donnelly and Woodruff, 2007; Liu and Fearn, 2000). For instance, Mann et al. (2009) suggest that periods of more frequent hurricane landfalls in the last 1500 years correlate to times of warmer Atlantic SSTs and more La Niña-like conditions. However, the active interval for intense hurricanes at Mullet and SCP ending at around 600 yrs BP is not predicted with the basin-wide statistical

model of Mann et al. (2009). This may indicate that variability in the Mullet Pond and SCP reconstructions represent changes more specific to the northeastern Gulf of Mexico, and in turn potentially forced by more regional forms of environmental change.

Alternatively, discrepancies between the combined SCP/Mullet Pond reconstructions and the Mann et al. (2009) proxy record may indicate that other factors in addition to SST, ENSO and the NAO are more dominant drivers of past changes in hurricane activity in the Gulf of Mexico. For instance, a better metric for the stability of the free troposphere, which in part governs the theoretical maximum wind speed that hurricanes can attain, is described by the difference between SST and temperature of the upper troposphere relative to SST rather than absolute SST alone (Emanuel, 1986, 1988). Further, SST is often assumed to represent the temperature of the upper ocean mixed layer; however, this SST proxy provides very little information regarding the depth of the mixed layer, which in part determines how quickly cooler water from below can be mixed to the surface during the passage of a hurricane (Emanuel et al., 2004).

It is possible that past variability in the position of the Loop Current in the Gulf of Mexico might explain regional changes in the frequency of intense hurricane landfalls represented by the SCP and Mullet Pond reconstructions (Lane and Donnelly, 2012). The Loop Current is a surface-ocean current (part of the North Atlantic Western Boundary Current) that flows from the Caribbean Sea, northward through the Yucatan Channel into the Gulf of Mexico, loops to the east, and exits through the Florida Straits to join the Gulf Stream (Poore et al., 2003; Lund and Curry, 2004). It is difficult to identify the Loop Current in the Gulf with SST alone; however, the importance of the Loop Current in controlling intense hurricane landfall frequency resides in how the current changes the Gulf's oceanic thermal structure rather than SST. In general the mixed layer of ambient warm surface waters in the Gulf of Mexico has a relatively

shallow average depth of 30-40 m (Chouinard et al., 1997). As storms intensify, they quickly mix up cooler waters from below (Price, 1981; Sriver and Huber, 2007), and this process limits further storm development (Emanuel et al,. 2004). In the Loop Current, however, the mixed layer can be as deep as 200 m below the surface providing several times more available energy to developing cyclones by limiting the role of storm-induced upwelling (Goni and Trinanes, 2003).

The deep, warm waters of the Loop Current occasionally meander northward into the eastern Gulf of Mexico and make a clockwise loop before exiting. These meanders periodically break off from the flow to form anti-cyclonic warm core eddies that propagate westward as they dissipate. The frequency of eddy formation and the extent to which the Loop Current penetrates into the Gulf is thought to be aperiodic on sub-decadal timescales; however, lower-frequency variations in wind stress may drive periodicities on longer timescales (Sturges and Leben, 2000). The relative abundance of the foraminifer *Globigerinoides sacculifer* in marine cores taken from the Pigmy Basin in the northern Gulf has been offered as a proxy for the extent and/or frequency of Loop Current incursions into the Gulf (Poore et al., 2003, 2004, 2011; Richey et al., 2007). Though not contemporaneous with regional SST cooling in Pigmy Basin at 1000 yrs BP as derived by Mg/Ca reconstructions, the significant decline in intense hurricane frequency occurring around 600 cal. yrs. B.P. at both SCP and Mullet Pond is concurrent with an abrupt decrease in *G. sacculifer* abundance at the Pigmy site (Richey et al., 2007). The decline in *G. sacculifer* has been interpreted to reflect reduced advection of Caribbean surface waters into the Gulf of Mexico and a shoaling of the thermocline caused by a more southerly residence of the Loop Current (Poore et al., 2004). A transition to less penetration of the Loop Current into the Gulf following 600 yrs BP would lower the ocean heat content available to tropical cyclones in the northeastern Gulf and might help to explain the 600 yrs BP drop in intense hurricane

frequency observed both at SCP and Mullet Pond. Additional reconstructions are required, however, to confirm the hypothesized Loop Current proxy derived from Pigmy Basin.

## 2.7. Conclusions

Sediments recovered from Spring Creek Pond, a coastal sinkhole located in northwest Florida, contain a ~2500 year record of hurricane activity in this area. We identify and date 34 storms layers and analyze each for %coarse material and $D_{90}$ grain size. An inverse modeling technique is developed to constrain the landfall wind speed of the storms from the $D_{90}$ grain size of their resultant deposits. We find that 1) applying the inverse model to the sediment deposits from the historic (post-1851 CE) record results in landfall wind speeds that are consistent with storms reported in the best-track data-set, 2) all deposits throughout the ~2500 year record are capable of being produced by hurricanes, including a seemingly anomalous layer dated to 600 yrs BP, and 3) the SCP time-series of intense hurricane occurrence is consistent with a nearby reconstruction previously obtained from Mullet Pond, with both records indicating a period of increased intense hurricane frequency between ~1700 and ~600 yrs BP and decreased intense storm frequency from ~2500 to ~1700 and ~600 yrs BP to the present. The variation in intense hurricane strike frequency, particularly the drop in activity at 600 years BP, is potentially the result of inferred shifts in Loop Current penetration into the Gulf of Mexico.

## 2.8. Acknowledgments

This work was supported by the National Science Foundation. We thank J. Elsner and J. Warner for valuable modeling assistance; K. Emanuel for sharing the data from the MIT model and his insightful comments and edits to an earlier version of the text; and S. Ahmed, A. Hawkes, D. MacDonald, S. Madsen, S. Moret, A. Sheldon, R. Sullivan, M. Toomey, P. van

Hengstum, and S. Zipper for their field and laboratory assistance. This article benefited from constructive reviews by M. Huber, J. Anderson, and one anonymous reviewer.

Table 2.1: List of $^{14}C$ Ages for SCP

| Sample | Depth in Core (cm) | Material | Mass (mg) | Age ± error ($^{14}C$ year B.P.) | Calibrated Age (year B.P.) |
|---|---|---|---|---|---|
| 1[a] | 170 | Bark | 11.8 | 1300 ± 20 | 1270 ± 15 |
| 2[b] | 172 | Grass blade | 3.6 | 240 ± 25 | 295 ± 10 |
| 3[c] | 174.5 | Leaf | 1.3 | 95 ± 25 | 235 ± 15 |
| 4[a] | 180 | Bark | 16.3 | 480 ±25 | 520 ± 10 |
| 5[a] | 209 | Bark | 3.3 | 390 ± 15 | 485 ± 15 |
| 6[a] | 225 | Bark | 8.9 | 735 ± 25 | 675 ± 10 |
| 7 | 254 | Bark | 17.3 | 735 ± 25 | 675 ± 10 |
| 8 | 307 | Bark | 9.3 | 1260 ± 15 | 1220 ± 20 |
| 9 | 355 | Twig | 4.7 | 1680 ± 30 | 1575 ± 35 |
| 10 | 441.5 | Bark | 4.6 | 2500 ±20 | 2565 ± 30 |

[a] excluded from chronology due to anomalously old age

[b] used the oldest 2-σ age of 415±5 yrs. BP; see text for discussion

[c] age inconsistent with $^{210}Pb$ and $^{137}Cs$ chronology

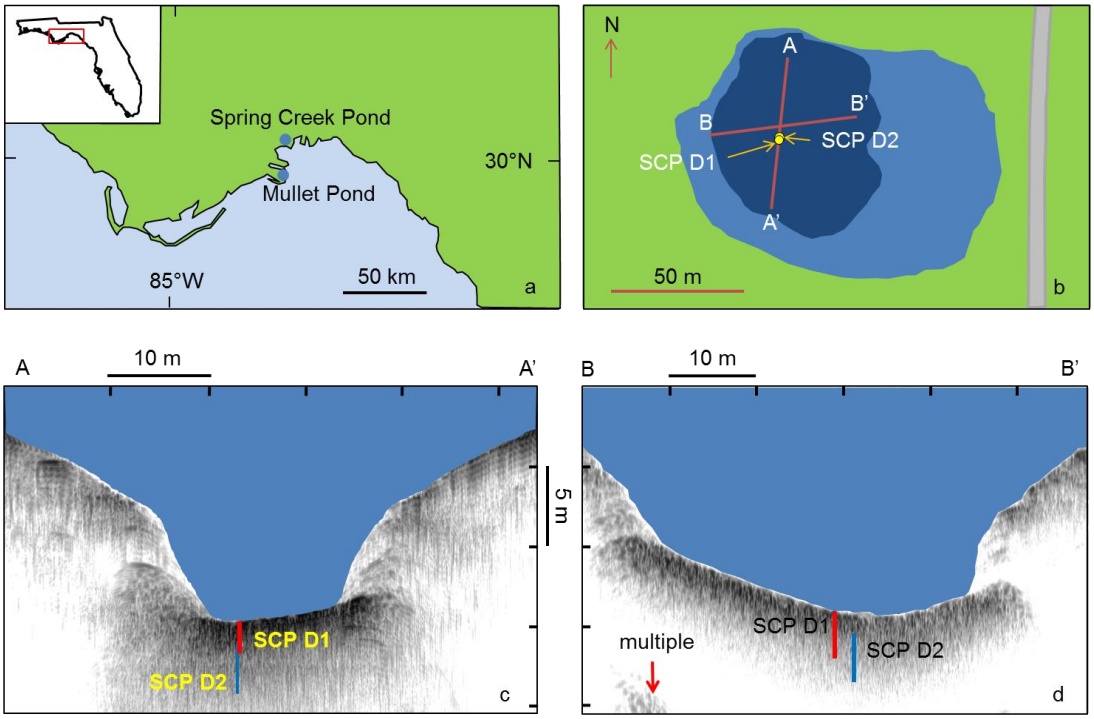


Figure 2.1: (a) Location of Spring Creek and Mullet Ponds on the coast of Apalachee Bay, Florida. Inset shows location of this area along Florida's coast. (b) Spring Creek Pond (light blue) and its sinkhole (dark blue). The two red lines correspond to sonar transects. Locations of cores SCP D1 and SCP D2 are shown. (c) Sub-bottom profile along line A-A'. Cores are shown at their proper location and depth. (d) Sub-bottom profile along transect B-B'. Cores are shown at their proper location and depth. "Multiple" refers to an instrument artifact and not a real subsurface feature.

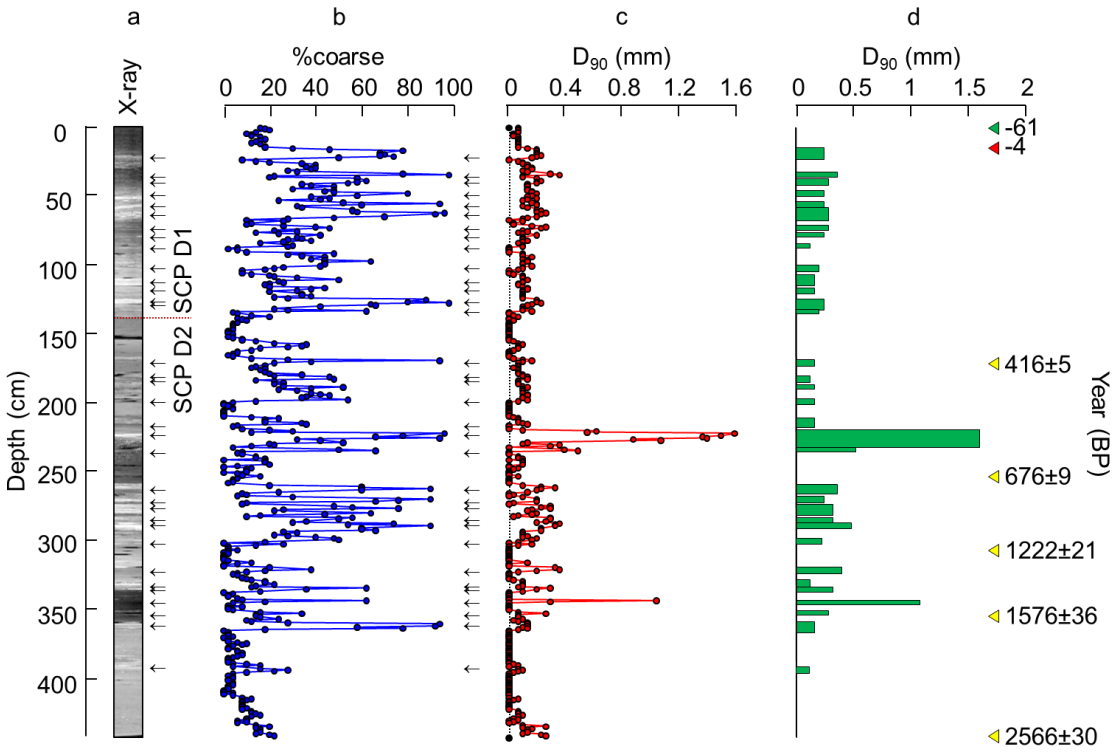


Figure 2.2: (a) Combined x-radiograph image of the SCP D1 and SCP D2 cores (separated by the dashed red line) extracted from Spring Creek Pond, showing density variations (lighter colors are denser). Arrows indicate inundation deposits. (b) Percentage of coarse material (grain size > 0.063 mm) sampled at 1 cm intervals. Peaks in %coarse (indicated with arrows) correlate with denser layers in x-radiograph. (c) Grain sizes at the 90$^{th}$ percentile ($D_{90}$), sampled at 1 cm intervals. The vertical dashed line at 0.063 mm indicates the silt-sand transition. (d) $D_{90}$ grain size of the hurricane inundation layers. The vertical width of the bar is equal to the thickness of the deposit (as determined by the width of the $D_{90}$ peak). $^{14}C$ data are shown with the yellow triangles, $^{137}Cs$ data with the red triangle, and the date of extraction (2011 CE) with the green triangle.

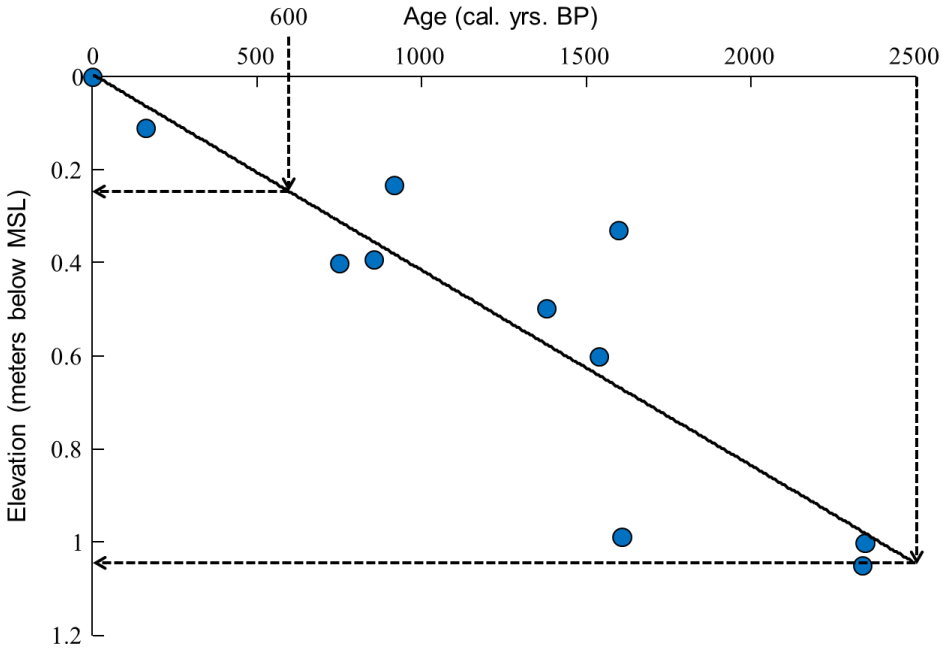


Figure 2.3: Sea level curve for the Gulf of Mexico using data from Wright et al. (2005) and Törnqvist et al. (2006). A linear fit to the data (solid line) yields a sea-level rise rate of 0.4 mm/yr. The sea-level at 600 yrs. BP, corresponding to the deposition of the anomalous deposit, and 2500 yrs BP, corresponding to the start of the Spring Creek record, are shown with the dashed lines.

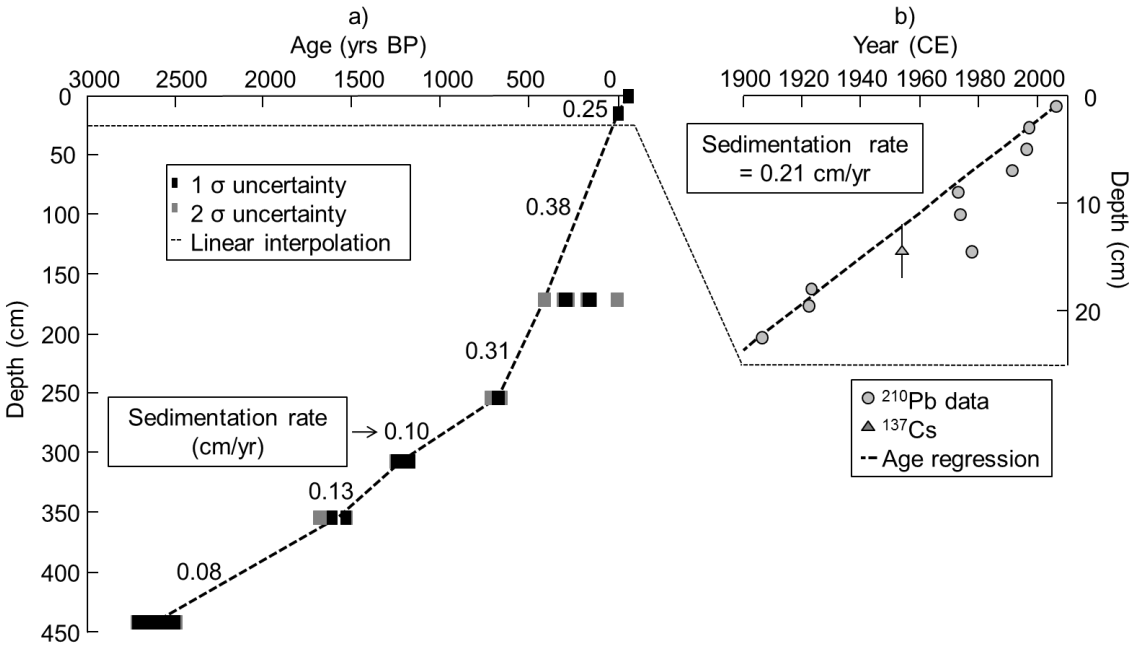


Figure 2.4: (a) Age model for SCP D1 and D2 using $^{14}C$, $^{210}Pb$, and $^{137}Cs$ data. 1-σ errors in the $^{14}C$ data are plotted as black boxes and 2-σ errors are plotted as gray boxes. The linearly-interpolated sedimentation rate between each $^{14}C$ and $^{137}Cs$ data point is displayed. (b) A close-up of the $^{210}Pb$ and $^{137}Cs$ data. The 1-σ error in 1954 CE onset of $^{137}Cs$ due to the sampling interval is shown as a vertical line.

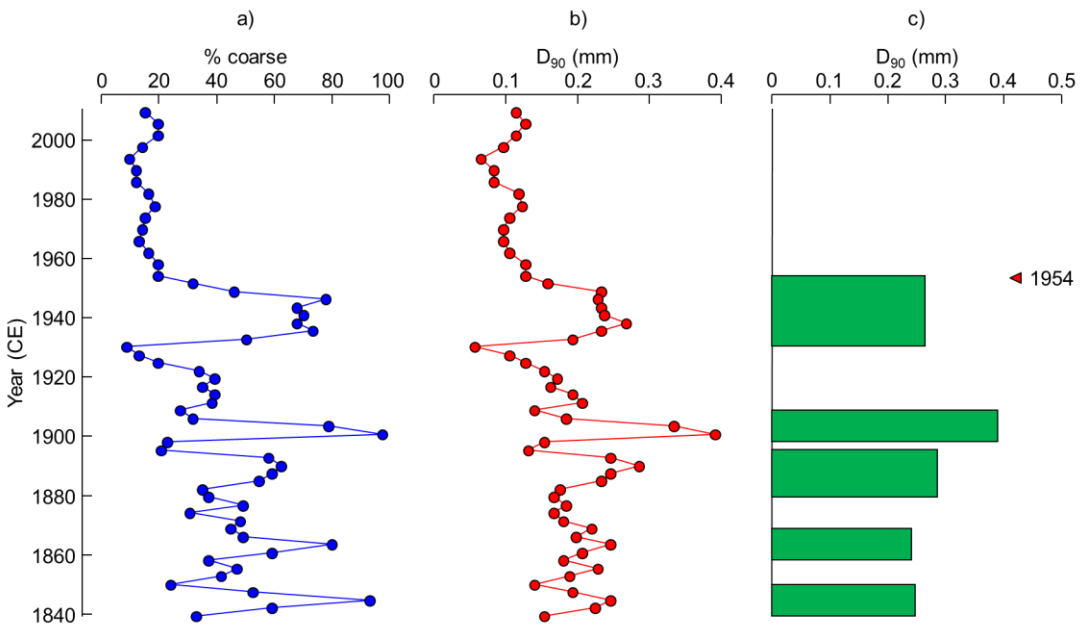


Figure 2.5: (a) %coarse (portion of material with diameters ≥0.063 mm) for the post-1840 CE portion of the sediment core. This age range is used to capture a storm whose temporal error bars put it within the historic period (post-1850 CE). (b) $D_{90}$ grain size for the post-1840 CE portion. (c) $D_{90}$ grain size for the inundation layers. The vertical height of the bar corresponds to the thickness of the deposit (measured using the width of the $D_{90}$ spike). $^{137}Cs$ age constraint is shown with a red triangle.

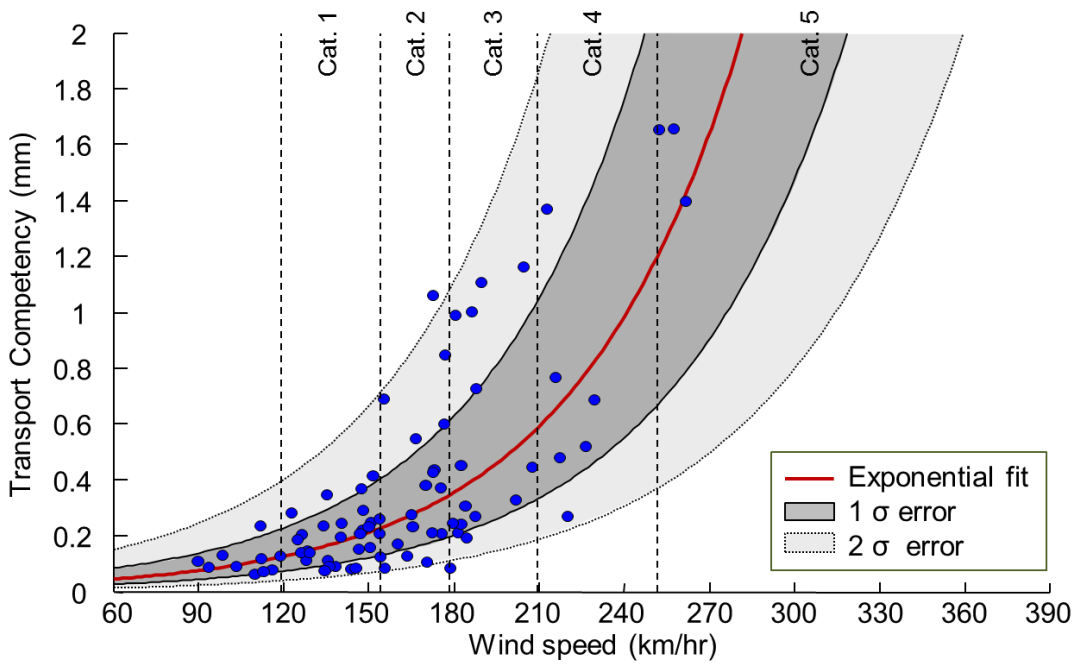


Figure 2.6: A plot of the surge competence and maximum landfall wind speed for each of the 80 storm surges (blue circles) which can transport a $D_{90}$ grain size ≥ 0.063 cm. The red line is the exponential fit to the data. The dark gray area denotes the 1-σ error and the light gray area denotes the 2-σ error in the model. Vertical dashed lines indicate the boundaries of the wind speeds for each Saffir-Simpson hurricane category.

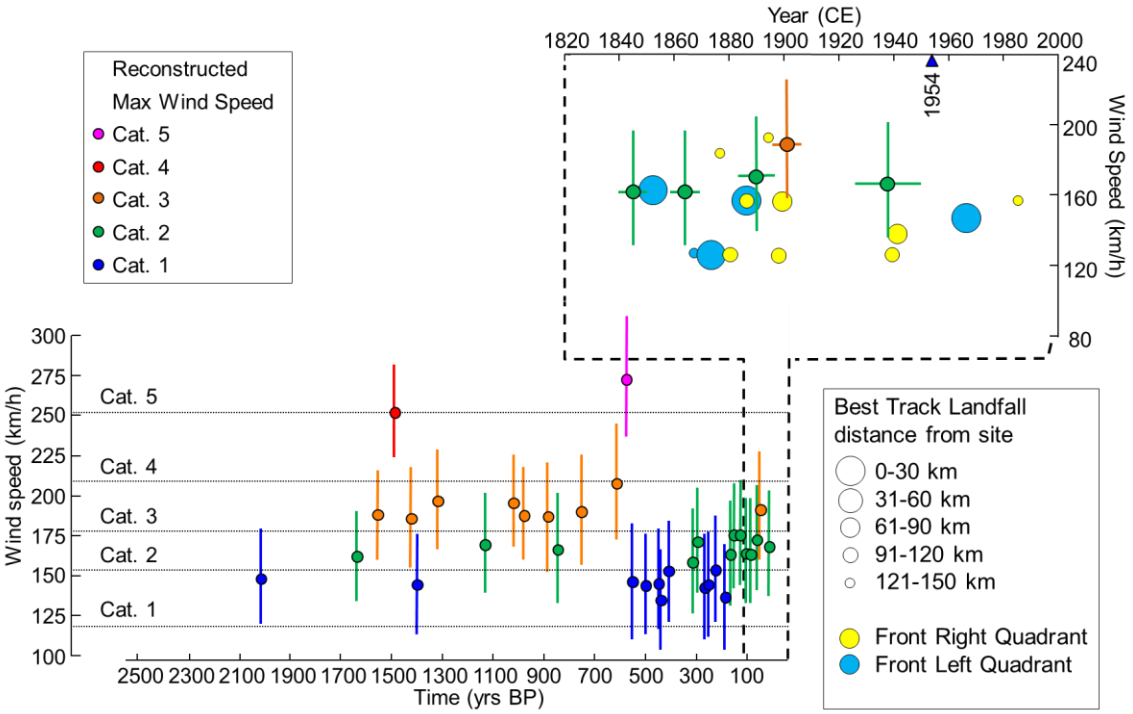


Figure 2.7: Time series of hurricane inundation events at Spring Creek Pond with calculated hurricane wind speeds and 1-σ error bars. Horizontal black lines indicate wind speeds denoting the Saffir-Simpson hurricane categories. Colors also correspond to Saffir-Simpson category: blue=cat. 1, green=cat. 2, orange=cat. 3, red=cat. 4, magenta=cat. 5.

Inset: A comparison between storms from the best-track data set (blue and yellow circles) and the wind speed calculated from the five historic (post-1850 CE) inundation deposits in the Spring Creek Pond record (green and orange circles). Vertical error bars denote the 1-σ error in wind speed and horizontal bars denote error in dating of the deposit associated with sampling interval and thickness of deposit. The size of the circle of the best-track storms denotes the landfall distance from the site with larger circles corresponding to a smaller distance. Yellow circles are storms whose right-front (stronger) quadrant struck Spring Creek Pond and blue circles are storms whose left-front (weaker) quadrant struck the site. $^{137}$Cs age constraint is shown with the blue triangle.

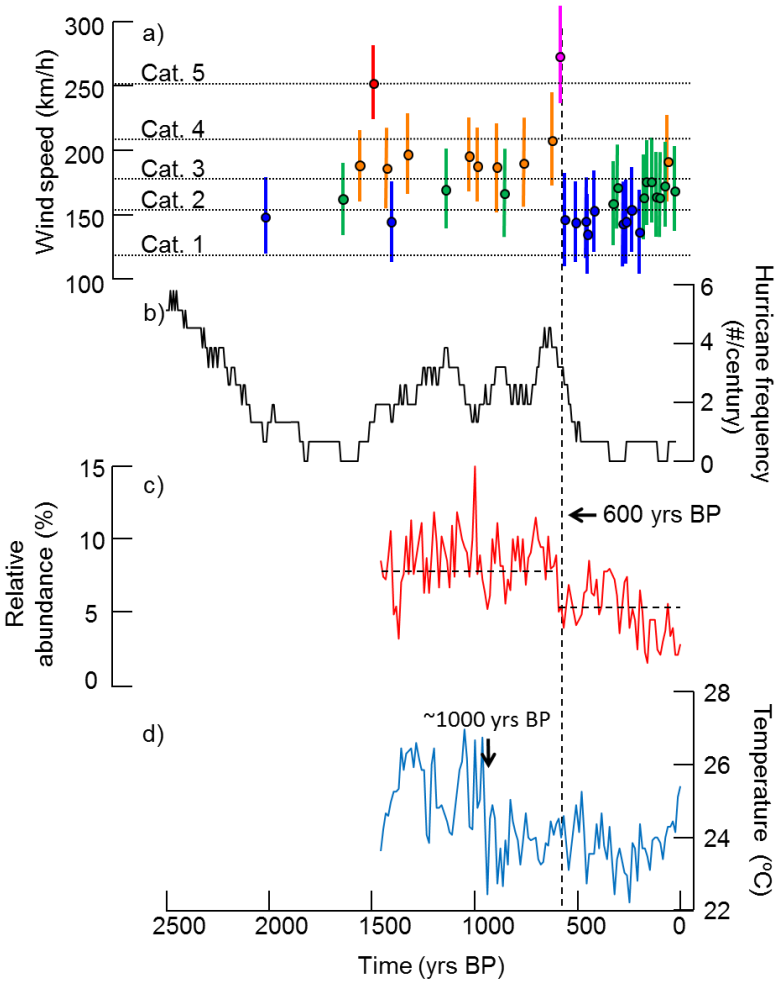


Figure 2.8: (a) Hurricane strike record at Spring Creek Pond spanning the past ~2500 years, compared to (b) the reconstructed frequency of intense hurricane events from the nearby site at Mullet Pond (MP) by Lane et al., (2011). The color scheme in "a" is the same as in Figure 2.7 and the y-axis of the MP record is intense (≥ category 3) hurricane frequency (storms/century). (c) The relative abundance of *G. sacculifer* in the Pygmy Basin over the last ~1500 years. Increasing relative abundance of *G. sacc.* corresponds to greater penetration of the Loop Current into the Gulf of Mexico. The hortizontal dashed lines represent the mean value of *G. sacc.* abundance, showing an abrupt decrease at 600 yrs BP (vertical dashed line), as presented by Richey et al., (2007). (d) SST record, reconstructed from foraminiferal Mg/Ca ratios in the Pygmy Basin over the past ~1500 years (Richey et al., 2007). The arrow indicates the drop in SST ~1,000 yrs BP identified by the authors.

# CHAPTER 3

# HOW UNIQUE WAS HURRICANE SANDY? SEDIMENTARY RECONSTRUCTIONS OF EXTREME FLOODING FROM NEW YORK HARBOR

## 3.1 Abstract

The magnitude of flooding in New York City by Hurricane Sandy is commonly believed to be extremely rare, with estimated return periods near or greater than 1000 years. However, the brevity of tide gauge records result in significant uncertainties when estimating the uniqueness of such an event. Here we compare resultant deposition by Hurricane Sandy to earlier storm-induced flood layers in order to extend records of flooding to the city beyond the instrumental dataset. Inversely modeled storm conditions from grain size trends show that a more compact yet more intense hurricane in 1821 CE probably resulted in a similar storm tide and a significantly larger storm surge. Our results indicate the occurrence of additional flood events like Hurricane Sandy in recent centuries, and highlight the inadequacies of the instrumental record in estimating current flood risk by such extreme events.

## 3.2 Introduction

On October 29, 2012 Hurricane Sandy inundated New York City, NY, raising water levels to 3.4 m above 2012 mean sea level (MSL) at the Battery (located at the south end of lower Manhattan). The return period of this storm tide is estimated to be 1570 years based on generalized extreme value return curves from existing tide gauge data (Sweet et al., 2013), and simulated hurricane climatology ranks this storm as a 1-in-900 year event (Lin et al., 2012). However, tide gauge data alone is generally too short to either obtain accurate extreme value statistics or evaluate the skill of extreme flood probabilities derived solely from numerical

simulations (Irish et al. 2011). Thus there is a real need for longer flood reconstructions, particularly for critically important coastlines like New York City. Historical documentation of storm activity for the city (i.e. newspapers, nautical logs, etc.) can extend storm records back to the mid-1600s for the U.S. east coast (Redfield, 1831; Ludlum, 1963; Boose, 2001; Scileppi and Donnelly, 2007). While these records provide valuable information on the occurrence of storms, detailed quantitative information on specific storm characteristics prior to 1844 (Talke et al., 2014) is limited, particularly with respect to flood magnitudes.

Storm surge and storm tide are two separate metrics that describe the storm-induced rise in water levels. Storm surge is the anomalous rise in water level above the predicted astronomical tide (excluding the impacts of waves), and storm tide is the total rise in water level due to the combination of storm surge and astronomical tides. Hurricane Sandy's peak hourly averaged water levels occurred at high tide at the Battery with a storm tide of 3.4 m above 2012 MSL and a storm surge of 2.8 m. Peak monthly water levels verified by the National Oceanic and Atmospheric Administration (NOAA) extend back to 1927 CE, and with the merging of an additional nearby tide gauge, provide a reconstruction of peak annual flood heights at the Battery back to 1893 CE (Zervas, 2013). Hurricane Sandy's storm tide exceeded past maxima in these records by over 1 meter (Hurricane Donna's 1960 CE storm tide held the previous record at 2.3 m).

Sandy's storm surge was also record breaking but to a lesser degree, exceeding the previous maxima in the vetted NOAA data set by roughly 40 cm (the Great Appalachian Storm of 1950 was the previous storm surge of record at 2.4 m). A more recent analysis of archived tide gauge data from the New York City area extends storm tide and storm surge records for the Battery back to 1844 and 1860 CE, respectively (Talke et al., 2014), with Hurricane Sandy remaining the event of record in both.

While Hurricane Sandy was record breaking compared to published tide gauge records, earlier historical accounts suggest that a major hurricane in 1821 CE may have had a similar storm tide and a substantially larger storm surge (Ludlum, 1963; Scileppi and Donnelly, 2007). During this 1821 hurricane the *New Bedford Mercury* newspaper reported a rise in water of 13 feet 4 inches or 4.06 m above low water in the East River (Redfield, 1831; Boose, 2001). The 1821 hurricane struck New York City at low tide with roughly 4.0 to 4.1 m of storm surge, compared to Sandy's 2.8 m of storm surge. Assuming this account is referenced to near the Battery, a 4.0 m storm surge would far exceed all events recorded within the instrumental tide gauge record, including Hurricane Sandy. Other flood descriptions support the 1821 hurricane as a significant flood event, including a 10 foot (3.0 m) rise in water level at Pungoteague, VA (Ludlum, 1963), drift caught in the trees 9 feet (2.7 m) above the ground at Cape May, NJ (Ludlum, 1963), and a tide several feet above normal at New London, CT (Boose, 2001). Because peak flooding for the 1821 hurricane occurred at low tide, its storm tide was smaller than its overall surge. Scileppi and Donnelly (2007) estimated a storm tide of roughly 3.2 m for the event, which is slightly less than that observed for Hurricane Sandy at 3.4 m.

Proxy records of extreme storm surge, such as overwash deposits preserved in coastal ponds and marshes, provide the opportunity for an independent assessment of early historical flood events (Donnelly et al., 2001a, b; Donnelly and Woodruff, 2007; Boldt et al., 2010; Lane et al., 2011; Brandon et al., 2013; Denommee et al., 2014; Wallace and Anderson, 2010; Donnelly et al., 2004). Specific to the New York City region, Scileppi and Donnelly (2007) developed a proxy record of hurricane flooding just to the east of the city using dated storm deposits preserved within a series of back-barrier saltmarshes in western Long Island. This reconstruction contained evidence of four significant flood events within the early historic period that were attributed to hurricane strikes in 1693, 1788, 1821 and 1893. Sedimentary reconstructions from

the central coast of New Jersey contain evidence for the 1821 event and/or a hurricane in 1788, but no deposits associated with the 1893 and 1693 hurricanes (Donnelly et al., 2004). The lack of evidence regarding a significant 1893 flood for New York City is also consistent with the recent analysis of archived tide gauge data (Talke et al., 2014), which, when combined with the Long Island and New Jersey storm proxies, suggest that the 1893 flood event may have been focused farther to the east along Long Island.

Discrepancies between archived tide gauge data in New York Harbor and the dated 1893 storm deposits on Long Island highlight the need for flood reconstructions obtained directly from New York Harbor itself. Furthermore, an important component to any paleo-storm reconstruction is the ability to sample and analyze a modern deposit laid down by an event of known intensity. Derived sedimentary proxies of hurricane overwash from the modern Sandy layer, therefore, are extremely valuable for improved identification and analyses of older storm deposits preserved in the region. Towards this end, we present here the first sedimentary reconstruction of significant flooding in New York Harbor based on event deposits preserved within a back-barrier pond on Staten Island, and informed with recent deposition in 2012 by Hurricane Sandy.

### 3.3 Local Geology and Field Site

Staten Island, one of the five boroughs of New York City, is located along the west side of New York Harbor (Fig. 3.1a). Proper interpretations of overwash deposition on the island require some background on its glacial legacy. The Harbor Hill terminal moraine, which forms the island's southwestern coast, was deposited during the Last Glacial Maximum and marks the southernmost extent of the Laurentide ice sheet (Borns, 1973; Fig. 3.1b). Grain sizes within the Harbor Hill moraine are poorly sorted, ranging in size from clay to boulder. Most of the fine

grains within this reddish-brown till (which gets its distinctive color from an abundance of hematite) are derived from the Triassic "red beds" located directly to the north (Soren 1988).

Seguine Pond is a small ~1.2 m deep coastal, back-barrier pond on the southern coast of Staten Island (Fig. 3.1c). The pond occupies a narrow, drowned fluvial valley that cuts through the terminal moraine. A small, 250 m long barrier beach roughly 1-2 m in height forms the southern shore of the pond and separates it from the open waters of Lower New York Bay. This 20-40 m wide barrier beach is secured in place on either end by two coastal bluffs composed of glacial till. The barrier is fairly uniform in height with the exception of a narrow (~5 m wide) topographic low at its eastern end, which serves as an occasional freshwater outlet for the pond.

A small stream network drains into the north side of the pond with a total catchment area of roughly 1 sq. km (Garin et al., 2009). The Seguine catchment is currently composed primarily of lowland suburban terrain draining initially into conservation marshlands. These wetlands are interrupted by a series of deeper natural kettle and artificial retention ponds, which both provide internal sediment traps that likely limit stream-borne fluxes directly into Seguine Pond.

## 3.4 Results

### 3.4.1 Hurricane Sandy's Impact at Seguine Pond

An interpolation of surveyed high water marks collected by the United States Geological Survey after Hurricane Sandy highlight how storm surges are amplified in the New York Bight region, particularly within funnel-shaped embayments tapering to the west (Fig. 3.1a). Such is the case in Raritan Bay, along the west side of New York City's Lower Harbor, and bordering the southern side of Staten Island. This area experienced the highest storm tide in New York (Fig.

3.1a), with a range between 3.7 and 4.0 m above 2012 MSL for Staten Island's southern coast (Blake et al., 2013).

Satellite and aircraft images acquired both prior to and immediately after the event highlight the effect of the storm on coastal environments (USGS, 2014). Specific to Seguine Pond, two newly deposited overwash fans are evident along the backside of the fronting barrier, with widespread marine-derived debris floating within the pond (Fig. 3.1d). Much of the coastline surrounding the site was stripped of its vegetation during the storm, exposing escarpments of reddish-brown till along the coastal bluffs. Fine grained sediment from these newly eroded escarpments can be seen advecting away from the coast as reddish plumes in post-Sandy images.

### 3.4.2 Chronological Constraints

Shortly following Hurricane Sandy four cores were extracted from Seguine Pond along a shore-normal transect (Fig. 3.1c). Deposition associated with the storm was evident within all surficial sediments. In core photographs and x-radiographs the deposit can be identified as a surficial layer of red, anomalously dense sediment (Fig. 3.2a, b). The reddish color of the deposit is interpreted to represent the enrichment in fine-grained hematite eroded directly from the glacial till composing the site's coastal bluffs and the deposit's higher density is due to its low organic content (and in turn higher clastic content) relative to underlying material. The Sandy deposit is also identified by anomalously low mercury (Hg) and zinc (Zn) concentrations, two industrially derived heavy metals (Fig. 3.2c, d). The deposit's concurrent drop in Hg and Zn are most likely due to the low levels of contaminants within the clastic beach and glacial sediments from which the deposit is primarily derived (Yellen et al., 2014).

We use carbon-14 ($^{14}C$), cesium-137 ($^{137}Cs$), and the onset of Hg and Zn to temporally constrain the ages of the inundation deposits. Beginning at the sediment surface and moving down core, age constraints for the central core site (SG2, Fig. 3.1c) begin with the 2012 base of the Hurricane Sandy deposit at a depth of 8 cm (Fig. 3.2 and 3.3). The peak in $^{137}Cs$ associated with the 1963 CE peak in atmospheric nuclear testing is observed farther down at a depth of 67 cm, followed by the onset for $^{137}Cs$ at 75 cm associated with the onset of atmospheric nuclear testing in 1954 CE (Pennington et al., 1973). Hg and Zn concurrently begin to rise in core SG2 above a sediment depth of 114 cm, which has been identified previously as the 1850-1900 CE onset of industrialization (Woodruff et al., 2013a; Varekamp et al., 2003; Varekamp et al., 2005). Finally, a radiocarbon sample collected at 200 cm in SG2 provides a $^{14}C$ age of 370 ± 20 yrs BP, which, when calibrated to calendar years (Reimer et al., 2013), has a 2-σ uncertainty range between 1451 and 1629 CE.

### 3.4.3 Flood Deposit Chronology

Tide gauge records identify 6 floods with storm tides greater than 2 m at the Battery since archived records begin in 1844 CE (Talke et al, 2014). In order of CE age, and with their respective storm tides, these top flood years include 1865 (2.1 m), 1950 (2.1 m), 1953 (2.2 m), 1960 (2.3 m), 1992 (2.2 m) and 2012 (3.4 m). Other documentation provides further evidence of significant floods at the Battery in 1693, 1788, 1821, and potentially 1893 (Scileppi and Donnelly, 2007).

Below the surficial Hurricane Sandy deposit, additional anomalously dense event layers are evident down to the base of the core. In particular, the first prominent deposit below the industrial onset is a 4 cm thick deposit ending at a sediment depth of 121 cm, and with a median age for this depth that dates almost exactly to the 1821 hurricane (1823 CE, Fig. 3.3). Below the

1821 deposit, additional event layers at 129 and 159 cm also date to the timing of the early historical hurricanes in 1788 and 1693, respectively (median ages of 1789 CE and 1691 CE). A less prominent deposit is evident just below the industrial onset at 116 cm that dates roughly to 1865 (median age of 1852 CE), and is consistent with the timing of the largest storm tide reported within archived tide gauge data between 1844 and 1900 (Talke et al, 2014). Note that the median derived age for the deposit at 116 cm is more consistent with the 1865 flood than with the 1893 storm, which is just outside of the 2-σ uncertainty bounds of this deposit (Fig. 3.3). Thus an event deposit for the 1893 hurricane is noticeably absent from the record, which is consistent with archival tide gauge data that downgrades the flood magnitude of this event in New York Harbor (Talke et al, 2014).

Two of the most prominent deposits in SG2 that date to the 1900s occur at a depth of 47 and 70 cm. The deeper of these two deposits resides between the 1954 and 1963 CE onset and peak in $^{137}Cs$, and is consistent with the timing of Hurricane Donna in 1960. The origin of the shallower deposit at 47 cm is less clear but is within the 1-σ age uncertainty for the December Nor'easter of 1992, which represents the largest storm tide recorded at the Battery falling between Hurricane Donna in 1960 and Sandy in 2012. Finally, two additional deposits occur just below the 1954 onset of $^{137}Cs$ at 83 and 85 cm with ages that are consistent with floods in 1953 and 1950. In addition to the 1865, 1960, 1992 and 2012 storms, these two 1950s floods are the only other events since 1844 when storm tides exceeded 2 m at the Battery (Talke et al, 2014). All historical flood events in excess of a 2 m storm tide at the Battery therefore appear to be accounted for in core SG2, along with early historical hurricanes in 1693, 1788, and 1821.

### 3.4.4 Grain Size Analyses

Percent sand and grain size analyses of event deposits in Core SG2 are presented in Figure 3.4. The 1821 CE deposit emerges as the coarsest deposit observed in SG2 with 82% sand (i.e. grain size fraction >63 μm), followed by Hurricane Sandy with 65% sand. In terms of percent >38 μm, Hurricane Sandy and the 1821 events are roughly equivalent at 85% and 86%, respectively. Hurricane Sandy and the 1821 deposit are also the only two event layers in core SG2 with a median grain size >63 μm (Fig. 3.4d). All other samples are less than 50% sand, such that their $D_{50}$ grain sizes were less than the 63 μm sieving limit.

The $D_{50}$ grain size for the 1821 hurricane was 240 μm, over two times larger than Hurricane Sandy's $D_{50}$ of 90 μm. It is possible that the anomalously large grain sizes of the 1821 event are due to the dilution of coarse material with fines in the Hurricane Sandy deposit. However, the $D_{90}$ values of just the sand fraction (see Methods) show that the 1821 hurricane remains the coarsest event with a 480 μm $D_{90}$ grain size, compared to a $D_{90}$ of 220 μm for Hurricane Sandy's event layer. Thus, when considering just the sand size fraction, peak grain sizes within the 1821 deposit are still over twice as great as that observed within Hurricane Sandy sediments, thereby ruling out fine grained dilution as the sole reason for the smaller grain sizes observed in Hurricane Sandy's event layer.

### 3.4.5 Spatial Trends in Deposition

Deposition associated with Hurricane Sandy is evident in all four cores obtained from Seguine Pond (Fig. 3.5). Grain size remains relatively uniform in the vertical for the Sandy deposit at each of the sampling locations (i.e. no vertical grading), but with clear sorting trends in the horizontal (Fig. 3.6). The Sandy deposit is thickest in the core closest to the barrier (SG1) at 20 cm and thins monotonically landward to 8 cm, 6 cm, and 5 cm in cores SG2, SG3, and SG4,

respectively. When sieved, the grain size of the deposit fines landward, with the greatest percent sand observed in SG1 at 89%, and decreasing to 65%, 39%, and 33% in SG2, SG3, and SG4, respectively (Fig. 3.6a). The $D_{90}$ grain size also decreases landward, going from 470 µm in SG1 to 220 µm in SG2, and 190 µm in both SG3 and SG4.

Similar to deposition from Hurricane Sandy, the 1821 deposit also decreases in thickness landward from a maximum of 11 cm in core SG1, to 5 cm in both SG2 and SG3, and 2 cm in core SG4 (Fig. 3.6a). A similar general fining trend is observed in grain size within the 1821 deposit (Fig. 3.6b). Although $D_{90}$ grain size initially coarsens from 410 µm at SG1 to 450 µm in SG2, this is followed by a steady fining to 420 µm and 410 µm for cores SG3 and SG4, respectively. Sieve results reveal a similar pattern with 46% sand in SG1, increasing to 82% in SG2, and then decreasing to 37% in SG3 and 9% in SG4.

### 3.4.6 Constraints on Storm Intensity

Both the Hurricane Sandy and the 1821 deposits generally fine and thin landward, while exhibiting little distinguishable vertical grading (Fig. 3.6). These patterns in lateral sorting are similar to those observed within other storm deposits collected from previous back-barrier ponds, and consistent with depositional trends governed predominantly by the settling of particles out of suspension while being advected landward by waves (Donnelly et al., 2004; Woodruff et al., 2008b). For such storm deposits, observed trends in grain size and thickness have in the past provided additional information for constraining flood conditions.

Brandon et al. (2013) observed a scaling between peak storm surge height and the maximum grain size within storm deposits from a coastal sinkhole in Apalachee Bay, FL. This site was far inland with surge likely the primary governor of flow. However, the $D_{90}$ grain size of the 1821 event deposit at Seguine Pond is over twice that of Hurricane Sandy, while earlier

documentation suggests a similar storm tide for the two events (Ludlum, 1963; Scileppi and Donnelly, 2007). Therefore, either the 1821 event was substantially greater than that reported in the early documentation or some process other than overall storm tide is the primary governor of transport competence (i.e. the maximum grain sizes capable of being transported by a flow) during inundation at the site.

An alternative control on transport competence includes the wave climate during barrier inundation, which governs the higher frequency oscillations in the flow that likely produce peak shear stresses (Donnelly et al., 2006). Woodruff et al. (2008b) observed a scaling between the magnitude of excess wave run-up over a barrier and the maximum grain size observed in landward fining, back-barrier deposits along the coast of Vieques, Puerto Rico (where run-up is defined as the maximum wave-induced uprush of water on a beach above still water). Here the greatest transport competence is assumed to occur when waves breach and inundate the barrier via low-frequency infra-gravity waves (Stockdon et al., 2006), which then flood the pond as bores (Donnelly et al., 2006). Under such flooding conditions Woodruff et al. (2008b) relates maximum wave-induced run-up over the barrier ($R_{max}$) to maximum grain size at a sampling site with:

$$R_{max} = \left(\frac{x_L^2 w_s^2}{g}\right)^{1/3} + h_b \quad (3.1)$$

where g is the acceleration due to gravity, $h_b$ is the barrier height, and $w_s$ is the settling velocity of the peak grain size advected landward a distance of $x_L$ from the barrier. Here we define the maximum grain size with $D_{90}$ and convert to settling velocity using the grain size vs. particle settling velocity relationship presented in Ferguson and Church (2004). Using the observed $D_{90}$ of 220 µm for the Hurricane Sandy deposit at SG2 and an average barrier height of 1.5 m for the

site, equation (1) results in a $R_{max}$ of 2.1 m. Significant offshore wave heights ($H_o$) during Hurricane Sandy near landfall are documented at 9.9 m with a dominant wave period of 13.8 s (NDBC, 2014), and respective offshore wavelength ($L_o$; Stockdon, 2006) of roughly 300 m. Resulting off-shore wave steepness likely results in dissipative breaking conditions (Stockdon et al., 2006), where wave run-up has been empirically related to $H_o$ and $L_o$ as:

$$R_{max} = \alpha(H_o L_o)^{1/2} \quad (3.2)$$

with a best fit α of 0.043. This relationship provides a predicted wave run-up of 2.3 m for Hurricane Sandy, which is quite close to the run-up of 2.1 m independently derived based on the $D_{90}$ grain size of the Hurricane Sandy deposit at SG2.

The advective-settling model proposed by Woodruff et al. (2008b) is certainly an over-simplification of the overwash process; however, similar independent run-up predictions between it and that predicted by equation (2) for Hurricane Sandy provide support for the model's use in obtaining a rough estimate of run-up and respective storm conditions for the 1821 hurricane. Using equation (1), a $D_{90}$ of 450 µm at SG2 for the 1821 deposit results in a predicted $R_{max}$ of 2.6 m. Wave periods and resultant off-shore wave lengths for the 1821 event are unavailable but assumed similar to Hurricane Sandy with a $L_o$ of 300 m. In turn, equation (2) provides an off-shore significant wave height of roughly 12 m for an $R_{max}$ of 2.6 m. Ochi (2005) proposes the following empirical relationship between severe wind speed ($U_{wind}$) and significant off-shore wave height:

$$H_o = 0.235\, U_{wind} \quad (3.3)$$

Using an estimated $H_o$ of 12 m for the 1821 hurricane, equation (3) provides a respective wind speed of 51 m/s, roughly equivalent to a weak category 3 hurricane (Saffir and Simpson, 1974).

This intensity is also consistent with earlier assessments for the strength of the 1821 hurricane based on independent documentation of wind damage occurring during the event (Ludlum, 1963; Boose, 2001).

### 3.4.7 SLOSH simulations of the 1821 hurricane

Accounts of the 1821 event describe a storm surge of ~4 m inundating the Battery in just 1 hour (Redfield, 1831). However, it is unclear if a storm estimated as a weak, category 3 intensity would be capable of such a rapid rise in water. To further test this we perform storm surge simulations of the event using NOAA's Sea, Lake, and Overland Surges from Hurricanes (SLOSH) model (Jelesnianski et al., 1992) (see Methods section for details).

The documentary evidence suggests the 1821 hurricane was considerably smaller in size than Hurricane Sandy. Redfield (1831) describes the size of the storm, based on reports of wind damage, as "...confined within a circuit whose diameter does not appear to have greatly exceeded one hundred miles," or, therefore, having an 80 km radius. Graham and Hudson (1960) compute the radius of maximum winds as 31 miles (50 km) and report observations ranging from 30-40 miles (48-64 km) for this storm. The discrepancy between these two records is most likely due to their description of two different aspects of the storm with Redfield (1831) describing the diameter of the damaging winds and Graham and Hudson (1960) describing the radius of maximum wind speed. For comparison, a radius of maximum wind of just 50 km for the 1821 event is 3-4 times smaller than the size of Hurricane Sandy, which had a radius of maximum wind of 160-200 km near landfall.

The track and translation speed of the 1821 hurricane is fairly well constrained due to the large number of historical accounts of its passage (Redfield, 1831; Ludlum, 1963; Boose, 2001). Based on these observations, the 1821 storm was likely moving substantially faster than

Hurricane Sandy with an estimated translation speed of 61 km/hr (Graham and Hudson, 1960) (or 64 km/hr using Landsea et al., 2004), compared to 29 km/hr for Sandy.

Because the above parameters are not precisely known, storm surge simulations for the 1821 event were run using a range of storm sizes, central pressure differences, and translation speeds. The simulation of the 1821 hurricane that most closely reproduced the rapid rise in water level had a radius of maximum winds of 40 km, 58 m/s (~210 km/hr) sustained winds, and a translation speed of 65 km/hr, which is generally consistent with historical observations described above (Fig. 3.7). Storm surge simulation of these hurricane conditions results in a rise in water of roughly 4 m but over an interval of two hours rather than one. However, these simulations provide support for the magnitude of storm surge of roughly 4 m noted in the documentary record for the 1821 event, which is substantially greater than the 2.8 m of surge observed during Hurricane Sandy.

**3.5 Discussion**

Sedimentological dissimilarities between the 1821 and Hurricane Sandy deposits highlight the different nature of the two flooding events. While the 1821 deposit is the coarsest event layer observed in Seguine Pond, the resultant deposition by Hurricane Sandy is consistently the thickest deposit at the site (Fig. 3.6), with thickness potentially related to the total net transport into the pond during an event (Morton et al., 2007). The volume of sediment that overwashes a barrier during a flood event is related to the time-varying rate of overwash transport and the duration of flooding (Donnelly et al., 2009). Overwash sediment transport rates are commonly assumed to be a function of excess wave run-up (Donnelly et al., 2006, 2009), while flood duration is more related to the size and speed of the storm (Davis and Dolan, 1993; Weisberg and Zhang, 2006; Irish et al., 2008). Larger and slower storms like Hurricane

Sandy (translation speed of 29 km/hr and a radius of maximum winds of 160-200 km), therefore have significantly longer flood durations than that documented for the smaller and faster moving 1821 event (translation speed of 65 km/hr and radius of maximum winds of 40 km). In turn, the anomalous thickness of the Hurricane Sandy deposit relative to past flood layers preserved at the site is consistent with greater net transport during the 2012 event. Thus although significantly larger grain sizes for the 1821 deposit point to greater initial wave run-up and overall storm intensity, Hurricane Sandy's anomalous thickness relative to the 1821 deposit supports Hurricane Sandy being significantly greater in size and of significantly longer flood duration (Fig. 3.7).

The return period of Hurricane Sandy's 3.4 m storm tide at the Battery has been estimated to range between 900 (Lin et al., 2012) and 1600 years (Sweet et al., 2013). The probability that this event could occur during the last century can be calculated using

$$P = \frac{n!}{x!(n-x)!} p^x q^{n-x} \quad (3.4)$$

where n is the interval of time under consideration, x is the number of occurrences of the event, p is the probability of "success" (i.e. the event happens) and q is the probability of "failure" (i.e. the event doesn't happen) (Gray and Odell, 1973). Using the length of the instrumental period and a 1000 year storm (i.e. p = 1/1000 or 0.001), the probability of an event like Hurricane Sandy occurring during the last century is roughly 10% (Woodruff et al., 2013b). However, the probability of two 1000-year storm tides occurring over three successive centuries (i.e. similar storm tides for Hurricane Sandy and the 1821 hurricane over the length of the sediment record), is ~3%. The assessment serves to highlight the difficulties and large uncertainty associated with accurately assessing the return period for an event of Hurricane Sandy's magnitude, and the

value of extending records beyond the instrumental with natural archives such as those provided by the Seguine Pond reconstruction.

Relative sea-level change is an environmental factor that could affect sedimentation at the field site. However, the percent coarse fraction of deposits in core SG2 does not exhibit any systematic increases or decreases up core (Fig. 3.4c). A similar trend was observed within previous overwash reconstructions (Woodruff et al., 2008b), and provides support for a relatively stable barrier system in recent centuries in the face of relatively modest rates of sea-level rise (Woodruff et al., 2013b; Kemp and Horton, 2013). Assuming that barrier elevation has risen at a rate similar to regional rates of sea-level, variations between flood deposits in Seguine Pond likely represent differences in storm characteristics relative to sea-level at the time of flooding.

Documented accounts of flooding for the 1821 hurricane are also likely in reference to mean low water at the time of flooding (Ludlum, 1963) with the resulting storm tide of 3.2-3.4 m relative to 1821 MSL. An analysis of long-term trends with tide gauge data at the Battery reveals an average rate of sea-level rise of 2.77 mm/yr since records begin in 1856 CE (NOAA, 2014). Extrapolating this rate back to 1821 suggests roughly 0.5 m of sea-level rise between the 1821 hurricane and Hurricane Sandy in 2012. Independent evaluations of sea-level rise from marsh records result in a similar rate of 2.5 mm/yr or ~0.48 m since 1821 (Kemp and Horton, 2013). Relative to the datum of modern mean sea level, the 1821 hurricane's peak water levels would have been 0.5 m lower or 2.7-2.9 m above modern mean sea level. Further, in terms of total storm surge the 1821 flood probably exceeded that of Hurricane Sandy significantly: 4.0 m for the 1821 Hurricane relative to 2.8 m for Hurricane Sandy. Therefore, when compared to the 1821 Hurricane, Sandy's record breaking water level likely has more to do with its occurrence at high tide and the increase in mean sea-level since 1821.

In summary, an inundation record covering the past ~300 years was reconstructed from sediment cores taken from New York City, NY. Deposits in the record correspond to storms known to have affected New York Harbor, including early historic storms in 1693, 1788, and 1821. Sedimentary analysis reveals only two deposits, those of Hurricane Sandy and the 1821 hurricane, with a median grain size in the sand range (>63 μm). While the Hurricane Sandy deposit was much thicker than the 1821 deposit, it had a smaller maximum grain size. This is consistent with historic accounts and SLOSH model results that suggest that the 1821 hurricane was a smaller (radius of maximum winds of 40 km) but significantly more intense storm (maximum 1-minute sustained wind speed of ~210 km/hr), compared to Hurricane Sandy with a radius of maximum winds of 160-200 km and 130 km/hr sustained winds at landfall. Sea-level rise and peak surge occurring at high tide combined to give Sandy record-breaking water levels, but the 1821 hurricane probably had a significantly larger overall storm surge. Our results indicate that extreme flood events like Hurricane Sandy are not uncommon within sedimentary records and that the true return interval for such extreme events to New York City is probably significantly shorter than current estimates.

## 3.6 Methods

### 3.6.1 Field work

All cores were collected using a modified Vohnout/Colinvaux piston core following methods similar to Woodruff et al. (2013a). Beginning closest to the barrier and traversing landward, cores and locations include SG1 (N 40.52423°, W 74.16934° ± 4 m), SG2 (N 40.52438°, W 74.16921° ± 3 m), SG3 (N 40.52463°, W 74.16919° ± 4 m), and SG4 (N 40.52506°, W 74.16908° ± 4 m).

### 3.6.2 Analysis of sediment cores

X-radiograph images were initially obtained on all cores by scanning split sections at 500 µm resolution on an Itrax Core Scanner (Croudace et al., 2006). Black and white inverted x-radiographs reveal density variations in all cores and anomalously dense bands are used as a proxy for event-driven deposition by storms (Boldt et al., 2010; Lane et al., 2011; Brandon et al., 2013). Core SG2 was chosen for detailed sedimentary analysis due to its central location in the pond (Donnelly and Woodruff, 2007) and the abundance of well-preserved storm layers. Following identification with the x-radiographs, the dense layers in core SG2 were subsampled at 1 cm intervals. Samples were weighed, dried in an oven at 100 °C for 24 hours, and weighed again to determine the mass of water. Dried samples were then powdered using a mortar and pestle and transferred to ceramic crucibles. The crucibles were put in a muffle furnace for 2 hours at 550 °C to combust organic material.

Following combustion, samples were transferred to plastic vials, hydrated, and sonicated for 3 hours to disaggregate clay particles. Next, they were wet sieved at both 63 µm, corresponding to the transition between sand and silt (Wentworth, 1922), and 38 µm, which is near the coarse silt to medium silt transition. Retained samples were then dried at 100 °C for 24 hours to obtain the mass of the sand fraction (> 63 µm) and the mass of the approximate coarse silt fraction (< 63 µm and > 38 µm).

The coarse (> 63 µm) fraction was run through a digital image processing, size and shape analyzer (Retsch Technology Camsizer) with the size distribution analyzed for both percent coarse (unadjusted) and adjusted for the removed fines (Brandon et al., 2013). Grain size results presented in this study include the median ($D_{50}$) grain size and the size of the largest subset of grains in the sample, taken as $D_{90}$, or the size for which 90% of the particles in the size distribution are finer. Two grain size distributions are considered: the total distribution of all

grain sizes in a sample and the grain size distribution of just the sand fraction. In this study, we present the $D_{50}$ grain size of the total grain size distribution, but the $D_{90}$ grain size of just the sand fraction. The $D_{90}$ grain size is similar between the unadjusted and adjusted distributions but we believe that using the unadjusted $D_{90}$ grain size in the transport competence calculations is more representative of largest grain sizes transported to the location during flooding.

### 3.6.3 Dating techniques

Temporal constraints on sediment deposition were determined using radiocarbon, cesium-137 ($^{137}$Cs), and the onset of industrial heavy metals (as identified in concentration-depth profiles of Hg and Zn). The global onset of $^{137}$Cs in the sediment record corresponds to 1954 CE, or the start of atmospheric nuclear weapons testing, and the peak in $^{137}$Cs dates to 1963 CE, or just prior to the signing of the Nuclear Test Ban Treaty (Pennington et al., 1973). $^{137}$Cs was measured using a Canberra GL2020R Low Energy Germanium Detector. Sediment samples with a dry mass greater than 2 grams were powdered, put in 6 cm diameter plastic jars, and counted for 48-96 hours. $^{137}$Cs activities were computed spectroscopically using the 661.7 keV photopeak.

In the Northeastern U.S., concentrations of heavy metals increase significantly in sediment between 1850 and 1900 CE, corresponding to the rise of factories during the Industrial Revolution (Woodruff et al., 2013a; Varekamp et al., 2003; Varekamp et al., 2005). Depth profiles of Hg and Zn were employed to identify the depth of this industrial horizon. Hg measurements were obtained on dried sediments from core SG2 with a Teledyne Leeman Labs Hydra-C mercury analyzer following procedures described by Woodruff et al. (2013a). Zn activities were measured in all cores with the ITRAX Core Scanner using a Molybdenum tube and operating at 30 kV and 55 mA for 10 seconds per measurement, and at a 500 µm resolution. To

extend ages beyond heavy metal and $^{137}$Cs derived constraints, a radiocarbon date was obtained at a sediment depth of 200 cm from the SG2 core site. The radiocarbon age with 1 sigma uncertainties was converted to calendar age probabilities using the IntCal13 radiocarbon calibration curve (Reimer et al., 2013).

We employ Monte Carlo simulations similar to Haslett and Parnell (2008) and Parnell et al. (2008) to derive Bayesian age constraints between chronological controls in core SG2. For each of the large number of simulations a discrete age is drawn randomly from the sample's obtained probability radiocarbon-derived distribution. A specific age is defined for the 1963 CE and 1954 CE $^{137}$Cs constraints, and a randomly drawn age between 1850 and 1900 CE for the heavy metal onset, with probabilities evenly distributed over this 1850-1900 CE interval. A date of 2012 CE was also defined at the base of the surficial deposit associated with Hurricane Sandy. Random ages were generated at random depths between the radiocarbon, $^{137}$Cs, heavy metal, and Hurricane Sandy control points such that ages increase monotonically with depth (i.e. no age reversals). The median of all simulations for a particular depth is defined as the most likely age, with bounds presented for 68% and 95% uncertainties.

### 3.6.4 SLOSH model

The SLOSH model is a coastal inundation model used by the National Weather Service for storm surge inundation prediction and hindcasting (Jelesnianski et al., 1992). The user can "create" a hurricane in the model by inputting a track, translation speed, central pressure difference (between the hurricane's eye and the ambient atmosphere), and radius of maximum winds. The central pressure difference and radius of maximum winds yield a pressure gradient body force and a resultant time-varying, surface wind field. This, along with the translation speed and track, acts as the driving force to the ocean's surface. Finally, the storm surge is

modeled by solving differential equations governing fluid motion using finite-difference methods (Jelesnianski et al., 1992).

Hurricane Sandy's parameters are readily available (Unisys, 2014) and when input into SLOSH yield a storm surge at the Battery that is ~20 cm lower than the reported surge (< 10% error). While the track and translation speed are well constrained for the 1821 hurricane (Redfield, 1831; Ludlum, 1963; Boose, 2001), the radius of maximum winds and central pressure difference are less so. To refine constraints on these parameters, numerous SLOSH model runs were executed with different combinations of these two parameters within bounds set by historical observations of the storm. The combination that best reproduces the 1821 storm tide height and inundation period as documented by Redfield (1831) at the Battery is presented in Fig. 3.7.

### 3.7 Acknowledgements

Funding for this work was provided by the Hudson River Foundation Expedited Grant #004/12E, the Hudson River Foundation Graduate Fellowship 02-13, the National Science Foundation (instrument and facility support via grant IF-0949313), and the Dalio Explore Fund. We thank H. Baranes, O. Beaulieu, B. Douglas, H. Kinney, M. Koerth, L. Kumpf, and C. Maio for their laboratory and field assistance and A. Martini for help with Hg analyses.

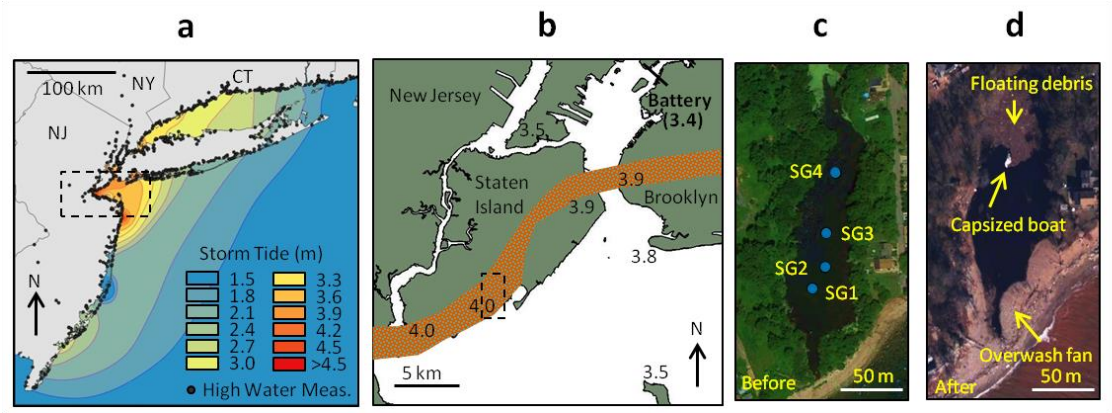


Figure 3.1: The Field Site. (a) Hurricane Sandy's storm surge, based on an interpolation between USGS high water measurements (black dots) using ArcGIS 10.0. Note that the offshore contours are extensions of these onshore observations, with uncertainty increasing with distance offshore. Upper scale bar is 100 km. Box shows the area indicated in b. (b) Location of Seguine Pond on the southern coast of Staten Island. Lower scale bar is 5 km. Brown area indicates the extent of the terminal moraine. Numbers are selected USGS high water marks for Hurricane Sandy given in meters above NAVD88. Box shows the area indicated in c and d. (c) Landsat satellite image of Seguine Pond in 2010 with core locations shown. Scale bar is 50 m. (d) Seguine Pond on Nov. 4, 2012, 6 days post-Sandy. Scale bar is 50 m.

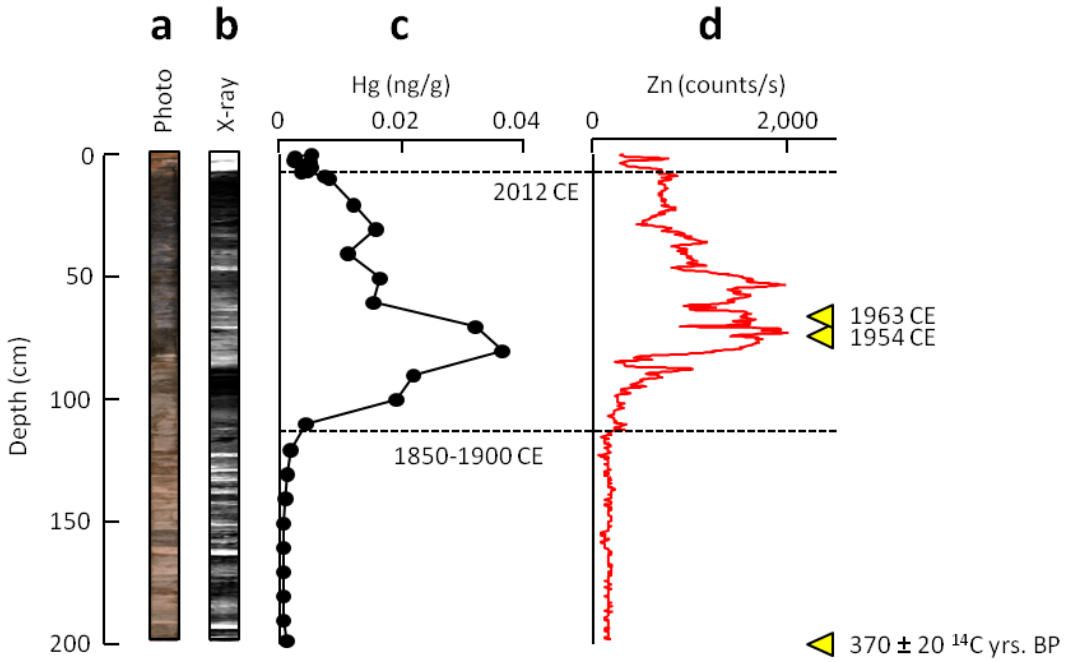


Figure 3.2: Core SG2 age constraints. (a) Optical photograph of SG2 showing red event beds, with the Hurricane Sandy deposit at the surface. (b) X-radiograph showing density variations in the core. White areas are denser than black and generally correspond to event deposits. (c) Mercury (Hg) and (d) Zinc (Zn) abundances. The upper dashed line indicates the base of the Hurricane Sandy deposit or 2012 CE. The lower dashed line marks the initial rise in heavy metals accompanying the onset of the Industrial Revolution (1850-1900 CE). In d, the yellow triangles indicate three more dating horizons: the 1963 peak in $^{137}Cs$ abundance due to atmospheric nuclear weapons testing, the 1954 onset of $^{137}Cs$, and a radiocarbon date indicating an age range between 1451 and 1629 CE.

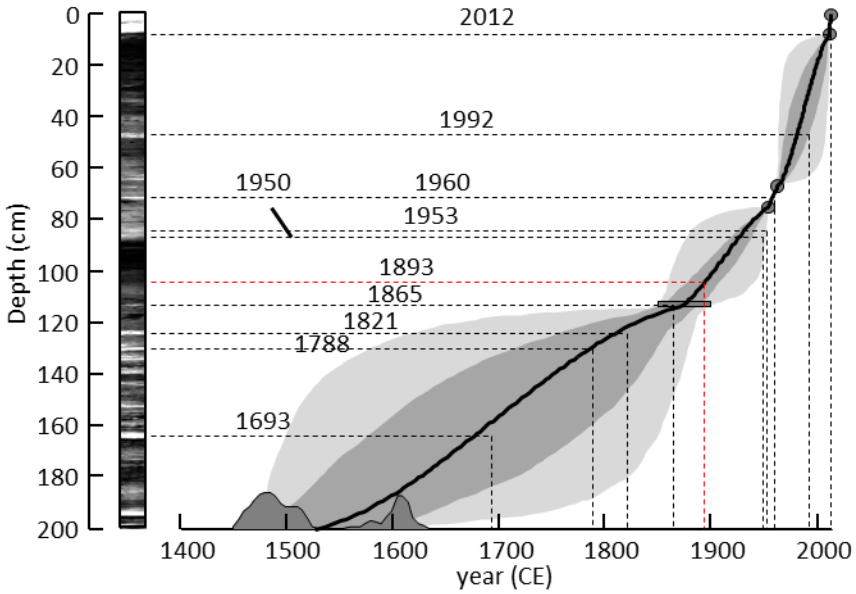


Figure 3.3: Bayesian analysis using chronological constraints from core SG2. The 1-σ age range is shown in medium gray and the 2-σ age range in light gray. 14C age probabilities are shown in dark gray just above the x-axis. The dark gray bar corresponds to the 1850-1900 onset of industrial heavy metals and circles indicate known ages based on $^{137}Cs$ and the depth of the 2012 Sandy deposit (Fig. 3.2). Vertical dashed lines correspond to the dates of significant surge events in New York Harbor and the horizontal dashed lines indicate their most likely deposit (seen in the x-radiograph). The 1893 event (red dashed lines) does not have a corresponding deposit.

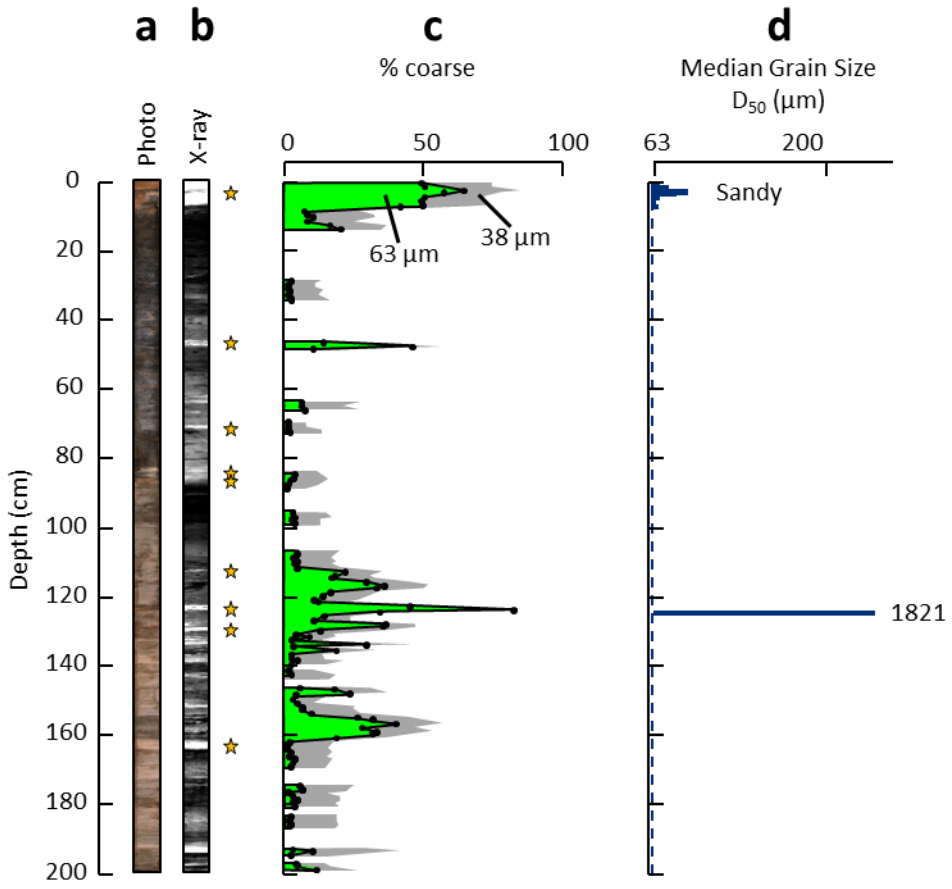


Figure 3.4: Sedimentary characteristics of storm deposits in core SG2. (a) Optical photograph of SG2 showing red flood derived deposits. (b) X-radiograph showing increased density of deposits. Deposits are indicated with orange stars. (c) Percentage of coarse material in each deposit. The percentage greater than 63 µm is shown in green and the percentage greater than 38 µm is shown in gray. (d) Median grain size ($D_{50}$) for deposits greater than 63 µm. The dashed blue line is the 63 µm sieving limit.

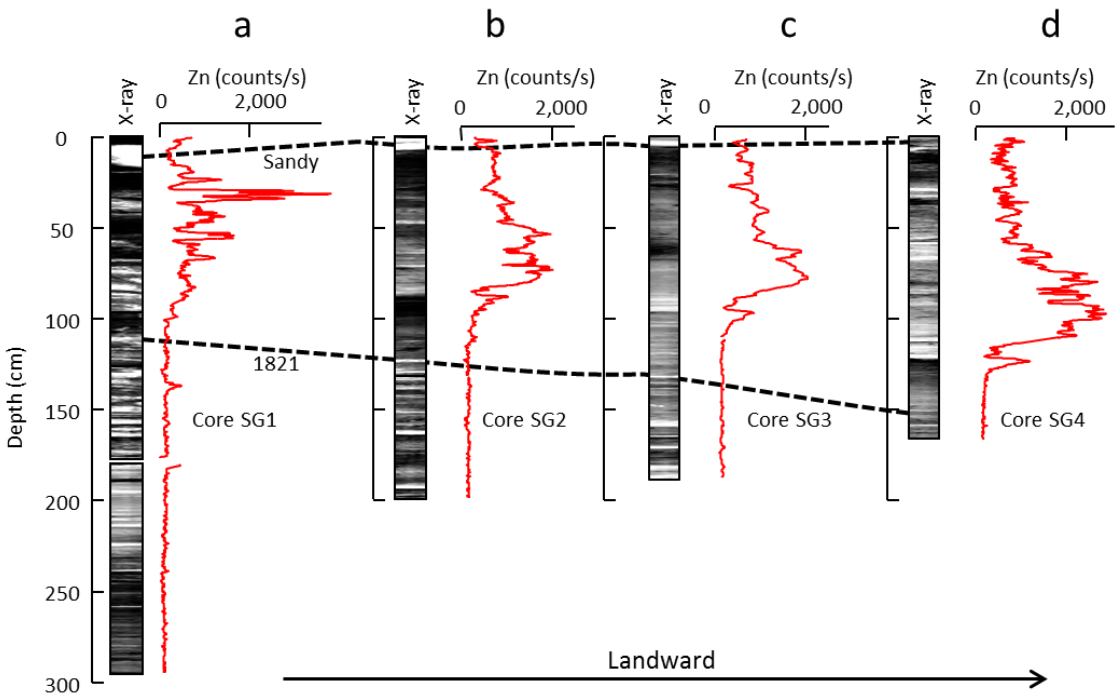


Figure 3.5: Core Transect from Seguine Pond. X-radiographs and Zn abundance (red lines) of (a) Core SG1, the core closest to the barrier, (b) core SG2, (c) core SG3, and (d) core SG4. Deposits associated with Hurricane Sandy and the 1821 hurricane deposits are indicated with the dashed lines.

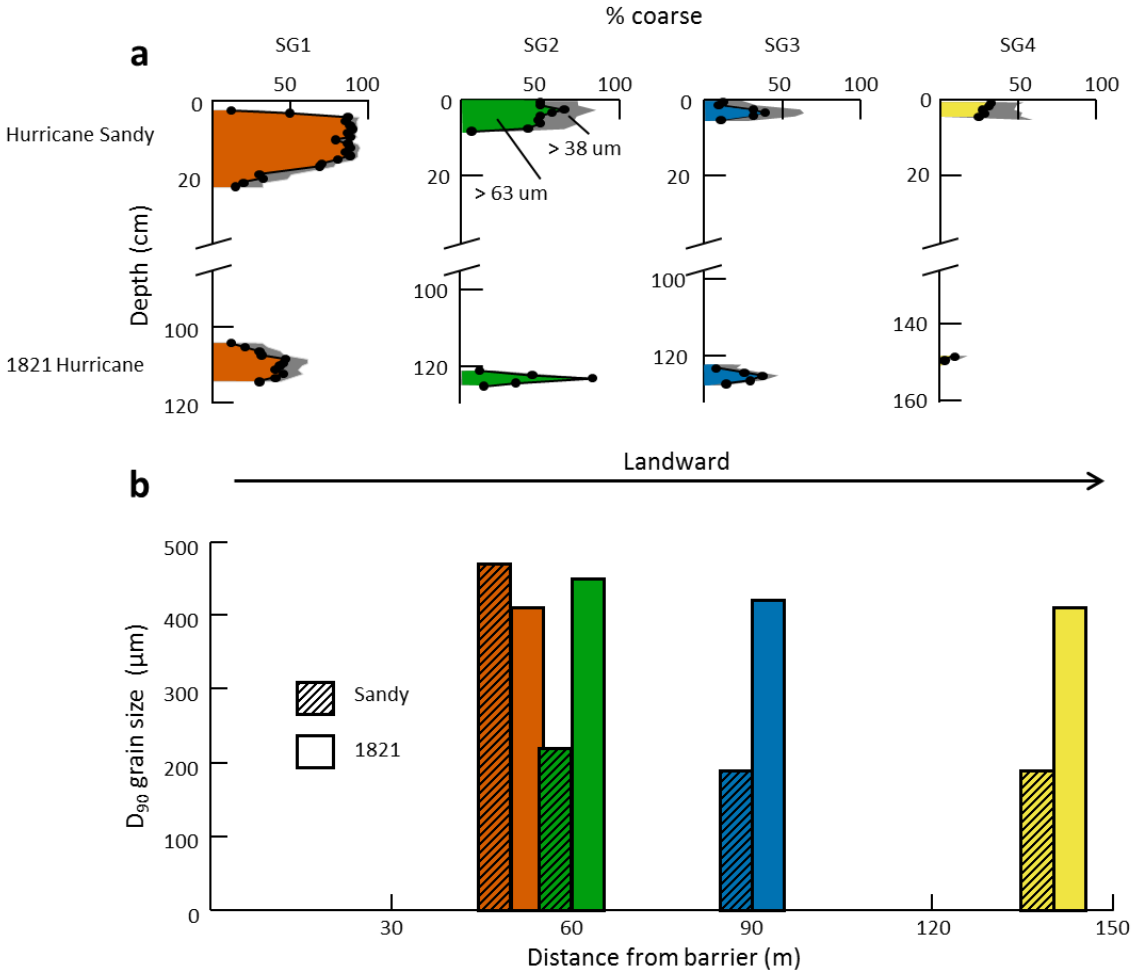


Figure 3.6: Hurricane Sandy vs. 1821 Hurricane deposition. (a) Percent coarse of the Hurricane Sandy and 1821 hurricane deposits in each core taken from Seguine Pond. The percentage of material >63 µm is in color and the percentage >38 µm is in gray. Core order starts closest to the barrier and extends landward (left to right). (b) $D_{90}$ grain size of the Hurricane Sandy (striped) and 1821 (solid) deposits in each core. Colors correspond to the same cores as in (a) and are shown in relative distance from the barrier.

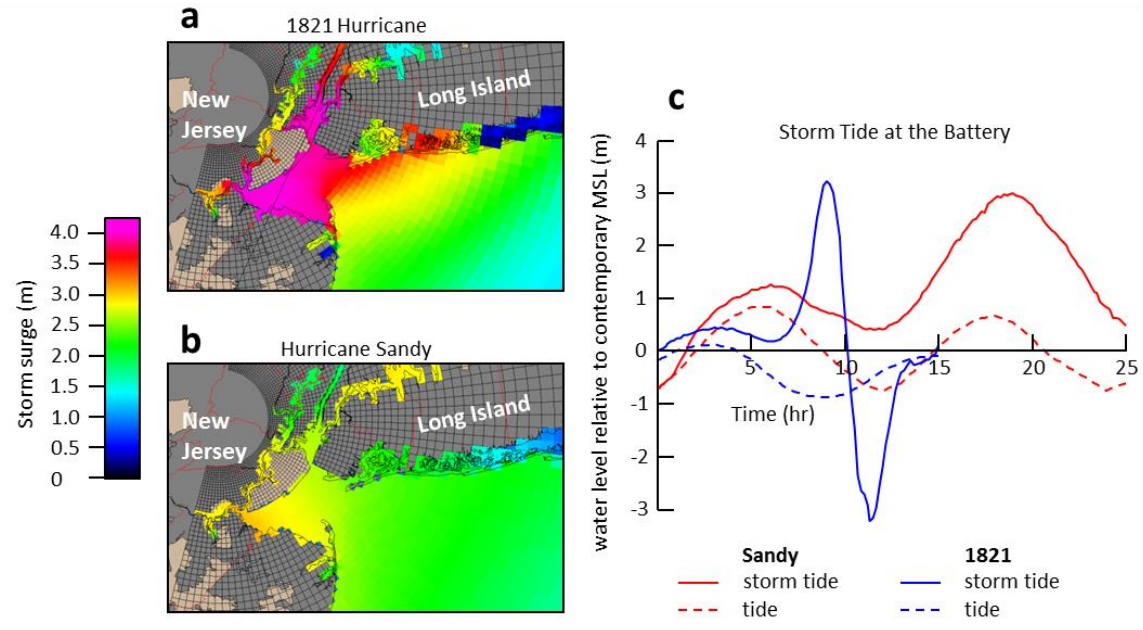


Figure 3.7: SLOSH model results of storm surge (i.e. not adjusted for tides) for (a) the 1821 hurricane and (b) Hurricane Sandy. Maps were generated using the SLOSH Display program (1.66a). (c) Tides (dashed lines) and storm tides (solid lines) for the 1821 hurricane (blue) and Hurricane Sandy (red). The beginning of the inundation for both storms is set to 0.

# CHAPTER 4

# INCREASED OVERWASH BY STORMS FOLLOWING EUROPEAN DISTURBANCE OF OYSTER BEDS IN NEW YORK CITY

## 4.1 Abstract

In the wake of Hurricane Sandy many ideas have been proposed to protect New York City from future flooding by hurricane storm surges and waves. One such strategy is to rebuild oyster beds that once blanketed the Hudson-Raritan estuary's shallows. Limited data exists, however, for assessing the effectiveness of these living barriers as a storm mitigation technique. Here we present the results of a "natural experiment" in which we employ event deposits preserved in the sediments from a series of coastal ponds and lakes to assess how the disturbance and decline of oyster beds in Raritan Bay following European settlement impacted the magnitude of overwash to these backbarrier settings. Resultant deposition from Hurricane Sandy is evident at all three of our field sites in Staten Island, New York City, and corresponds to a distinct surficial coarse grained layer and peak in magnetic susceptibility (MS). Following 1800 CE, each coarse grained layer at Seguine Pond (our primary field site) dates to the timing of significant flooding to the site. Prior to 1800, a dramatic decline in the number and percentage of coarse grained material in overwash deposits is observed back to ~1600 CE, preceded by a near absence of overwash between 1600 CE and the development of the barrier around 3000 yrs BP. Depth profiles of MS at our two additional field sites show similar temporal patterns in deposition, including the 1600-1800 CE onset of increased storm-induced overwash concurrent with rapid declines in nearby oyster populations. Conservative numerical simulations indicate a reduction in significant wave height at the coast by 30% when broad 1 m high reefs are implanted on the seabed just offshore of our field sites. Results are therefore consistent with

oyster reef decimation playing a role in driving observed increases in storm-induced overwash at Staten Island following European settlement.

**4.2 Introduction**

For centuries, various "hard" engineering strategies such as groins, jetties, sea walls, revetments, and breakwaters have been implemented to prevent wave-induced erosion and enhance sediment retention along the coastline. Recently, "green" engineering strategies which use natural materials or environments have been proposed as more sustainable and economical alternatives (Cheong et al., 2013; Temmerman et al., 2013). One strategy, suggested for New York Harbor, involves using oyster beds as "living breakwaters" to provide protection from wave damage (SCAPE, 2014). This idea has been described in previous work (Cheong et al., 2013; Temmerman et al., 2013) and has been tested using small-scale plots of oyster beds (Piazza et al., 2005; Scyphers et al., 2011) or in wave tanks (Campbell, 2004). While Piazza et al. (2005) and Scyphers et al. (2011) found decreased rates of shoreline retreat in low-energy environments, they did not find a discernable effect in high-energy environments. The authors admit that this could be due to the limited spatial extent of the oyster beds.

Larger scale studies on analogous structures (breakwaters and coral reefs) provide additional insight on how extensive oyster beds may affect coastlines. One involved the installation of a 1260 m long, submerged breakwater off the coast of Palm Beach, Florida (Dean et al., 1997) which showed increased shoreline retreat and scour between the breakwater and the shore. The authors suggest that this was probably due to the "ponding" of water as it flowed over the breakwater. The hydrodynamics of natural oyster beds may be best understood by studying coral reefs because their spatial extent and structure resemble those of oyster beds. Ferrario et al. (2014) presented the results of 255 studies on coral reefs and showed that they

decreased wave energy by 97% and wave heights by 84%. None of these studies, however, quite captures how natural oyster beds behave (which can be as extensive as coral reefs but with different material and structural properties). Therefore, information on how natural oyster beds affect wave heights and coastal erosion is needed.

Using oyster beds as breakwaters in New York Harbor is particularly appealing because, historically, this area once had extensive beds. Prior to European settlement, oyster reefs were extensive in the Hudson-Raritan estuary, with beds that followed most of its shoreline (Mitchell, 1951). However, these beds were severely overfished shortly following European colonization, and made evident with the passage of an ordinance in 1658 CE prohibiting oyster harvesting around Manhattan (O'Callaghan, 1868). Despite these efforts the natural beds in the Hudson-Raritan estuary were nearly depleted by the 1820's, at which time New York City began importing "oyster seed" from Virginia in an attempt to replace the dwindling native population (Ingersoll, 1881; Mitchell, 1951; McCay, 1998).

Sediments from coastal ponds can provide natural archives for the occurrence and severity of past storm-induced flooding (e.g. Woodruff et al., 2008a; Wallace et al., 2009; Brandon et al., 2013). In turn, these sedimentary archives provide the means for assessing how extreme wave conditions and resulting overwash deposition by storms in New York City and Harbor may potentially have been altered by man-made activities, including the overharvesting of oysters following European settlement. Towards this end we present here a new millennial-scale reconstruction of event deposition from Seguine Pond. To further assess regional coherence, we also provide additional and complimentary reconstructions of storm-induced overwash from two coastal ponds adjacent to Seguine Pond. Finally, we present results of a numerical modeling experiment that quantitatively assesses the magnitude to which oyster bed degradation could have impacted hurricane-induced wave conditions near our sites.

**4.3 Field Site**

Our study focuses on three adjacent coastal ponds/lakes located on the southern coast of Staten Island (Figure 4.1). This coast forms the northern border of Raritan Bay, a west-ward tapering, wedge-shaped embayment that is particularly susceptible to hurricane flooding (Coch, 1994). The Harbor Hill terminal moraine which was deposited during the Last Glacial Maximum about 20,000 years ago (Borns, 1973; Soren, 1988) is the major geomorphic feature controlling this coast's shape. The sediments in this moraine are derived primarily from the erosion of Triassic "red beds" to the north of the site (Sanders, 1974; Soren, 1988). Due to their enrichment in hematite, these moraine sediments are distinctively red in color.

The study's three coastal ponds are all likely formed by drowned fluvial valleys carved in the moraine and later separated from the ocean by small barrier beaches (Brandon et al., 2014). Seguine Pond is the most northeasterly of the three sites; Arbutus Lake lies about 0.6 km to the southwest of Seguine Pond and Wolfe's Pond lies ~1.3 km to the southwest of Arbutus Lake. Historical records support a stable barrier at Seguine Pond over the past few centuries (Brandon et al., 2014), but indicate that the barrier at Arbutus Lake and Wolfe's Pond have undergone some modifications. Most significant changes appear to have occurred in the late 19$^{th}$ and 20$^{th}$ centuries and thus significantly later than initial European settlement. Early historical maps of Arbutus Lake indicate a man-made groin present since at least 1890 CE (Bien and Vermeule, 1890) which likely resulted in a gradual widening of the barrier following its construction. Primary human modifications to Wolfe's Pond begin with a dam/seawall that was constructed in 1933 CE specifically to reduce the connection between the pond and the ocean (Day, 2007), followed by the raising of the berm in the 1950s, 1995 and 2011 after severe flooding of the barrier by three separate storm events (Stein, 2011).

Due to anthropogenic changes at Wolfe's Pond and Arbutus Lake, our initial, analysis focuses on Seguine Pond. This site has proven to be a reliable recorder of overwash deposition for storm surges exceeding 2 m at the Battery for at least the last ~200 years (Brandon et al., 2014). We then compliment this Seguine reconstruction with records from Arbutus Lake and Wolfe's Pond, whose barriers appear to have remained relatively untouched up until the late 19$^{th}$ century.

## 4.4 Methods

### 4.4.1 Field Work and Laboratory Analyses

The Seguine Pond cores presented in Brandon et al. (2014) were relatively short and unable to constrain relative flood magnitudes for events prior to 1800 CE. As a result the site was revisited and a longer core was extracted from the primary core site (SG2) using a vibra-core system. Cores were also collected from the Arbutus and Wolfe's sites using a combination of piston-push and vibra-coring (Figure 4.1), following methods similar to Brandon et al. (2014). All of the primary cores for each site were driven to the point of refusal in a basal unit of glacial material, with total respective core lengths of 5.5 m, 6.5 m and 5.0 m for Seguine, Arbutus and Wolfe's.

Once back in the lab all cores were initially split and then scanned on an ITRAX Core Scanner to obtain down-core profiles of magnetic susceptibility (5 mm resolution) and x-radiograph images (0.5 mm resolution). Magnetic susceptibility is used to reveal the relative abundance of elements that are responsive to induced magnetic fields, including iron-rich minerals like hematite that are abundant within the glacial moraine that forms the coastal escarpments of Staten Island's south shore (Smith, 1916). Density variations in the cores are revealed by the inverted x-radiograph with lighter areas in the image corresponding to greater

density. Storm layers typically appear as thin, white layers in these images, interbedded within lower density muds that appear dark in the x-radiographs (e.g. Brandon et al., 2014; Woodruff et al., 2015). High resolution optical images of all cores were also obtained with a GeoTek multi-scanner core logger at a resolution of 0.1 mm. Once identified, storm layers from the primary field site (Seguine Pond) were subsampled at 1 cm intervals, combusted, and sieved at 63 µm to assess organic content and percent coarse, following methods described in Brandon et al. (2014).

Chronologies for the primary core from each of the three field sites were constructed using common dating techniques including depth profiles of cesium-137 ($^{137}$Cs) and industrial associated heavy metals, as well as discrete radiocarbon ($^{14}$C) activities. All cores also contained a surficial event layer associated with overwash from Hurricane Sandy (Brandon et al., 2014) with the base of this storm deposit assigned an age of 2012 CE. $^{137}$Cs appears worldwide in the sediment record starting in 1954 CE, when atmospheric nuclear weapons tests began, and peaks in 1963 CE, just prior to the signing of the Nuclear Test Ban Treaty (Pennington et al., 1973). Bulk lead (Pb) and zinc (Zn) concentrations increase greatly in sediments from the northeast United States starting between 1850 CE and 1900 CE (e.g. Woodruff et al., 2013a; Brandon et al., 2014), with $^{14}$C dating used to obtain the ages of older sediments. Depth-to-age models and associated uncertainties at each site were obtained using the Bayesian approach described by Brandon et al. (2014) and Woodruff et al. (2015), and bounded by the above described age constraints.

### 4.4.2 Modeling

We use the coupled Advanced Circulation/Simulating Waves Nearshore (ADCIRC/SWAN) model to quantify significant wave height just offshore of our three field sites under severe storm conditions for two scenarios: 1) when oyster reefs are emplaced and 2) a control case

without oyster beds. ADCIRC is a coastal/shelf circulation, two-dimensional, vertically integrated model that solves the turbulent, incompressible Reynolds equations, simplified using the Boussinesq and hydrostatic pressure approximations (Luettich et al., 1992). SWAN is a spectral wave model that simulates both waves and currents in the nearshore, including the surf zone, and models such processes as wave generation, propagation, dissipation, and non-linear wave-wave interactions (Ris et al., 1994; Booij et al., 1996).

We explore the effects of oyster beds on significant wave height near shore to our sites by driving the model with wind and atmospheric pressure data from a severe nor'easter that occurred on December 12, 1992 CE. The 1992 Nor'easter produced the region's third highest storm tide in the past century (Talke et al. 2014), and is more typical of severe flood events impacting the region when compared to Hurricane Sandy, whose track and corresponding impact angle was extremely rare (Hall and Sobel, 2013).

Meteorological conditions for the nor'easter were obtained from OceanWeather Inc. and are in the form of a reanalysis described by Cardone et al. (1996). Validation of the 1992 Nor'easter's modeled storm tide compared to observations was carried out using data from NOAA's tide gauge at the Battery in New York City, and showed excellent agreement with a RMS error of 0.15 m. The model was run using the FEMA Region II, unstructured numerical grid (FEMA, 2014) with enhanced resolution (up to 70 m) in the New York/New Jersey area. This grid contains bathymetry and shore topographic information, including varying onshore bottom roughness based on land-use data. The model was extensively validated for the FEMA (2014) study and applied in another study that simulated waves and storm tides of future flood zones with sea level rise (Orton et al. 2015). Simulations were run both with and without oyster reefs.

Oyster reefs were added to the model at all locations in western and southern Raritan Bay with water depths between 1 and 6 m, roughly corresponding to areas of historical oyster

beds (Mount and Page, 1784-1794). Further confidence in these depth ranges is given by similar ranges of modern oyster beds in Chesapeake Bay (Hargis and Haven, 1999). Reef heights were modeled as a 1 m increase in seabed elevation; however, since reefs generally extend vertically to mean low water (Hargis and Haven, 1999), this is most likely an extremely conservative estimate of their true heights prior to disruption. A Mannings-n value of 0.035 was used in the modeling to represent the roughness-induced drag of the oysters on water currents and waves. Since no coefficients are available for oyster reefs, a value corresponding to equivalently-sized river cobbles (2.5-5 inch or 6.4-12.7 cm) was used instead (Bray, 1979). This is again a fairly conservative estimate of the actual roughness, as oysters are more irregularly shaped and have rougher surfaces than cobbles in rivers.

## 4.5 Results

### 4.5.1 Seguine Pond

The Seguine Pond sediment record exhibits a distinct change in color, magnetic susceptibility (MS), and %coarse data (Transition A in Figure 4.2). Red sediments extend from the top of the core down to ~200 cm where they transition to gray (Figure 4.2). Deeper, older gray sediments contain intact and broken oyster shells, which are absent within the younger, more surficial reddish sediments (Figure 4.2). The transition in color at ~200 cm was accompanied by an increase in the background MS, suggesting an increase in the amount of iron-bearing minerals within surficial sediments (Thompson and Morton, 1979).

Coarse grained event deposits are prevalent within the top unit of sediment compared to a near absence of deposits below Transition A. Hurricane Sandy's deposit is at the surface of the core and corresponds to a peak in MS. Prior analysis by Brandon et al. (2014) indicates that all other post-1840 CE hurricanes that produced storm surges in excess of 2 m (as measured in

the Battery Park tide gauge record; Talke et al., 2014) are also present in the sediment record, with new MS data presented here indicating accompanied peaks in MS (Figure 4.2). In particular, a prominent deposit located just below the 1850-1900 CE onset of heavy metals is consistent with an extremely damaging hurricane in 1821 CE, the only storm in the historic period that likely produced a larger storm surge than Hurricane Sandy (Redfield, 1831; Brandon et al., 2014). Each storm deposit post-1800 CE corresponds to a peak in MS, which supports these MS peaks as a reliable proxy of storm-induced overwash deposition. Below the 1821 CE deposit, the depth profile of %coarse and MS both exhibit a gradual, generally monotonic reduction in peak magnitude and number of coarse layers down to Transition A; below which a near absence of distinguishable event layers exists.

$^{14}$C samples extracted from the core provide additional age constraints on the timing of Transition A, as well as an approximate age for the first substantial overwash layer observed above this transition at 160 cm (Figure 4.2). Results are presented in Table 4.1 and Figure 4.3A. The sample collected just below Transition A yields an age range of 1463 to 1616 CE, indicating that the transition occurred sometime shortly following. The first substantial deposit above this age constraint occurs at a depth of 160 cm, with an estimated median age of ~1690 CE based on the depth-to-age model presented in Figure 4.2D. The first significant historical hurricane known to have impacted the New York City region was in 1693 CE (Ludlum, 1963), and is consistent with the age of this first significant deposit at 160 cm.

There is a near absence of coarse grained deposits below Transition A down to the depth of basal sediments at ~530 cm depth (Transition B in Figure 4.2), and dating to ~3000 yrs. BP based on the radiocarbon date obtained ~30 cm above this transition (Figure 4.2). Below Transition B, basal materials are evident as an increase in %coarse material. An increase in

background MS is also observed, but this increase is more subtle than at Transition A and is not accompanied by a significant change in sediment color.

### 4.5.2 Arbutus Lake and Wolfe's Pond

Modern age constraints for the Arbutus Lake chronology begin with base of the Hurricane Sandy layer at 1 cm, followed by the peak in $^{137}$Cs activity at 24 cm, the onset of $^{137}$Cs activity at 29 cm, and the onset of industrial pollution at 49 cm (Figure 4.3B). All are consistent with slower modern rates of deposition compared to Seguine Pond. Six $^{14}$C dates were taken from the Arbutus core (Table 4.1) and provide an age constraint just above the basal unit between 3600 and 3800 yrs. BP. This basal data is older yet still similar to that observed at Seguine Pond (~3000 yrs. BP), and is consistent with barrier beaches at both sites being initiated sometime between 3000 and 4000 yrs. BP.

The modern part of the Wolfe's Pond chronology is constrained by the base of the Hurricane Sandy layer at 3 cm and the onset of industrial pollution at 28 cm. Two additional $^{14}$C samples (Table 4.1) extend the chronology to the early part of the historic record and indicate similar, albeit somewhat slower modern deposition rates than at Arbutus Lake. Sediments extend down to basement material at ~500 cm and at a slightly shallower depth than Arbutus Lake. No dating was performed at the base of the Wolfe's Pond core, however, its extension into basement material at a depth just above that observed at Arbutus Lake, coupled with modern chronological constraints that indicate a slightly slower deposition rate, support a similar time of barrier initiation as Arbutus Lake, and in turn Seguine Pond of between 3000 and 4000 yrs BP.

Similar to Seguine Pond, a marked increase in background MS is observed above ~96 cm in Arbutus Lake and ~80 cm in Wolfe's Pond. This transition is accompanied just above by a transition to larger peaks in MS that correlate to individual overwash layers, including a surficial

layer at both sites directly linked to deposition from Hurricane Sandy. A transition in color and lithology is also observed that is similar to that at Seguine Pond, with dark muds gradually transitioning to more reddish sediments above a depth of 96 cm and 80 cm in Arbutus Lake and Wolfe's Pond, respectively. Both background levels of MS, as well as distinct peaks in MS, continue to increase most rapidly above this color transition up to a depth of 53 cm and 44 cm for Arbutus Lake and Wolfe's Pond, respectively, with this rapid rise in MS and accompanied transition towards more reddish sediments dating to a period between 1600 CE and 1800 CE at both sites (Figure 4.3).

### 4.5.3 Numerical Simulations

The numerical modeling results for the 1992 Nor'easter in Raritan Bay are presented in Figure 4.4, showing the storm's peak significant wave height. The control simulation (i.e. without oyster beds) produced 2.2 m high waves just offshore of Seguine Pond, compared to highs of 1.6 m for the case with oyster beds included. Thus, a ~30% reduction in wave height is observed. As mentioned earlier, simulations with oyster beds are rather conservative, both because: 1) the employed cobble derived roughness coefficient is likely smaller than for oyster beds and 2) pre-European reefs were often very large and intertidal, thus likely exceeding the 1 m elevation change used in the simulation (Hargis and Haven, 1999). Regardless, our conservative simulations still support a measurable reduction in near-shore wave activity due to off-shore dissipation by emplaced oyster reefs.

An increase in nearshore wave energy after reef removal is consistent with an increase in the sediment transport capacity by flooding waters during barrier inundation (Soulsby, 1997), and in turn an increase in the amount and extent of overwashing sediments that would be deposited and preserved as event deposits within the site's backbarrier ponds.

**4.6 Discussion**

Cores from all three sites show contemporaneous trends in deposition beginning with the transition from basal sediments to lacustrine mud between 3000 and 4000 yrs. BP. This is followed by a much more recent reddening of fine grained mud and a corresponding rise in background MS just following the1600's; as well as an increase in the number and magnitude of peaks in MS associated with storm induced overwash events beginning with the 1693 CE hurricane and stabilizing at substantially greater values near the timing of the 1821 Hurricane.

The onset of backbarrier sediments following ~3000 yrs. BP is consistent with the stabilization and/or reduced transgression of barrier beaches at each of the three sites following nearly an order of magnitude drop in rates of regional sea-level rise (Miller et al., 2013). Backbarrier marsh and pond cores from the southern coasts of Long Island (Scileppi and Donnelly, 2007) and New Jersey (Donnelly et al., 2004) suggest a similar timing for barrier beach stabilization and/or reduced transgression. The ~3000 yrs. BP initiation or transition to a more stable barrier is almost certainly due to natural causes; however, it is noteworthy considering projected rates of sea-level rise in the oncoming century will reach or exceed those experienced prior to 3000 yrs. BP when sedimentary shorelines appear to have been far less stable relative to present (Woodruff et al., 2013b).

One possible explanation for the lack of overwash deposits between ~3000 yrs. BP and ~350 yrs. BP could be a millennial-scale decrease in hurricane frequency. While the Scileppi and Donnelly (2007) and Donnelly et al. (2004) studies found periods of decreased hurricane activity from 250-900 yrs. BP and from 2200-2800 yrs. BP they also show an increase in activity between 2200 and 900 yrs. BP which is not captured in the overwash records from our three Staten Island field sites. Further, a new synthesis of sediment cores (Donnelly et al., in press)

demonstrates that the period between 1700 and 800 yrs. BP was a time of heightened hurricane activity across the entire western North Atlantic, including the Gulf of Mexico. Donnelly et al. (in press) also report another period of increased overwash deposition from 550 to 275 yrs. BP during which time 10 deposits are identified in Salt Pond (located in Cape Cod, Massachusetts). However, this is about 200 years earlier than the start of increased overwash activity at our three Staten Island pond sites (Figure 4.3). It seems unlikely that our site could experience no hurricane landfalls during the same 200 year period when the Salt Pond site just to the northeast experienced 10 landfalls and the Long Island sites experienced an increase in hurricane activity (Scileppi and Donnelly, 2007; Boldt et al., 2010). Therefore, the lack of overwash deposits at our site does not appear to be correlated to a regional shift in observed storm activity.

An increase in recent rates of regional sea-level rise might also explain the onset of storm-induced overwash activity at our New York Harbor field sites. Recent studies show that while sea-level rise was fairly steady for the past few thousand years, the rate of rise has increased starting around 1850 CE (Horton et al., 2013; Kemp et al., 2013). However, this increase in sea-level rise post-dates the onset for increased overwash in the late 1600's CE suggesting an additional mechanism is responsible for the initiation of substantial overwash at the site. Barrier transgression could also be a potential explanation; with the late 1600 CE onset for overwash marking the moment barriers at all three sites had migrated landward enough for overwash deposition to have occurred at each of the three coring locations. However, the cohesive terminal moraine that marks Staten Island's southern coast is less erodible than sandier coastlines along the open coasts of Long Island and New Jersey, thus likely resulting in slower rates of shoreline retreat. Further, it seems unlikely that the onset of recorded overwash

at all three core sites would be synchronous with early European colonization by chance and without a human-induced cause.

The increase in number of coarse-grained deposits does occur concurrently with documented land clearance on Staten Island (Cohen, 1987); however, the earlier work by Brandon et al. (2014) clearly shows that event deposits at the Seguine Pond site are marine derived. Evidence for their marine origin includes: 1) the correlation of all historical event deposits with hurricanes of significant storm surge including Hurricane Sandy; 2) a landward fining in grain size and decrease in thickness away from the barrier beach; and 3) photographs showing new overwash fans at Seguine Pond that were deposited by Hurricane Sandy. Additionally, stream-borne flux of sediment to the ponds are limited by the small and flat watersheds that feed them, as well as upstream interruption of sediment transport by wetlands, relic glacial depressions, and kettle ponds (Brandon et al. 2014). It is possible that European land clearance resulted in increased sediment availability that allowed barriers to form concurrently on Staten Island's south coast, however, coastal pond sediments exist at all three sites back to roughly 3000 yrs. BP, indicating that each of the sites' barriers have likely existed throughout the last few millennia.

The European disturbance and destruction of the oyster reefs offshore of Staten Island is well documented (Ingersoll, 1881; Smith 1970; Kochiss, 1974; MacKenzie, 1992; McCay, 1998; Kirby, 2004), with a date concurrent to the 1600-1800 CE transition towards increased overwash along Staten Island's south shore. Between the arrival of the Europeans and up until the early 20$^{th}$ century, New York City was famous for its oyster trade (Ingersoll, 1881; Smith, 1970; Kochiss, 1974), with Raritan Bay one of the most prominent harvest areas (Smith, 1970; Kochiss, 1974). Historic evidence, such as the increasing number of laws in the 1600's and 1700's limiting the harvesting of oysters (McCay, 1998; Kirby, 2004), suggests that natural oyster beds were

being depleted significantly over this period (Ingersoll, 1881; Smith 1970). The oyster trade survived by importing oyster seed from Virginia, but the continued decline in oyster trade strongly suggests that in terms of their distribution, these planted beds were not as extensive as the natural beds that existed prior to colonization. The decimation of the oyster population is also consistent with the decrease in abundance of oyster shell material for sediments deposited following ~1600 CE at all three sites (e.g. Figure 4.2E and 4.2F). Model simulations for a fairly conservative distribution of oyster beds also indicate a measurable decrease in significant wave height relative to current conditions (Figure 4.4). Thus model results and historical records support the depletion of oyster beds as a viable cause of the increase in overwash sedimentation beginning in the late 1600's.

**4.7 Conclusion**

In this study we utilize event deposits preserved in the sediments from a series of coastal ponds and lakes to assess the sensitivity of these sites to both natural and manmade changes. A transition from basal sediments to backbarrier lacustrine mud occurs around 3000 yrs. BP and is linked to the initiation of barrier beaches in their current form following a decrease in rates of regional sea-level rise. The second concurrent trend is an increase in the number and magnitude of storm induced overwash events beginning with the 1693 CE hurricane. Model results and historical records support that the depletion of oyster beds may have contributed to this increase in overwash sedimentation. Results highlight changes in sea-level rise and oyster reef destruction as two of the most important governors of coastline stability and overwash frequency for backbarrier environments internal to New York City's harbor system.

**4.8 Acknowledgments**

Funding for this work was provided by the Hudson River Foundation Expedited Grant #004/12E, the Hudson River Foundation Graduate Fellowship 02–13, the National Science Foundation (RAPID grant #1313859 and instrument and facility support via grant IF-0949313), and the Dalio Explore Fund. We thank H. Baranes, O. Beaulieu, B. Douglas, H. Kinney, M. Koerth, L. Kumpf, S. Madsen, C. Maio, and R. Sullivan for their laboratory and field assistance. We also thank C. Dellatte at the Staten Island Museum for her assistance with the historical research. Modeling was supported, in part, by a NOAA-RISA funded project (Consortium for Climate Risk in the Urban Northeast) and a grant of computer time from the City University of New York High Performance Computing Center under NSF Grants CNS-0855217, CNS-0958379 and ACI-1126113

Table 4.1: $^{14}C$ Sample Ages

| Sample | Sediment Depth (cm) | Material | Mass (mg) | Age ± Error ($^{14}C$ yr B. P.) | Calibrated Age Range (CE) | Probabilities |
|---|---|---|---|---|---|---|
| Arbutus | | | | | | |
| 1 | 59 | leaf | 5.8 | 385 ± 45 | 1446-1521 | 0.746 |
| | | | | | 1591-1620 | 0.254 |
| 2 | 92 | leaf | 42.8 | 335 ± 20 | 1497-1507 | 0.104 |
| | | | | | 1511-1526 | 0.166 |
| | | | | | 1556-1601 | 0.531 |
| | | | | | 1616-1632 | 0.199 |
| 3 | 127 | grass | 1.1 | 685 ± 35 | 1276-1302 | 0.699 |
| | | | | | 1367-1382 | 0.301 |
| 4 | 220 | twig? | 15.2 | 1540 ± 15 | 434-453 | 0.256 |
| | | | | | 470-487 | 0.278 |
| | | | | | 534-557 | 0.466 |
| 5 | 344.5 | twig | 10 | 2050 ± 25 | 100-36 BCE | 0.823 |
| | | | | | 30-20 BCE | 0.087 |
| | | | | | 11-2 BCE | 0.09 |
| 6 | 488 | twig | 9.9 | 2840 ± 30 | 1039-971 BCE | 0.763 |
| | | | | | 960-937 BCE | 0.237 |
| 7 | 649 | wood | 13.2 | 3450 ± 25 | 1869-1846 BCE | 0.213 |
| | | | | | 1775-1735 BCE | 0.518 |
| | | | | | 1717-1694 BCE | 0.269 |
| Seguine | | | | | | |
| 5[a] | 193 | grass | 4 | 640 ± 20 | 1295-1310 | 0.37 |
| | | | | | 1360-1387 | 0.63 |
| 6 | 204 | bark | 28.5 | 370 ± 20 | 1463-1513 | 0.73 |
| | | | | | 1600-1616 | 0.27 |
| 7 | 227 | leaf | 18.9 | 465 ± 25 | 1428-1445 | 1 |
| 8 | 242 | leaf | 14 | 715 ± 20 | 1273-1286 | 1 |
| | 356.5 | grass | 4.8 | 1980 ± 20 | 2-54 | 1 |
| | 505 | twig | 23 | 2460 ± 30 | 750-683 BCE | 0.399 |
| | | | | | 668-637 BCE | 0.138 |
| | | | | | 623-615 BCE | 0.027 |
| | | | | | 591-509 BCE | 0.395 |
| | | | | | 497-494 BCE | 0.011 |
| Wolfe's | | | | | | |
| 9 | 56 | bark | 4.7 | 155 ± 15 | 1678-1686 | 0.115 |
| | | | | | 1731-1765 | 0.531 |
| | | | | | 1773-1776 | 0.023 |
| | | | | | 1800-1808 | 0.129 |
| | | | | | 1927-1940 | 0.202 |
| 10 | 85.5 | leaf | 7.8 | 290 ± 25 | 1524-1559 | 0.595 |
| | | | | | 1564-1569 | 0.059 |
| | | | | | 1631-1649 | 0.346 |

[a] Excluded because it is anomalously old


Figure 4.1: A) The three field sites on June 17, 2010 (pre-Hurricane Sandy). Inset: Field site locations on the southern coast of Staten Island (red box). B) The three field sites on November 3, 2012 or five days after Hurricane Sandy's landfall. The colored circles indicate the position of the cores described in the text.

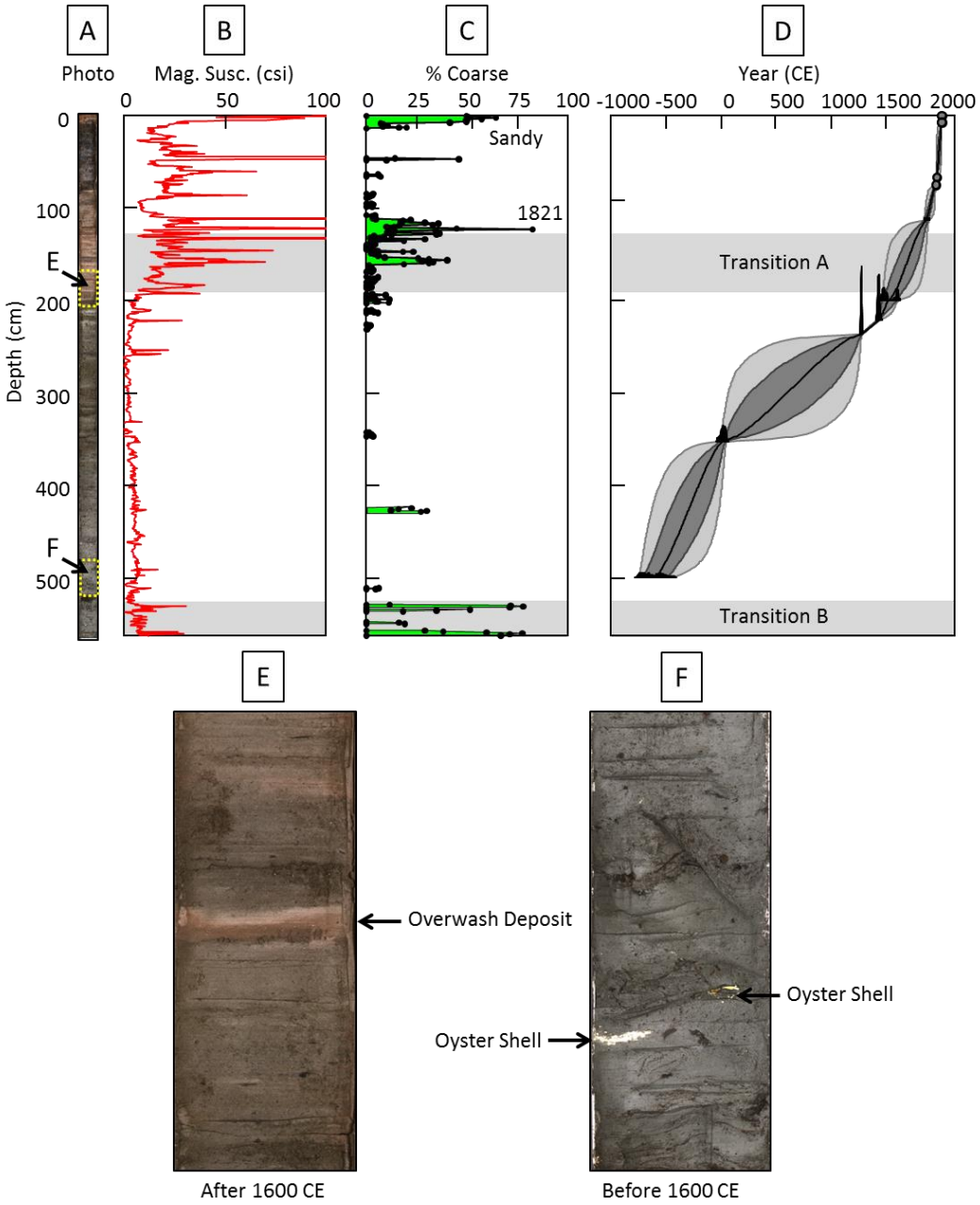


Figure 4.2: Sediment results from Seguine Pond. A) A photograph of the ~5.5 m long core. Note the transition from gray sediments to red sediments at just above 200 cm. B) Magnetic susceptibility results. Recent spikes correspond to coarse-grained overwash deposits as identified with depth profile of %coarse in C. D) Bayesian age-depth model for core. Black line denotes median ages, and dark and light shading represents 1 and 2 sigma uncertainties. E) Image of sediments from above the transition shown in A, compared to F) sediments from below the transition.

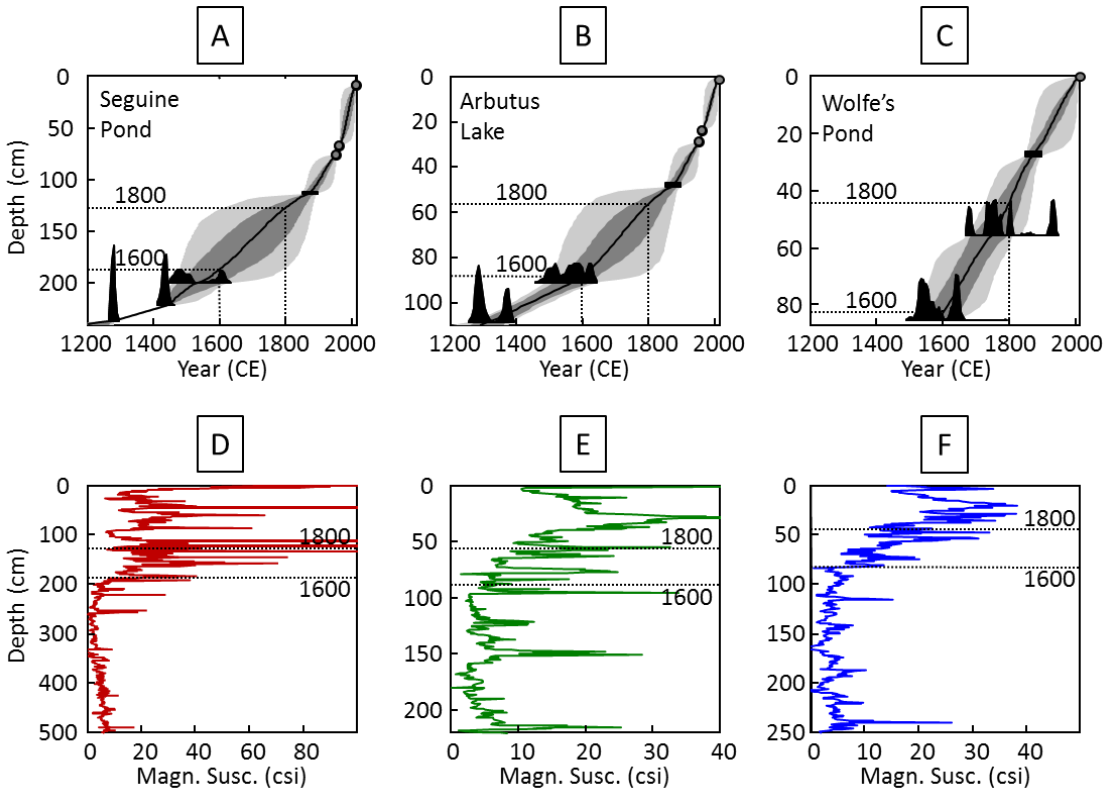


Figure 4.3: Transition A as seen in all three ponds. Chronologies of the sediments at A) Seguine Pond, B) Arbutus Lake, and C) Wolfe's Pond using a format identical to Fig. 4.2D. Dashed horizontal lines indicate depths dating to median ages of 1600 CE and 1800 CE. Magnetic susceptibility depth-profiles are shown below each site's respective age model; D) Seguine Pond, E) Arbutus Lake, and F) Wolfe's Pond.

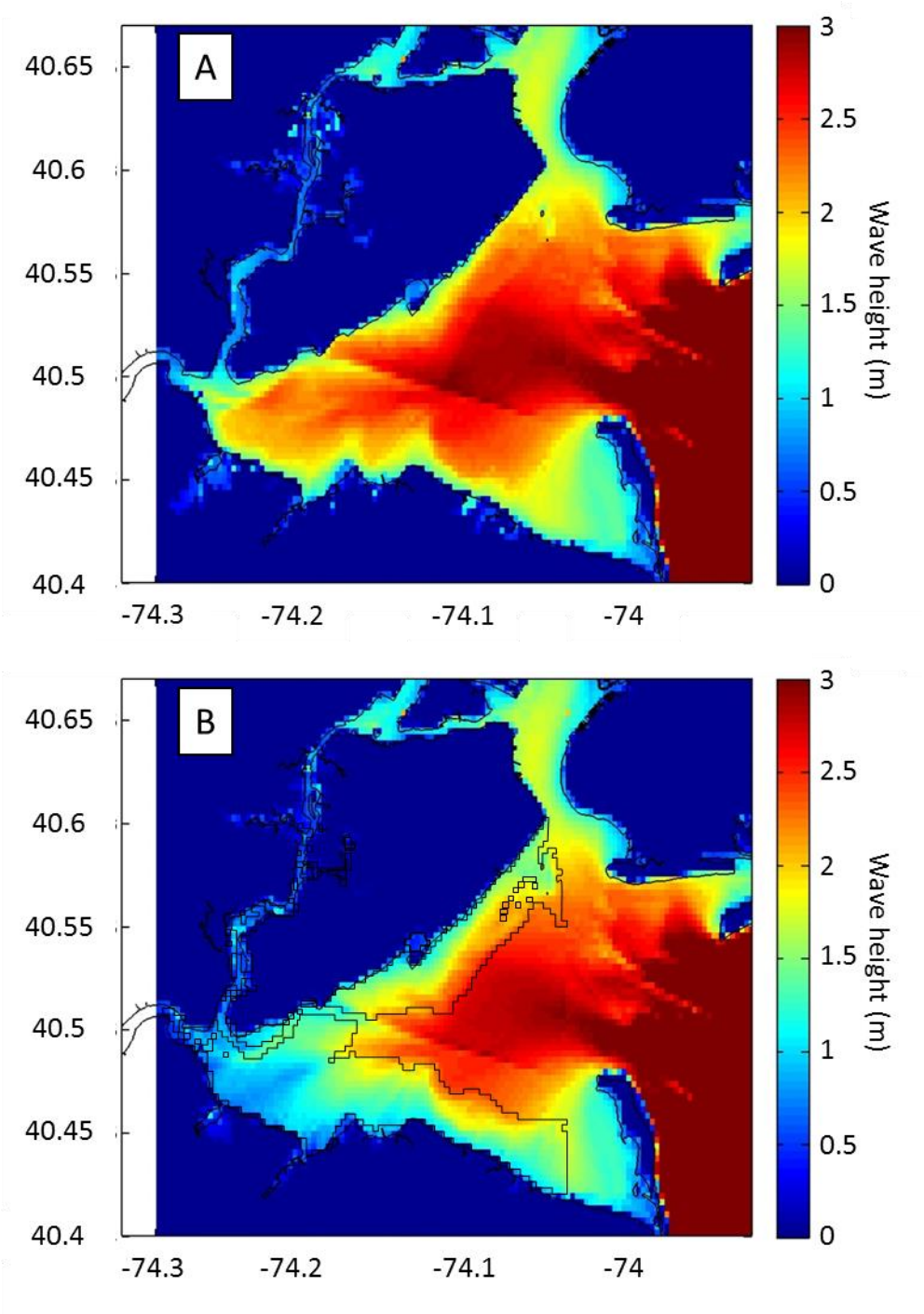


Figure 4.4: A comparison of the wave heights produced by the 1992 Nor'easter for A) present-day bathymetry and B) a hypothetical modified bathymetry where oyster beds of 1 m elevation were added to areas of the bay shallower than 6 m (black outline). Colors represent wave heights based on color scale to the right of each panel.

# CHAPTER 5

## CONCLUSION

In chapter 2 a new numerical model is presented which relates the maximum grain size in a storm surge deposit to the landfall wind speed of the hurricane which produced the surge. The constraints placed on wind speed allow the differentiation between major (≥ category 3) and minor (< category 3) hurricanes in a 2500 year long sediment record from St. Marks, FL. While the frequency of minor hurricanes remained fairly constant over this interval, the frequency of major hurricanes showed millennial-scale variations, including a period of heightened activity between 1700 and 600 yrs. BP. This corresponds to a time when the Loop Current was much closer to the field site than at present and may be responsible for sustaining hurricane strength into landfall.

Chapter 3 develops a ~300 year long record of hurricane inundation from a coastal pond on Staten Island, NY. Hurricane Sandy's overwash deposit provides a modern constraint that allows comparison with older deposits. It is found that every storm after 1840 CE that produced a ≥ 2 m surge, as well as storms in 1693, 1788, and 1821, are recorded in the sediments. In particular, a deposit produced by the 1821 Hurricane, known from historical records as the most destructive hurricane to affect New York City prior to Sandy, was found. The larger maximum grain size of its deposit suggests that it had a higher landfall wind speed than Hurricane Sandy, and indeed, SLOSH model results suggest the 1821 Hurricane was a weak category 3 storm (Sandy was a category 1 at landfall). The thickness of the two deposits was qualitatively related to the inundation periods of the storms with Sandy's thicker deposit suggesting that it had a longer inundation period than the 1821 Hurricane.

Chapter 4 describes a ~3000 yearlong reconstruction of hurricane activity from the same site as chapter 3 and presents supporting analyses from nearby sites. Two distinct transitions in

sediment color, magnetic susceptibility, and %coarse are observed in the sediments from all three sites. The first is a transition from sediments with high %coarse and magnetic susceptibility to sediments with lower values, dating to between 3000 and 4000 yrs. BP. This most likely corresponds to the reduced transgression of the barrier beach which may be related to the decrease in rates of sea-level rise at that time. The second transition occurs ~400 years ago. Older, finer gray sediments transition to younger, coarser red sediments; the background magnetic susceptibility increases; and overwash deposition begins. The color change and increase in magnetic susceptibility are most likely related to land clearance by European colonists and therefore represent an increase in input of terrestrially derived sediments to the ponds. The onset of overwash deposition is concurrent with overfishing of the offshore oyster beds between 1600 and 1800 CE. Modeling results conservatively show that the presence of oyster beds could have reduced the significant wave heights of the 1992 Nor'easter by ~30%, suggesting that oyster beds played a significant role in preventing overwash before their decimation.

This dissertation describes the wealth of information that can be learned from analyzing long records of overwash deposition at coastal sites. For example, changes in the background accumulation of sediments can reveal shifts in sediment source. Comparisons of different paleotempest records from the same region (e.g. New Jersey, Staten Island, and Long Island) can reveal patterns of local disturbances such as the overharvesting of oysters in Raritan Bay leading to increased overwash deposition on Staten Island. When paleotempest records from the entire western North Atlantic are examined, past shifts in major hurricane frequency can be linked to climatic and oceanic circulation changes. The spatial and temporal coverage of these studies is still sparse and future advances in this field will come from the addition and comparison of sediment records from new field sites.

**BIBLIOGRAPHY**


Appleby PG, Oldfield F. 1978. The calculation of lead-210 dates assuming a constant rate of supply of unsupported 210Pb to the sediment. *Catena* **5**(1): 1-8. doi:10.1016/S0341-8162(78)80002-2.

Besonen MR, Bradley RS, Mudelsee M, Abbott MB, Francus P. 2008. A 1,000-year, annually-resolved record of hurricane activity from Boston, Massachusetts. *Geophysical Research Letters 35*(14), L14705, doi: 10.1029/2008GL033950.

Bien J, Vermeule CC. 1890. Richmond County (Staten Island). Bien & Company: New York. http://www.davidrumsey.com/luna/servlet/detail/RUMSEY~8~1~25381~1020008:Richmond-Co-,-Staten-Island-?sort=Pub_List_No_InitialSort%2CPub_Date%2CPub_List_No%2CSeries_No&qvq=w4s:/where/Staten+Island+%28New+York,+N.Y.%29;sort:Pub_List_No_InitialSort%2CPub_Date%2CPub_List_No%2CSeries_No;lc:RUMSEY~8~1&mi=0&trs=9 Date of access: 12/26/2014.

Blake ES, Kimberlain TB, Berg RJ, Cangialosi JP, Beven II JL. 2013. *Tropical Cyclone Report: Hurricane Sandy*. National Hurricane Center **12** http://www.nhc.noaa.gov/data/tcr/AL182012_Sandy.pdf , Date of access: 01/05/2014.

Blum MD, Carter AE, Zayac T, Gobel R. 2002. Middle Holocene sea-level and evolution of the Gulf of Mexico coast. *Journal of Coastal Research* **36**: 65-80, ISSN/ISBN: 0749-0208.

Boldt KV, Lane P, Woodruff JD, Donnelly JP. 2010. Calibrating a sedimentary record of overwash from Southeastern New England using modeled historic hurricane surges. *Marine Geology* **275**(1-4): 127-139. doi: 10.1016/j.margeo.2010.05.002.

Booij N, Holthuijsen LH, Ris RC. 1996. The SWAN wave model for shallow water. In *Coastal Engineering 1996: Proceedings of the 25th International Conference on Coastal Engineering*, 1, Edge BL (ed). American Society of Civil Engineers; 668-676. DOI: http://dx.doi.org/10.9753/icce.v25.

Boose ER, Chamberlin KE, Foster DR. 2001. Landscape and regional impacts of historical hurricanes in New England. *Ecological Monographs* **71**: 27–48.

Borns Jr HW. 1973. Late Wisconsin fluctuations of the Laurentide ice sheet in southern and eastern New England. In *The Wisconsin Stage*, Black RF, Goldthwait RP, Williman HB (eds). GSA Memoirs **136**: Boulder; 37-45. DOI: 10.1130/MEM136-p37

Brandon CM, Woodruff JD, Lane DP, Donnelly JP. 2013. Tropical cyclone wind speed constraints from resultant storm surge deposition: A 2500 year reconstruction of hurricane activity from St. Marks, FL. *Geochemistry, Geophysics, Geosystems* **14**: 2993–3008.

Brandon CM, Woodruff JD, Donnelly JP, Sullivan RM. 2014. How unique was Hurricane Sandy? Sedimentary reconstructions of extreme flooding from New York Harbor. *Scientific Reports* **4**: 7366. DOI: 10.1038/srep07366.

Bray DI. 1979. Estimating average velocity in gravel-bed rivers. *Journal of the Hydraulics Division* **105** (HY9): 1103-1122.

Campbell MD. 2004. Analysis and Evaluation of a Bioengineered Submerged Breakwater. MSc thesis, Louisiana State University.

Cardone V, Jensen R, Resio D, Swail V, Cox A. 1996. Evaluation of contemporary ocean wave models in rare extreme events: the "Halloween Storm" of October 1991 and the "Storm of the Century" of March 1993. *Journal of Atmospheric and Oceanic Technology* **13**(1): 198-230. DOI: 10.1175/1520-0426(1996)013<0198:EOCOWM>2.0.CO;2

Chen Z, Saito Y, Kanai Y, Wei T, Li L, Yao H, Wang Z. 2004. Low concentration of heavy metals in the Yangtze estuarine sediments, China: a diluting setting. *Estuarine, Coastal, and Shelf Science* **60**(1): 91-100. doi: 10.1016/j.ecss.2003.11.021.

Cheong SM, Silliman B, Wong PP, van Wesenbeeck B, Kim CK, Guannel G. 2013. Coastal adaptation with ecological engineering. *Nature Climate Change* **3**: 787-791. DOI:10.1038/nclimate1854

Chouinard L, Liu C, Cooper C. 1997. Model for Severity of Hurricanes in Gulf of Mexico. *Journal of Waterway, Port, Coastal, and Ocean Engineering* **123**: 120-129, doi: 10.1061/(ASCE)0733-950X(1997)123:3(120).

Coch, NK. 1994. Hurricane hazards along the northeastern Atlantic Coast of the United States. Journal of Coastal Research, Special Issue 12: 115-147.

Cohen DS. 1987. Dutch-American Farming: crops, livestock, and equipment, 1623-1900. In *New World Dutch Studies: Dutch Arts and Culture in Colonial America, 1609-1776*, Blackburn RH, Kelley NA (eds). Albany Institute of History and Art: Albany; 185-200.

Croudace IW, Rindby A, Rothwell RG. 2006. ITRAX: description and evaluation of a new multi-function X-ray core scanner. In *New Techniques in Sediment Core Analysis*, Rothwell RG (ed). Geological Society of London Special Publication **267**: London; 51-63.

Davis RE, Dolan R. 1993. Nor'easters. *American Scientist* **81**: 428-439.

Day L. 2007. Field Guide to the Natural World of New York City. The Johns Hopkins University Press: New York.

Dean RG, Chen R, Browder AE. 1997. Full scale monitoring study of a submerged breakwater, Palm Beach, Florida, USA. *Coastal Engineering* **29**: 291–315. DOI:10.1016/S0378-3839(96)00028-2

Denommee KC, Bentley SJ, Droxler AW. 2014. Climatic controls on hurricane patterns: a 1200-y near-annual record from Lighthouse Reef, Belize. *Scientific Reports* **4**: 3876. doi: 10.1038/srep03876

Donnelly JP, Bertness MD. 2001. Rapid shoreward encroachment of salt marsh cordgrass in response to accelerated sea-level rise. *Proceedings of the National Academy of Sciences* **98**(25): 14218-14223. doi: 10.1073/pnas.251209298.

Donnelly JP, Bryant SS, Butler J, Dowling J, Fan L, Hausmann N, Newby P, Shuman B, Stern J, Westover K. 2001a. 700 yr sedimentary record of intense hurricane landfalls in southern New England. *Geological Society of America Bulletin* **113**(6): 714-727.

Donnelly JP, Roll S, Wengren M, Butler J, Lederer R, Webb III, T. 2001b. Sedimentary evidence of intense hurricane strikes from New Jersey. *Geology* **29**(7): 615-618.

Donnelly JP, Butler J, Roll S, Wengren M, Webb T. 2004. A backbarrier overwash record of intense storms from Brigantine, New Jersey. *Marine Geology* **210**(1): 107-121.

Donnelly CK, Kraus N, Larson NM. 2006. State of knowledge of measurement and modeling of coastal overwash. *Journal of Coastal Research* **22**: 965-991.

Donnelly JP, Woodruff JD. 2007. Intense hurricane activity over the past 5,000 years controlled by El Niño and the West African monsoon. *Nature* **447**(7143): 465-468. doi: 10.1038/nature05834.

Donnelly JP, Giosan L. 2008. Tempestuous highs and lows in the Gulf of Mexico. *Geology* **36**(9): 751-752.

Donnelly C, Hanson H, Larson M. 2009. A numerical model of coastal overwash. *Proceedings of the Institution of Civil Engineering-Maritime Engineering* **162**: 105-114.

Donnelly JP, Hawkes AD, Lane P, MacDonald D, Shuman BN, Toomey MR, van Hengstum PJ, Woodruff JD. In press. Climate forcing of unprecedented intense-hurricane activity in the last 2,000 years. *Earth's Future*.

Dukhovskoy DS, Morey SL. 2011. Simulation of the Hurricane Dennis storm surge and considerations for vertical resolution. *Natural Hazards* **58**(1): 511-540.

Elsner JB, Jagger TH, Liu K. 2008. Comparison of hurricane return levels using historical and geological records. *Journal of Applied Meteorology and Climatology* **47**(2): 368-374.

Emanuel KA. 1986. An air-sea interaction theory for tropical cyclones. Part I: steady-state maintenance. *Journal of the Atmospheric Sciences* **43**(6): 585–605. doi: http://dx.doi.org/10.1175/1520-0469(1986)043<0585:AASITF>2.0.CO;2

Emanuel KA. 1988. The maximum intensity of hurricanes. *Journal of the Atmospheric Sciences* **45**(7): 1143-1155.

Emanuel KA, DesAutels C, Holloway C, Korty R. 2004. Environmental control of tropical cyclone intensity. *Journal of the Atmospheric Sciences* **61**(7): 843-858.

Emanuel KA, Ravela S, Vivant E, Risi C. 2006. A statistical deterministic approach to hurricane risk assessment. *Bulletin of the American Meteorological Society* **87**(3), 299-314.

Faure G. 1986. *Principles of Isotope Geology.* J. Wiley: New York. ISSN/ISBN: 0471864129 9780471864127.

Federal Emergency Management Agency (FEMA). 2014. Redefinition of the Coastal Flood Hazard Zones in FEMA Region II: Analysis of the Coastal Storm Surge Flood Frequencies, Fairfax, VA. https://www.rampp-team.com/documents/region2/storm_surge/Supporting%20Documents%202011_11_10.pdf Date of access: 01/05/15.

Ferguson RI, Church M. 2004. A simple universal equation for grain settling velocity. *Journal of Sedimentary Research* **74**: 933-937.

Ferrario F, Beck MW, Storlazzi CD, Micheli F, Shepard CC, Airoldi L. 2014. The effectiveness of coral reefs for coastal hazard risk reduction and adaptation. *Nature Communications* **5**: 3794. DOI:10.1038/ncomms4794

Frappier AB, Sahagian D, Carpenter SJ, González LA, Frappier BR. 2007. Stalagmite stable isotope record of recent tropical cyclone events. *Geology* **35**(2): 111-114.

Garin J. *et al*. 2009. Bluebelt beginnings – green preserves blue on Staten Island. *Clear Waters* **39**: 10-20.

Gehrels WR, Kirby JR, Prokoph A, Newnham RM, Achterberg EP, Evans H, Black S, Scott DB. 2005. Onset of recent rapid sea-level rise in the western Atlantic Ocean. *Quaternary Science Reviews* **24**(18): 2083-2100.

Goni G, Trinanes J. 2003. Ocean thermal structure monitoring could aid in the intensity forecast of tropical cyclones. *Eos* **84**(51): 573-580.

Graham HE, Hudson GN. 1960. National Hurricane Research Project Report No. 39: Surface winds near the center of hurricanes (and other cyclones). *U. S. Department of Commerce*.

Gray HL, Odell PL. 1973. *Probability for Practicing Engineers.* Barnes & Noble: New York.

Hall TM, Sobel AH. 2013. On the impact angle of Hurricane Sandy's New Jersey landfall. *Geophysical Research Letters* **40** (10): 2312-2315. DOI: 10.1002/grl.50395

Hargis WJ, Haven DS. 1999. Chesapeake oyster reefs, their importance, destruction and guidelines for restoring them. In *Oyster Reef Habitation Restoration: A synopsis and Synthesis of Approaches*, Luckenbach MW, Mann R, Wesson JA (eds). Virginia Institute of Marine Science Press: Gloucester Point; 329-358.

Haslett J, Parnell A. 2008. A simple monotone process with application to radiocarbon-dated depth chronologies. *Journal of the Royal Statistical Society C-Applied Statistics* **57**: 399-418.

Hauck-Lawson A, Deutsch J. 2009. *Gastropolis: Food and New York City.* Columbia University Press: New York. ISBN: 978-0-231-51006-6

Haug GH, Hughen KA, Sigman DM, Peterson LC, Röhl U. 2001. Southward migration of the Intertropical Convergence Zone through the Holocene. *Science* **293**(5533): 1304-1308.

Herman PMJ, Middleburg JJ, Van de Koppel J, Heip CHR. 1999. Ecology of Estuarine Macrobenthos. In *Advances in Ecological Research: Estuaries*, Nedwell DB, Raffaelli DG (eds). Academic Press **29**: Cornwall; 196-240. DOI:10.1016/S0065-2504(08)60194-4

Hine AC, Belknap DF, Hutton JG, Osking EB, Evans MW. 1988. Recent geological history and modern sedimentary processes along an incipient, low-energy, epicontinental-sea coastline: northwest Florida. *Journal of Sedimentary Research* **58**(4): 567-579.

Hondula, DM, Dolan R. 2010. Predicting severe winter coastal storm damage, *Environmental Research Letters* **5**: 034004. DOI: 10.1088/1748-9326/5/3/034004

Horton BP, Engelhart SE, Hill DF, Kemp AC, Nikitina D, Miller KG, Peltier WR. 2013. Influence of tidal-range change and sediment compaction on Holocene relative sea-level change in New Jersey, USA. *Journal of Quaternary Science* **28**: 403–411. DOI: 10.1002/jqs.2634

Ingersoll E. 1881. The Oyster Industry. In *The History and Present Condition of the Fisheries Industry* Baird SF, Goode GB (eds). Government Printing Office: Washington D. C.

Irish JL, Resio DT, Ratcliff JJ. 2008. Influence of storm size on hurricane surge. *Journal of Physical Oceanography* **38**: 2003-2013.

Irish JL, Youn KS, Chang K -A. 2011. Probabilistic hurricane surge forecasting using parameterized surge response functions. *Geophysical Research Letters* **38**: L03606.

Jelesnianski CP, Chen J, Shaffer WA. 1992. *SLOSH: Sea, Lake, and Overland Surges from Hurricanes*. US Department of Commerce, National Oceanic and Atmospheric Administration, National Weather Service. <http://slosh.nws.noaa.gov/sloshPub/pubs/SLOSH_TR48.pdf>, Date of access: 15/04/2014.

Julien PY, Wargadalam J. 1995. Alluvial channel geometry: theory and applications. *Journal of Hydraulic Engineering* **121**(4): 312-325.

Kemp AC, Horton BP. 2013. Contribution of relative sea-level rise to historical hurricane flooding in New York City. *Journal of Quaternary Science* **28,** 537-541.

Kemp AC, Horton BP, Vane CH, Bernhardt CE, Corbett DR, Engelhart SE, Anisfeld SC, Parnell AC, Cahill N. 2013. Sea-level change during the last 2500 years in New Jersey, USA. *Quaternary Science Reviews* **81**: 90–104. DOI: 10.1016/j.quascirev.2013.09.024

Kirby MX. 2004. Fishing down the coast: historical expansion and collapse of oyster fisheries along continental margins. *Proceedings of the National Academy of Sciences* **101** (35): 13096-13099. DOI: 10.1073/pnas.0405150101.

Kirwan ML, Murray AB, Donnelly JP, Corbett DR. 2011. Rapid wetland expansion during European settlement and its implication for marsh survival under modern sediment delivery rates*. Geology* **39***:* 507–510*.* DOI:10.1130/G31789.1

Kochiss JM. 1974. Oystering from New York to Boston. Wesleyan University Press: Middletown.

Koide M, Bruland KW, Goldberg ED. 1973. Th-228/Th-232 and Pb-210 geochronologies in marine and lake sediments. *Geochimica et Cosmochimica Acta* **37**(5): 1171-1187.

Landsea CW, Anderson C, Charles N, Clark G, Dunion J, Fernandez-Partagas J, Hungerford P, Neumann C, Zimmer M. 2004. The Atlantic hurricane database re-analysis project: Documentation for the 1851-1910 alterations and additions to the HURDAT database*.* In *Hurricanes and Typhoons: Past, Present and Future*, Murnane RJ, Liu K-b (eds). Columbia University Press: New York; 177-221.

Lane DP. 2011. *Late Holocene hurricane activity and climate variability in the Northeastern Gulf of Mexico*, PhD dissertation, Dept. of Earth, Atmospheric and Planetary Sciences, Massachusetts Institute of Technology, Cambridge, Massachusetts

Lane P, Donnelly JP 2012. Hurricanes and typhoons: will tropical cyclones become stronger and more frequent? *PAGES newsletters* **20**(1): 33.

Lane P, Donnelly JP, Woodruff JD, Hawkes AD. 2011. A decadally-resolved paleohurricane record archived in the late Holocene sediments of a Florida sinkhole. *Marine Geology* **287**(1-4): 14-30.

Lin N, Emanuel KA, Oppenheimer M, Vanmarcke E. 2012. Physically based assessment of hurricane surge threat under climate change. *Nature Climate Change* **2**: 462-467.

Liu KB, Fearn ML. 1993. Lake-sediment record of late Holocene hurricane activities from coastal Alabama. *Geology* **21**(9): 793-796.

Liu K, Fearn ML. 2000. Reconstruction of prehistoric landfall frequencies of catastrophic hurricanes in northwestern Florida from lake sediment records. *Quaternary Research* **54**(2): 238-245.

Lough JM. 2007. Tropical river flow and rainfall reconstructions from coral luminescence: Great Barrier Reef, Australia. *Paleoceanography* **22**(2): PA2218.

Ludlum DM. 1963. *Early American Hurricanes*. American Meteorological Society: Boston.

Luettich RA, Westerink AA, Scheffner, NW. 1992. ADCIRC: An advanced three-dimensional circulation model for shelves, coasts, and estuaries Report 1: Theory and methodology of

ADCIRC-2DDI and ADCIRC-3DL Technical report DRP-92-6. U. S. Army Corps of Engineers. http://www.dtic.mil/dtic/tr/fulltext/u2/a261608.pdf Date of access: 12/26/14.

Lund DC, Curry WB. 2004. Late Holocene variability in Florida Current surface density: Patterns and possible causes. *Paleoceanography* **19**(4): PA4001.

MacKenzie CL. 1992. The Fisheries of Raritan Bay. Rutgers University Press: New Brunswick. ISBN: 978-0813518404

Malmquist D. 1997. Oxygen isotopes in cave stalagmites as a proxy record of past tropical cyclone activity. 22nd Conference on Hurricanes and Tropical Meteorology, American Meteorological Society: Fort Collins.

Mann ME, Woodruff JD, Donnelly JP, Zhang Z. 2009. Atlantic hurricanes and climate over the past 1,500 years. *Nature* **460**(7257): 880-883.

McCay B. 1998. Oyster Wars and the Public Trust: Property, Law, and Ecology in New Jersey History. The University of Arizona Press: Tuscon. ISBN: 0-8165-1804-1.

Meyer-Peter E, Müller R. 1948. Formulas for bed-load transport. Proceedings of the 2nd Meeting of the International Association for Hydraulic Structures Research: 39-64.

Miller DL, Mora CI, Grissino-Mayer HD, Mock CJ, Uhle ME, Sharp Z. 2006. Tree-ring isotope records of tropical cyclone activity. *Proceedings of the National Academy of Sciences* **103**(39): 14294-14297.

Miller KG, Kopp RE, Horton BP, Browning JV, Kemp AC. 2013. A geological perspective on sea-level rise and its impacts along the U.S. mid-Atlantic coast. *Earth's Future* **1**: 3-18. DOI: 10.1002/2013EF000135.

Milliken K, Anderson JB, Rodriguez AB. 2008. A new composite Holocene sea-level curve for the northern Gulf of Mexico. In *Response of Gulf Coast Estuaries to Sea-Level Rise and Climate Change, Geological Society of America, Special Paper* **443**: 1-11.

Mitchell J. 1951. The Bottom of the Harbor. The New Yorker.

Morris IK. 1898. Morris's Memorial History of Staten Island New York. Memorial Publishing Company: New York. https://archive.org/details/morrissmemorialh02morr, Date of access: 12/11/14.

Morton RA, Paine JG, Blum MD. 2000. Responses of stable bay-margin and barrier-island systems to Holocene sea-level highstands, western Gulf of Mexico. *Journal of Sedimentary Research* **70**(3): 478-490.

Morton RA, Gelfenbaum G, Jaffe BE. 2007. Physical criteria for distinguishing sandy tsunami and storm deposits using modern examples. *Sedimentary Geology* **200**: 184-207.

Mount J, Page T. 1784-1794. A chart of New York Harbour : with the banks, soundings and sailing marks from the most accurate surveys & observations. http://digitalcollections.nypl.org/items/510d47da-eed7-a3d9-e040-e00a18064a99, Date of access: 12/11/14.

Murnane RJ, Barton C, Collins E, Donnelly J, Eisner J, Emanuel K, Ginis I, Howard S, Landsea C, Liu K, Malmquist D, McKay M, Michaels A, Nelson N, O'Brien J, Scott D, Webb III T. 2000. Model estimates hurricane wind speed probabilities. *Eos Transactions American Geophysical Union* **81**(38): 433-438.

National Data Buoy Center. 2014. *Station 44065 (LLNR 725) — New York Harbor Entrance — 15 NM SE of Breezy Point, NY*. http://www.ndbc.noaa.gov/station_page.php?station=44065, Date of access: 06/06/2014.

National Oceanic and Atmospheric Administration/National Weather Service. 2012. Tropical Cyclone Climatology. *National Weather Service, National Hurricane Center.* http://www.nhc.noaa.gov/climo/#returns Date of access: 28/08/2012

National Oceanic and Atmospheric Administration. 2013. *Tides & Currents*. http://tidesandcurrents.noaa.gov/waterlevels.html?id=8518750&units=standard&bdate=20121028&edate=20121030&timezone=GMT&datum=MLLW&interval=6&action=, Date of access: 13/01/2014.

Noren A J, Bierman PR, Steig EJ, Lini A, Southon J. 2002. Millennial-scale storminess variability in the northeastern United States during the Holocene epoch. *Nature* **419**(6909): 821-824.

Nott J. 2004. Paleotempestology: the study of prehistoric tropical cyclones- a review and implications for hazard assessment. *Environmental International* **30**(3): 433-447.

Nyberg J, Malmgren BA, Winter A, Jury MR, Kilbourne KH, Quinn TM. 2007. Low Atlantic hurricane activity in the 1970s and 1980s compared to the past 270 years. *Nature* **447**(7145): 698-701.

O'Callaghan EB. 1868. Laws and Ordinances of New Netherland 1638-1674. Weed, Parsons, and Company: Albany.

Ochi MK. 2005. *Ocean Waves: The Stochastic Approach.* Cambridge University Press **6**: New York.

Orton P, Vinogradov S, Georgas N, Blumberg A, Lin N, Gornitz V, Little C, Jacob K, Horton R. 2014. Chapter 4: Dynamic coastal flood modeling. In *Building the Knowledge Base for Climate Resiliency*, Rosenzweig C, Solecki W (eds). Annals of the New York Academy of Sciences: New York.

Otvos EG. 2001. Assumed Holocene Highstands, Gulf of Mexico: Basic Issues of Sedimentary and Landform Criteria: Discussion. *Journal of Sedimentary Research* **71**(4): 645-647.

Parnell AC, Haslett J, Allen JRM, Buck CE, Huntley B. 2008. A flexible approach to assessing synchroneity of past events using Bayesian reconstructions of sedimentation history. *Quaternary Science Reviews* **27**: 1872-1885.

Pennington W, Tutin T, Cambray R, Fisher E. 1973. Observations on lake sediments using fallout 137Cs as a tracer. *Nature* **242**: 324-326. doi: 10.1038/242324a0

Peterson L, Overpeck J, Kipp N, Imbrie J. 1991. A high-resolution late Quaternary upwelling record from the anoxic Cariaco Basin, Venezuela. *Paleoceanography* **6**(1): 99-119.

Piazza BP, Banks PD, La Peyre MK. 2005. The potential for created oyster shell reefs as a sustainable shoreline protection strategy in Louisiana. *Restoration Ecology* **13**: 499-506. DOI: 10.1111/j.1526-100X.2005.00062.x

Poore R, Dowsett H, Verardo S, Quinn TM. 2003. Millennial-to century-scale variability in Gulf of Mexico Holocene climate records. *Paleoceanography* **18**(2): 1048.

Poore R, Quinn T, Verardo S. 2004. Century-scale movement of the Atlantic Intertropical Convergence Zone linked to solar variability. *Geophysical Research Letters* **31**(12): L12214.

Poore RZ, DeLong KL, Richey JN, Quinn TM. 2009. Evidence of multidecadal climate variability and the Atlantic Multidecadal Oscillation from a Gulf of Mexico sea-surface temperature-proxy record. *Geo-Marine Letters* **29**(6): 477-484.

Poore RZ, Verardo S, Caplan J, Pavich K, Quinn T. 2011. Planktic foraminiferal relative abundance and trends in gulf of mexico holocene sediments: Records of climate variability. In *Gulf of Mexico: Its Origins, Waters, Biota, and Human Impact*, Buster NA, Holmes CW (eds). Geology **3**: Texas A&M University: College Station; 367-379. ISSN/ISBN: 1-60344-290-1.

Price JF. 1981. Upper Ocean Response to a Hurricane. *Journal of Physical Oceanography* **11**(2): 153–175.
doi: http://dx.doi.org/10.1175/1520-0485(1981)011<0153:UORTAH>2.0.CO;2

Puri HS, Vernon RO. 1964. *Summary of the Geology of Florida and a Guidebook to the Classic Exposures*, Special Publication **5**: Florida Geological Survey: Tallahassee.

Randazzo AF, Jones DS. 1997. *The Geology of Florida*. University Press of Florida Gainesville, Florida.

Redfield WC. 1831. Remarks on the prevailing storms of the Atlantic Coast of the North American States. *American Journal of Science* **20**: 17–51.

Reimer PJ, Bard E, Bayliss A, Beck JW, Bertrand CJH, Blackwell PG, Buck CE, Burr GS, Cutler KB, Damon PE, Edwards RL, Fairbanks RG, Friedrich M, Guilderson TP,Hogg AG, Hughen KA, Kromer B, McCormac G, Manning S, Bronk RC, Reimer RW, Remmele S, Southon JR, Stuiver M, Talamo S, Taylor FW, van der Plicht J, Weyhenmeyer CE. 2004. IntCal04 terrestrial radiocarbon age calibration, 0–26 cal kyr BP. *Radiocarbon* **46**(3): 1029-1058.

Reimer PJ, Bard E, Bayliss A, Beck JW, Blackwell PG, Bronk Ramsey C, Buck CE, Cheng H, Edwards RL, Friedrich M, Grootes PM, Guilderson TP, Haflidason H, Hajdas I, Hatté C, Heaton TJ, Hoffmann DL, Hogg AG, Hughen KA, Kasier KF, Kromer B, Manning SW, Niu M, Reimer RW, Richards DA, Scott EM, Southon JR, Staff RA, Turney CSM, van der Plicht J. 2013. IntCal13 and Marine13 radiocarbon age calibration curves 0-50,000 years cal BP. *Radiocarbon* **55**(4): 1869-1887. doi: 10.2458/azu_js_rc.55.16947

Richey JN, Poore RZ, Flower BP, Quinn TM. 2007. 1400 yr multiproxy record of climate variability from the northern Gulf of Mexico. *Geology* **35**(5): 423-426.

Ris RC, Holthuijsen LH, Booij N. 1994. A spectral model for waves in the near shore zone. Proceedings of the 24th International Conference on Coastal Engineering: Kobe; 68-78. DOI: 10.9753/icce.v24

Robbins JA, Edgington DN. 1975. Determination of recent sedimentation rates in Lake Michigan using Pb-210 and Cs-137. *Geochimica et Cosmochimica Acta* **39**(3): 285-304.

Saffir H, Simpson R. 1974. The hurricane disaster potential scale. *Weatherwise* **27**: 169-186.

Sanders JE. 1974. Geomorphology of the Hudson Estuary. In *Hudson River Colloquium* Roels OA (ed). Annals of the New York Academy of Sciences **250**: 5-38. DOI: 10.1111/j.1749-6632.1974.tb43894.x

SCAPE Landscape Architecture. 2014. Living Breakwaters: IP edition, Staten Island and Raritan Bay. http://www.rebuildbydesign.org/wordpress/wp-content/uploads/briefing/SCAPE_IP_Briefing_Book.pdf Date of access: 12/05/14.

Scileppi E, Donnelly JP. 2007. Sedimentary evidence of hurricane strikes in western Long Island, New York. *Geochemistry, Geophysics, Geosystems* **8**(6): Q06011. doi: 10.1029/2006GC001463

Scyphers SB, Powers SP, Heck KL, Byron D. 2011. Oyster reefs as natural breakwaters mitigate shoreline loss and facilitate fisheries. *Public Library of Science ONE* **6**: e22396. DOI: 10.1371/journal.pone.0022396

Shaw J, You Y, Mohrig D, Kocurek G. 2014. Tracking hurricane-generated storm surge with washover fan stratigraphy. *Geology*, online, doi: 10.1130/G36460.1

Smith TT. 1916. The magnetic properties of hematite. *Physical Review* **8**(6): 721-738. doi: http://dx.doi.org/10.1103/PhysRev.8.721

Smith DV. 1970. Staten Island: Gateway to New York. Chilton Book Company: Philadelphia.

Soren J. 1988. *Geologic and geohydrologic reconnaissance of Staten Island, New York U.S. Geologic Survey, Water-Resources Investigations Report 87-4048*. http://pubs.usgs.gov/wri/1987/4048/report.pdf, Date of access: 06/01/2014.

Soulsby R. 1997. *Dynamics of Marine Sands: A Manual for Practical Applications*. Thomas Telford: London. ISBN: 978-0-7277-2584-X.

Sriver RL, Huber M. 2007. Observational evidence for an ocean heat pump induced by tropical cylones. *Nature* **447**: 577-580. doi:10.1038/nature05785

Stapor Jr FW, Mathews TD, Lindfors-Kearns FE. 1991. Barrier-island progradation and Holocene sea-level history in southwest Florida. *Journal of Coastal Research* **7**(3): 815-838.

Stein M. 2011. Freshwater Wolfe's Pond has already been refilled, but it's with salt water from Raritan Bay; solution to problem yet to be figured out. Staten Island Advance. http://www.silive.com/southshore/index.ssf/2011/09/freshwater_wolfes_pond_has_alr.html Date of access: 12/01/2014.

Stockdon HF, Holman RA, Howd PA, Sallenger Jr AH. 2006. Empirical parameterization of setup, swash, and runup. *Coastal Engineering* **53**: 573-588.

Sturges W, Leben R. 2000. Frequency of ring separations from the Loop Current in the Gulf of Mexico: A revised estimate. *Journal of Physical Oceanography* **30**(7): 1814-1819. doi: http://dx.doi.org/10.1175/1520-0485(2000)030<1814:FORSFT>2.0.CO;2

Sweet W, Zervas C, Gill S, Park J. 2013. Hurricane Sandy inundation probabilities today and tomorrow. *Bulletin of the American Meteorological Society* **94**: S17-S20.

Talke SA, Orton P, Jay DA. 2014. Increasing storm tides in New York Harbor, 1844-2013. *Geophysical Research Letters* **41**: 3149-3155. doi: 10.1002/2014GL059574

Tanner WF. 1992. 3000 years of sea level change. *Bulletin of the American Meteorological Society* **73**(3): 297-303.

Temmerman S, Meire P, Bouma TJ, Herman PMJ, Ysebaert T, De Vriend HJ. 2013. Ecosystem based defense in the face of global change. *Nature* **504**: 79-83. DOI: 10.1038/nature12859

The City of New York. Wolfe's Pond Park. NYC Parks. http://www.nycgovparks.org/parks/wolfes-pond-park/highlights/12301 Date of access: 12/01/2014.

Thompson R, Morton DJ. 1979. Magnetic susceptibility and particle-size distribution in recent sediments of Loch Lomond drainage basin, Scotland. *Journal of Sedimentary Petrology* **49**(3): 0801-0811. DOI: 10.1306/212F7851-2B24-11D7-8648000102C1865D

Tjerry S, Fredsøe J. 2005. Calculation of dune morphology. *Journal of Geophysical Research* **110**(F4): F04013. doi: 10.1029/2004JF000171

Törnqvist TE, González JL, Newsom LA, van der Borg K, de Jong AF, Kurnik CW. 2004. Deciphering Holocene sea-level history on the US Gulf Coast: A high-resolution record from the Mississippi Delta. *Geological Society of America Bulletin* **116**(7-8): 1026-1039.

Törnqvist TE, Bick SJ, van der Borg K, de Jong AF. 2006. How stable is the Mississippi Delta? *Geology* **34**(8): 697-700.

Unisys. 2014. *2012 Hurricane/Tropical Data for Atlantic.* <http://weather.unisys.com/hurricane/atlantic/2012H/SANDY/track.dat>, Date of access: 02/10/2014.

USEPA. 1999. *Ecological condition of estuaries in the Gulf of Mexico, EPA 620-R- 98-004*, 80 U.S. Environmental Protection Agency, Office of Research and Development, National Health and Environmental Effects Research Laboratory, Gulf Ecology Division, Gulf Breeze, Florida

United States Geological Survey. 2014. *Coastal Change Hazards: Hurricanes And Extreme Storms*. <http://coastal.er.usgs.gov/hurricanes/sandy/field-measurements/>, Date of access: 05/06/2014.

Varekamp J, Kreulen B, Buchholtz ten Brink MR, Mecray E. 2003. Mercury contamination chronologies from Connecticut wetlands and Long Island Sound sediments. *Environmental Geology* **43**: 268-282. doi: 10.1007/s00254-002-0624-x

Varekamp JC, Mecray EL, Maccalous TZ. 2005. Once spilled, still found: metal contamination in Connecticut coastal wetlands and Long Island Sound sediment from historic industries. In *America's Changing Coasts: Private Rights And Public Trust*, Whitelaw DM, Visgilio GR (eds). Edward Elgar Publishing, Inc.: Northampton.

Wallace DJ, Anderson JB, Rodriguez AB. 2009. Natural versus anthropogenic mechanisms of erosion along the upper Texas coast. Geological Society of America Special Papers **460**: 137-147. DOI: 10.1130/2009.2460(10).

Wallace DJ, Anderson JB. 2010. Evidence of similar probablility of intense hurricane strikes for the Gulf of Mexico over the late Holocene. *Geology* **38**(6): 511-514.

Wallace DJ, Woodruff JD, Anderson JB, Donnelly JP. 2014. Palaeohurricance reconstructions from sedimentary archives along the Gulf of Mexico, Caribbean Sea and western North Atlantic Ocean margins. The Geological Society of London Special Publication **388**: SP388.12. DOI: 10.1144/SP388.12.

Warner JC, Sherwood CR, Signell RP, Harris CK, Arango HG. 2008. Development of a three-dimensional, regional, coupled wave, current, and sediment-transport model. *Computers & Geosciences* **34**(10): 1284-1306.

Weisberg RH, Zheng L. 2006. Hurricane storm surge simulations for Tampa Bay. *Estuaries and Coasts* **29**: 899-913.

Wentworth CK. 1922. A scale of grade and class terms for clastic sediments. *Journal of Geology* **30**: 377-392.

Woodruff JD,Donnelly JP, Emanuel K, Lane P. 2008a. Assessing sedimentary records of paleohurricane activity using modeled hurricane climatology. *Geochemistry, Geophysics, Geosystems* **9**(9): Q09V10. doi:10.1029/2008GC002043

Woodruff JD, Donnelly JP, Mohrig D, Geyer WR. 2008b. Reconstructing relative flooding intensities responsible for hurricane-induced deposits from Laguna Playa Grande, Vieques, Puerto Rico. *Geology* **36**(5): 391-394. doi: 10.1130/G24731A.1

Woodruff JD, Martini A, Elzidani E, Naugton T, Kekacs D, MacDonald DG. 2013a. Off-river waterbodies on tidal rivers: Human impact on rates of infilling and the accumulation of pollutants. *Geomorphology* **184**: 38-50. doi: 10.1016/j.geomorph.2012.11.012

Woodruff JD, Irish J, Camargo S. 2013b. Coastal flooding by tropical cyclones and sea-level rise. *Nature* **504**: 44-52. doi: 10.1038/nature12855

Woodruff JD, Kanamaru K, Kundu S, Cook TL. 2015. Depositional evidence for the Kamikaze typhoons and links to changes in typhoon climatology. *Geology* **43**(1): 91-94. DOI:10.1130/G36209.1

Wright EE, Hine AC, Goodbred SL, Locker SD. 2005. The effect of sea-level and climate change on the development of a mixed siliciclastic–carbonate, deltaic coastline: Suwannee River, Florida, USA. *Journal of Sedimentary Research* **75**(4): 621-635.

Yellen B, Woodruff JD, Kratz LN, Mabee SB, Morrison J, and Martini AM. 2014. Source, conveyance and fate of suspended sediments following Hurricane Irene. New England, USA. *Geomorphology* **226**: 124-134.

Zervas C. 2013. *Extreme water levels of the United States 1893-2010 NOAA Technical Report NOS CO-OPS 067.* <http://tidesandcurrents.noaa.gov/publications/NOAA_Technical_Report_NOS_COOPS_067a.pdf>, Date of access: 18/10/2014.

Zhou H-y, Peng X-t, Pan J-m. 2004. Distribution, source and enrichment of some chemical elements in sediments of the Pearl River Estuary, China. *Continental Shelf Research* **24**(16): 1857-1875. DOI: 10.1016/j.csr.2004.06.012